MODELING FLOW IN PULP LIFTER CHANNELS OF GRINDING MILLS WITH COMPUTATIONAL FLUID DYNAMICS

by

Dilek Alkac

A dissertation submitted to the faculty of
The University of Utah
in partial fulfillment of the requirements for the degree of

Doctor of Philosophy

Department of Metallurgical Engineering

The University of Utah

December 2011

The University of Utah Graduate School

STATEMENT OF DISSERTATION APPROVAL

The dissertation of **Dilek Alkac**

has been approved by the following supervisory committee members:

Raj K. Rajamani	, Chair	**09/06/2011** Date Approved
Jan D. Miller	, Member	**09/06/2011** Date Approved
Chen-Luh Lin	, Member	**09/06/2011** Date Approved
Felipe Calizaya	, Member	**09/06/2011** Date Approved
Michael G. Nelson	, Member	**09/06/2011** Date Approved

and by **Jan D. Miller**, Chair of the Department of **Metallurgical Engineering**

and by Charles A. Wight, Dean of The Graduate School.

ABSTRACT

The current study is aimed at improving the performance of autogenous grinding and semiautogenous grinding mills. In particular, the material transport issue is the focus since the efficiency of mill discharge via grate, pulp lifter channels, and discharge trunnion determines the mill throughput.

The objective of this study is to develop a computational tool, and a simulation model which is built on fundamental physics of the process. Mainly, the simulation model is expected to give reasonably accurate predictions of free surface profiles inside the pulp lifter channels and volumetric flow rate out of the pulp lifter channels.

Employing the computational fluid dynamics as the central component, the study puts forward the mathematical modeling of the pulp flow in the pulp lifter channels along with experimental validation of simulation results.

First, past modeling studies of grinding mills are reviewed, with the focus on the material transport. Then the experimental methodology is presented. The explanations of flow dynamics are given from a theoretical point of view. Primarily, the free surface profiles and the dynamic discharge profiles are captured experimentally. The proposed model that includes rotation of the pulp lifter channel is validated by comparing the predictions of the model to experimental results.

Having proved the pulp flow dynamics by the experimental study, the computational fluid dynamics methodology is employed for the prediction of plant scale mill data.

The free surface profiles inside the mill are well captured by the CFD methodology, giving insight into understanding the pulp flow. The volumetric flow rate predictions conform to the experimental data as well as the plant scale mill survey data.

Modeling of pulp flow in the pulp lifter channel by computational fluid dynamics is beneficial in the sense that it yields comprehensive information about the specifics of the operation, making it possible to investigate in detail such phenomena as flow back and carry over flow in semiautogenous grinding mill pulp lifter channels.

Dedicated to my father, Hasan Alkac

TABLE OF CONTENTS

LIST OF TABLES

Table **Page**

NOMENCLATURE

F	force	(N = kg.m.s^{-2})
m	mass	(kg)
a_{NET}	net acceleration	(m.s^{-2})
g	gravitational acceleration	(m.s^{-2})
u	velocity component in x-direction	(m.s^{-1})
v	velocity component in y-direction	(m.s^{-1})
w	velocity component in z-direction	(m.s^{-1})
P	static pressure	(Pa = N.m^{-2})
ρ	density	(kg.m^{-3})
μ	dynamic viscosity	(Pa.s = kg.m^{-1}.s^{-1}) (1 Pa.s = 1000 mPa.s)
μ_T	turbulent viscosity	(kg.m^{-1}.s^{-1})
τ_{xx}	shear stress in x-direction – force per unit area in the x-direction on a plane perpendicular to x-direction	(N.m^{-2})
τ_{yy}	shear stress in y-direction – force per unit area in the y-direction on a plane perpendicular to y-direction	(N.m^{-2})
τ_{zz}	shear stress in z-direction – force per unit area in the z-direction on a plane perpendicular to z-direction	(N.m^{-2})
τ_{xy}	shear stress in x-direction – force per unit area in the y-direction on a plane perpendicular to x-direction	(N.m^{-2})
τ_{yx}	shear stress in y-direction – force per unit area in the x-direction on a plane perpendicular to y-direction	(N.m^{-2})

τ_{xz} shear stress in x-direction – force per unit area in the z-direction on a plane perpendicular to x-direction ($N.m^{-2}$)

τ_{zx} shear stress in z-direction – force per unit area in the x-direction on a plane perpendicular to z-direction ($N.m^{-2}$)

τ_{yz} shear stress in y-direction – force per unit area in the z-direction on a plane perpendicular to y-direction ($N.m^{-2}$)

τ_{zy} shear stress in z-direction – force per unit area in the y-direction on a plane perpendicular to z-direction ($N.m^{-2}$)

α volume fraction (.)

u_i', u_j' velocity fluctuations around the mean velocity ($m.s^{-1}$)

k kinetic energy of turbulence ($m^2.s^{-2}$)

ε turbulence energy dissipation rate ($m^2.s^{-3}$)

σ_k Prandtl number constant for kinetic energy of turbulence (.)

σ_ε Prandtl number constant for turbulence energy dissipation rate (.)

$C_{1\varepsilon}$ constant in equation for turbulence energy dissipation rate (Equation 4.13) (.)

$C_{2\varepsilon}$ constant in equation for turbulence energy dissipation rate (Equation 4.13) (.)

C_μ constant in equation for turbulent viscosity (Equation 4.18) (.)

∂ **and** ∂**x** partial differential operator in x-direction

∂ **and** ∂**y** partial differential operator in y-direction

∂ **and** ∂**z** partial differential operator in z-direction

δ_{ij} Kroneckor delta ($\delta_{ij} = 1$, if $i = j$ and $\delta_{ij} = 0$, if $i \neq j$)

Abbreviations

AG Autogenous Grinding

CFD Computational Fluid Dynamics

DEM Discrete Element Method

DGB Discrete Grain Breakage

HFS High Fidelity Simulations

PBM Population Balance Model

PDP Position Density Plot

RANS Reynolds averaged Navier Stokes

RPM Revolutions per Minute

SAG Semi Autogenous Grinding

SDV Superficial Discharge Velocity

SPH Smoothed Particle Hydrodynamics

TPH Tons per Hour

VCM Virtual Comminution Machine

VOF Volume of Fluid

ACKNOWLEDGEMENTS

I would like to thank Dr. Raj K. Rajamani for his supervision. I also want to thank the examining committee members, Dr. Jan D. Miller, Dr. C. L. Lin, Dr. Felipe Calizaya, and Dr. Michael G. Nelson, for their interest in the study.

I am grateful to Dr. Jose A. Delgadillo for inspiring me to see what I already had underneath my hands, and eventually put it to use. His contribution on gathering some of the experimental data is acknowledged.

The computational time and assistance provided by computer aided design and engineering (CADE) laboratory is greatly appreciated.

I want to express my gratitude for the financial support of PolyCorp Limited as well as for assistance of PolyCorp personnel in acquiring the plant scale mill survey data.

Last but not least, my sincerest thanks go to my family for their moral support during the course of the study.

CHAPTER 1

INTRODUCTION

Tumbling mills are cylindrical vessels used for the grinding process in mineral processing applications. The mill charge, containing the grinding media and the rock and ore particles, tumbles inside the mill to achieve the required size reduction. The tumbling action can either be cascading resulting in breakage by abrasion or cataracting resulting in breakage by impact.

Autogenous grinding mills and semiautogenous grinding mills are tumbling mills in which the grinding media is fully or partially made up of rock and ore particles in the mill charge. The processes taking place in AG and SAG mills cover all stages of size reduction and material transport. The material transport may be deemed more critical in the sense that failure to efficiently transport the slurry out of the mill affects the breakage field adversely, softening the impact of balls and rock particles. As a result, the milling efficiency is reduced.

The slurry is transported out of the mill in two stages: flow through the grate and discharge through the pulp lifter channels. Although both stages are equally important, the discharge capacity through the pulp lifter channels is the primary factor that determines the overall mill performance.

Modeling of the processes, including all stages of size reduction and material transport, in AG and SAG mills has received extensive recognition in mineral processing industry. These studies have revealed beneficial data on process specifics. Empiricism has mostly marked the basis of the modeling approach. Thus, the applicability of the models developed has been limited to certain cases. On the other hand, incorporating the physics governing the flow behavior requires models to use fundamental knowledge of the interactions between process variables to define the model structure.

The process fundamentals of pulp flow in the pulp lifter channels were initially studied by Mokken et al. (1975), noting the inefficiency of the pulp lifter channels for complete pulp removal. Detailed discussion of flow patterns was given with supporting mathematical arguments.

In 1996, Morrell and Stephenson published fully empirical models relating the volume of slurry in AG and SAG mills with the flow capacity of the grate. Morrell and Latchireddi (2000) expanded the model to the grate and pulp lifter discharge system.

Royston (2000, 2007a, 2007b) demonstrated the importance of practical mill operating experience in his work, mainly focusing on mill liner design, and curved pulp lifter channels. The slurry pooling issue was addressed in the study by Powell and Valery (2006) in which the overall system efficiency was discussed.

There have also been some studies using particulate models to study the slurry effects (Cleary et al. 2006, 2007; Herbst 2004).

As portrayed by the above discussion, though the design and operating variables related to AG and SAG mills have been studied, the number of publications discussing the material transport, specifically out of the pulp lifter channels, is scarce. Consequently,

a study of the pulp flow dynamics is essential to understand the efficiency of AG and SAG mills.

Therefore, in this study, the aim is to give a full model of pulp flow in the pulp lifter channel, including all the fundamental aspects, which in turn will enhance optimal configuration leading to more efficient operation. Inclusion of all aspects of the physics of flow is important in modeling while the validation of the model puts emphasis on the experimental work. For that reason, experimental work is an integral part in the study. Accordingly, a detailed experimental campaign is conducted. High speed photography is utilized for recording the flow scenes. Due to the insight gained from such experiments, the proposed model utilizes relevant computational tools and mathematical principles. Three-dimensional simulation of pulp flow, consisting of only fluid with no solid addition, is presented. However, the effect of slurry on the flow behavior is mimicked by use of glycerol solutions prepared at certain concentrations in the experimental part of the study. The characteristic values for slurry density and slurry viscosity, as given by the mill survey data, are used in plant scale mill simulations.

1.1. Research Objectives

The objective in the study is to design a computational tool that gives reasonable predictions of free surface profiles, discharge profiles inside the pulp lifter channels, and the volumetric flow rate out of the pulp lifter channels through a simulation model which is built on fundamental physics of the process.

Intrinsically, the flow behavior inside the single pulp lifter channel is modeled via computational fluid dynamics to represent the flow behavior inside the mill which is

made up of a number of pulp lifter channels. In other words, detailed understanding of pulp flow is the ultimate objective.

Supporting physical experiments are also conducted, as a measure of the accuracy of modeling. The experimental data have been collected, both for free surface profile and discharge profile experiments, by varying mill rotational speed, volume filling of fluid, solution density, and solution viscosity. The simulations are run on the basis of the same set of variables. Furthermore, the methodology is tested on the plant scale survey data published in the literature as well as on the survey data of an AG mill, having a diameter of 9.76 m and length of 3.5 m. The data from the physical experiments and plant scale mill surveys and the simulation results are compared to validate the proposed CFD methodology.

The proposed model basically incorporates transient multiphase turbulent flow subject to a force field. The following is essential to meet the objective:

(i) Understanding of the motion of solution and slurry in pulp lifter channels with physical experiments.

(ii) Using the gained knowledge to develop a model that will make it possible to predict the free surface profiles of the fluid volume carried by the pulp lifter channel.

(iii) Establishing a model for predicting the volume discharged by the pulp lifter channel besides the volumetric flow rate out of the pulp lifter channel.

(iv) Predicting volumetric flow rate through pulp lifter channels and comparing it with published mill survey data.

1.2. Structure of Dissertation

The outline of the dissertation is presented as follows:

Chapter 1 starts with the general introduction of AG and SAG mills, continuing with the description of the mill discharge assembly including grate, pulp lifter channels, and discharge trunnion.

Review of current modeling studies of AG and SAG milling is given in ***Chapter 2***. The milling variables that form the basis of the studies are introduced, with particular reference to the terminology used in AG and SAG milling.

Experimental set-ups along with the data collection strategy and the presentation of plant scale mill data make up contents of ***Chapter 3***. The set-ups for the dynamic free surface profile experiments and the dynamic discharge experiments are presented. Then the data collection strategy is explained. The plant scale mill data from the mill surveys published in literature is outlined together with the data of the ArcelorMittal Mont-Wright AG mill. Additionally, brief discussion of the modeling theory is given**,** addressing the proposed model assumptions. ***Chapter 4*** discusses the mathematical description of the process, specifically based on the CFD methodology. The principle CFD models, namely the multiphase flow model and turbulence model, are explained. Analyses of the experimental results and the CFD simulation results are taken up in ***Chapter 5***. ***Chapter 6*** covers the discussion of plant scale data and the corresponding CFD simulation results. ***Chapter 7*** concludes with a summary of the study.

CHAPTER 2

LITERATURE REVIEW

The current chapter begins with the description of the field related terms in autogenous grinding and semiautogenous grinding milling. Systematically, all the components of the grinding mill are introduced, underlining the modeling studies related to each component. Thorough discussion of the process taking place in the grinding mills is given in regards to the modeling aspects.

Bearing in mind that the aim is to put forward a general view of the modeling studies of the grinding process to delineate an overall picture, the discussion of the modeling studies of discharge dynamics follows. The discussion continues with the modeling studies of charge motion and power draft. Finally, full process simulation modeling studies, including all the stages of the process, are presented.

AG and SAG mills are known to be “high aspect ratio” mills, having diameters 1.5 – 3 times larger than length. The overall process inside the mill can be summarized as breakage, classification, and discharge. The material fed into the mill undergoes size reduction in the mill interior, and the broken material first is classified through the grate according to fineness. The material larger than grate opening size is retained inside the mill while the material fine enough passes into the pulp lifter channels. Then, the fine material in the channels is discharged out of the mill via the discharge end.

Size reduction is achieved in the breakage stage, via cascading and/ or cataracting motion of the charge. The breakage takes place in the mill interior which is the part spanning the distance between the feed trunnion and the discharge trunnion (Figure 2.1). A detailed view of grate and pulp lifter channels assembly is provided by Figure 2.2 (Taggart 1945).

The efficiency of size reduction is determined by the mill shell as it is the means of power delivery to the bed of ore particles housed inside the mill shell. Therefore**,** the design of shell liners and shell lifters plays a crucial role in achieving the maximum work done per unit time. In addition to its part in controlling the charge motion in the mill shell, the mill liner, in general, provides replaceable surfaces all throughout the mill. The grate makes up the principle classification unit, allowing the passage of the suspension containing particles of size less than grate opening.

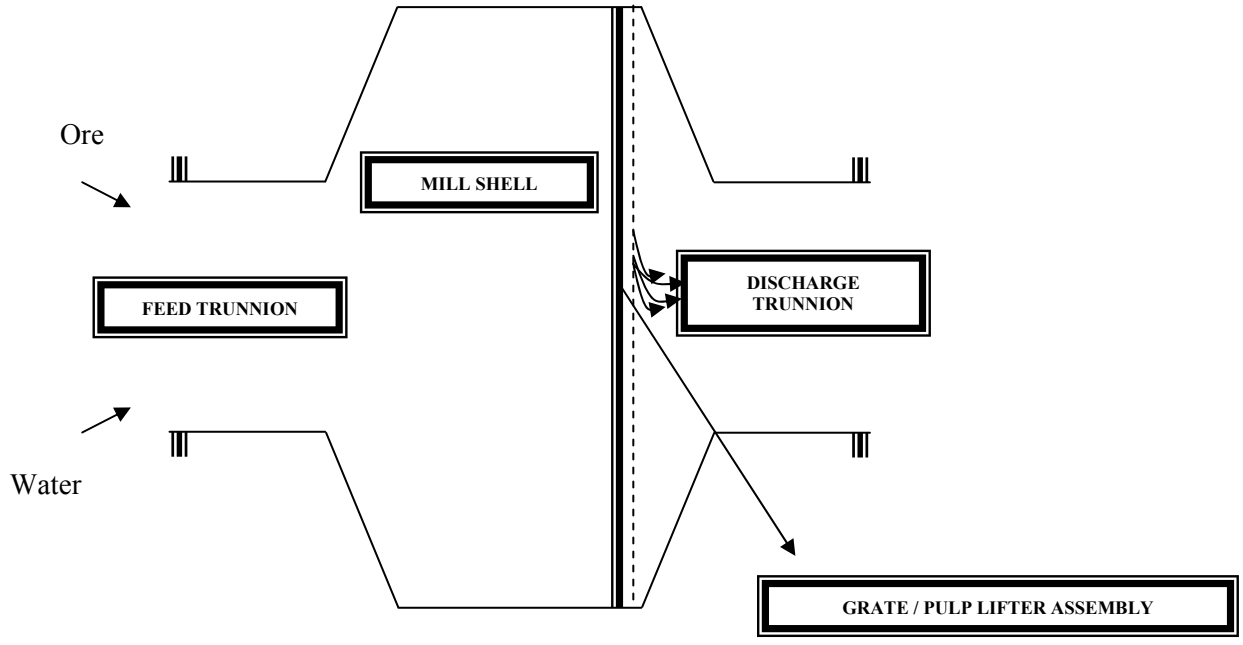

Figure 2.1 – Schematic of AG and SAG mills

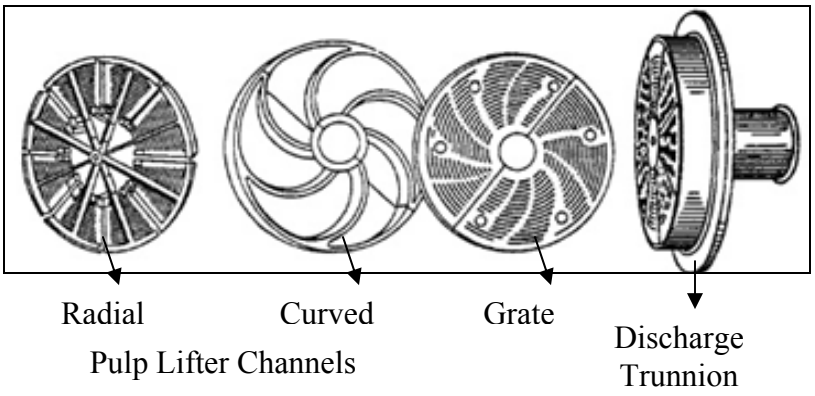

Figure 2.2 – Conventional design of grate, pulp lifter channels, and discharge trunnion (Adapted from Taggart 1945)

The slurry, in other words the fluid with fine solid particles resembling a pulp, acts as the transporting agent. Grate design proves to be one of the most important factors for optimum milling performance in the sense that it is the very first unit for transporting the broken material out of the mill. The variables that make up the grate design are basically the percent grate open area, and the spatial distribution of grate openings. The allocation of grate openings with respect to the central axis of the mill is termed as relative radial position. The relative radial position is an important variable in determining the discharge efficiency since the discharge of slurry most readily occurs through the outermost grate openings (Royston 2007a). For that reason, high values of relative radial position are preferable.

The slurry flowing through the grate is first accumulated within the pulp lifter channels and then discharged through, as the mill rotates. Each pulp lifter channel transports the ore slurry to the discharge trunnion. The major types of pulp lifter channels used in AG and SAG mills are radial and curved pulp lifter channels. Curved pulp lifter channels offer the advantage of faster discharge due to their shape. However, the

unidirectional rotation requirement associated with curved pulp lifter channel design renders this choice less preferable.

The slurry hold up is defined as the volume of slurry inside the mill, held within the interstices of the charge. A crash stop survey, in which the mill is fully stopped without any inflow and outflow, is performed to measure the slurry level and mill filling as well as the shell lifter wear patterns.

The system with pulp lifter channels discharges less slurry than the system without pulp lifter channels (Latchireddi & Morrell 1997, 2003a, 2003b). Thus, the free flow of the pulp is hindered by the pulp lifter channel, causing some significant phenomena such as flow back, slurry pooling, and carry over.

The pulp lifter channel, once filled up with the slurry, lifts the slurry till it flows towards the center of the mill. All through the lifting stage, the slurry inside the channel is stationary under the effect of centrifugal and gravitational force. The slurry starts to flow down, leveling out in the channel, when the pulp lifter channel passes the horizontal. Some of the slurry flows back into the mill through the grate openings as it levels out. In some instances, flow back volume results in formation of a slurry pool, excessively accumulating inside the mill. The slurry pooling adversely affects the power draft (Morrell & Kojovic 1996; Powell & Valery 2006).

Carry over is observed at high mill rotational speeds, and is described as the volume of slurry being carried around due to incomplete discharge of the pulp lifter channel in the preceding revolution of the mill.

Mathematical modeling has a good reputation in engineering applications, such that the results are to be used as guides once the model outputs are fully proven. As far as

the grinding process is concerned, there have been modeling studies dealing with charge motion and power draft, discharge dynamics, and full process simulation.

The models have mostly had empirical roots, principally linking the mill design and operating variables based on experimental data. Later introduction of particulate models has put the focus on the fundamental physics once again. The particulate models do solve the related conservation equations for the case being studied. Numerical roots of the methodology, however, necessitate use of discretization schemes for the defining equations as well as the geometrical discretization of the domain.

Breakage mechanics is principally described by the population balance model, in which the mass balance equations are solved. Discrete element modeling is well known for the simulation of charge motion, providing detailed information on the interaction, energy spectra, and hence mill power draft. The slurry effects are studied by smoothed particle hydrodynamics as the particulate model.

2.1. Modeling Studies on Discharge Dynamics

Theoretical investigation of pulp flow in the pulp lifter channel was first taken up in 1975 by Mokken et al., pointing out the limitations of the capacity of pulp lifter channels. The importance of mill rotational speed was specifically emphasized with regard to the breakage rates. The authors opted for an end peripheral discharge arrangement, seeing that the capacity of pulp lifter channels was inversely correlated with the speed of rotation. Improvement in power utilization as well as increase in amount of pulp flow was reported upon the change to the end peripheral discharge system.

It was also noted that the conventional pebble mills always processed less compared to the amount handled by peripheral discharge mills.

Investigating the effects of flow rate and viscosity of slurry on slurry hold up, Moys (1986) published a quasi-mechanistic model. The model was developed on a 2.5-kW pilot grinding mill, and it accounted for the details of grate design as well as the flow rate and viscosity of slurry. The results of the study demonstrated that both grate and mill load caused significant resistance to flow of slurry.

The effect of grate design along with some operating variables in AG and SAG mills was later studied by Morrell and Stephenson (1996). The authors developed empirical model equations defining slurry hold up on the basis of grate design and operating variables on a laboratory scale mill, of size 0.3 m in diameter and 0.15 m in length. The equations were calibrated to be used on pilot scale and plant scale mills, with successful predictions.

Detailing the effect of slurry transport on power draft by use of empirical equations, Morrell and Kojovic (1996) showed that insufficient grate and pulp lifter assembly discharge capacity can adversely affect the mill performance. The study performed on the Leinster AG mill, of size 9.4 m in diameter and 6.76 m in length, indicated progressive drop in power draft due to the formation of a slurry pool.

A qualitative laboratory scale study on discharge characteristics, particularly on the capacity, of pulp lifter channels was conducted in 1997 by Latchireddi and Morrell. It was shown that the capacity of the system with pulp lifter channel was always less than that of grate only configuration. The authors attributed the difference to flow back and carry over phenomena, in addition to insufficient capacity of pulp lifter channels.

Emphasizing the advantage offered by curved pulp lifter channels, Royston and Denlay (1999) developed a mathematical model for comparing radial and curved pulp

lifter channel performance. The spreadsheet model made use of a single solid particle representing the charge in the rotating mill. By balancing the gravitational force, the centrifugal force, and the friction force on the single particle, the model outputs mathematically verified the notion that the curved pulp lifter channel discharged faster.

In the same line with the study published in 1997, Latchireddi and Morrell (2003a) detailed their qualitative study of slurry flow by studying the systems individually: grate only discharge system and grate and pulp lifter assembly discharge system. Having studied the effects of flow rate, mill speed, charge volume, and grate design, the authors concluded that hold up was more controlled by the charge volume compared to grate open area, especially when the flow occurred through the porous charge. Switching to pilot scale set-up, of size 1 m in diameter and 0.5 m in length, in the second part of the study, Latchireddi and Morrell (2003b) once again noted the inefficiency of pulp lifter channels, reporting that the performance improved as the volume of the pulp lifter channel was increased while there was a decrease in discharge flow as the mill speed was increased. The authors also reported that even though the system with curved pulp lifter channels discharged better, the capacity of the system with curved pulp lifter channels was not equivalent to the grate only discharge system**.**

Royston (2005) discussed pulp lifter channel design and discharge cone design. Again, a single particle motion model was referred to demonstrate the effect of flow back phenomena, in particular as the source of wear in pulp lifter channels. Addressing the flow back phenomena as “reverse flow” of fluid pulp, Royston commented on the necessity of minimizing the reverse flow for efficient performance.

The slurry pooling issue was thoroughly analyzed by Powell and Valery (2006), pointing to the fact that discharge capacity directly determined the mill throughput. The detailed analysis of the issue was taken up by way of presentation of nine sets of plant scale data. The authors formulated the slurry and pebble discharge capacity in terms of superficial discharge velocity, defined simply as the volumetric flow rate per unit grate open area, to assess the slurry pooling. Emphasizing once again the importance of sufficient pulp discharge capacity, the range of SDV for slurry flow was given as $100 – 150\ m.h^{-1}$.

Incorporating the slurry effects into a particulate model via SPH, Cleary et al. (2006) proposed and demonstrated a DEM-SPH framework, in which the charge was presented as dynamic porous media, for modeling slurry motion in mills. Prediction of the slurry distribution in a 10.36 m diameter mill was presented, focusing on the effects of slurry viscosity, charge permeability, and slurry volume.

2.2. Modeling Studies on Charge Motion and Power Draft

The population balance model makes use of material balance principles in a similar manner to that of a path function, that is it integrates all possible information on how the process evolves to arrive at the resulting output. In that regard, the selection function gives information about how much of particles of size i undergoes size reduction per unit time while the breakage function represents how much of particle of size j is produced from broken particles of size i, where size i is greater than size j.

The mean residence time for solid particles is defined as the time required to break the feed material to a size less than grate openings, which is the ratio of solid hold up to solid feed rate.

Modeling the mass transport in SAG and AG mills by use of PBM code, Austin et al. (1987) identified three distinct breakage zones as normal breakage, abnormal breakage, and self breakage. The shell balance approach around the SAG mill and AG mill was used in developing the model equation for fractional solid hold up of any size class. The resulting equation consisted of selection functions, breakage functions, classification functions, and mean residence time. Stating that the transport of material of sizes less than grate opening was dependent on the ease of slurry flow, the residence time was formulated based on the volumetric slurry flow rate. The formulation for the volumetric slurry flow rate was given in terms of mill diameter, percent grate open area, and fractional mill critical speed. The model was used to compare the performance of a SAG mill with an aspect ratio of 2 to that of an AG mill with an aspect ratio of 0.5. The results showed that two AG mills were required to achieve the same capacity as that of a SAG mill.

Rajamani and Mishra (1996) studied the charge motion in SAG mills with DEM code. The study focused on the effect of shell lifter height and shell lifter configuration, angle and spacing, on overall dynamics of charge, as well as the shell liner wear. The results indicated that the charge profile changes with changes in shell lifter spacing and shell lifter angle.

In 2001, Rajamani and Mishra presented the study of charge motion via a three-dimensional DEM code. The study was conducted on a 10.75 m diameter SAG mill, investigating the effects of design of lifters and liners. By changing the number of shell lifters and lifter face angles, the authors reported significant differences in the resulting charge profiles. The effect of mill speed was also discussed in the same study.

Simulation of size reduction by a modified DEM approach, namely the discrete grain breakage model, was discussed by Nordell and Potapov (2001). DGB code is a combination of PBM and DEM algorithms, numerically solving the energy conservation equations for crack propagation in solid particles consisting of discrete grains. Stating that the performance of DGB code could be demonstrated with regard to shell lifter design, particle shape, and discharge performance, analysis of a 10.4 m diameter mill with different configurations was presented. The authors reported the detailed results in terms of charge behavior, wear patterns, and power draft specifically by identifying the key variables for enhancement of breakage performance.

Dong and Moys (2003) presented the power draft calculations based on the torque-arm model by describing the load orientation with position density plots, which are digital, visual, and statistical representations of charge distribution in a mill.

It was shown that the amount of cataracting material increased as the mill speed increased. The authors also noted that PDPs provided more detailed information on the load orientation than the conventional approach using dynamic angle of repose, shoulder and toe angles. With the increasing mill speed, an increase in shoulder angle was reported while there was a decrease in toe angle.

Acknowledging the crucial function of mill liners in the grinding process, Royston (2007b) drew attention to the design of mill liners in relation to shell lifters and grate and pulp lifter assembly. Royston recommended double-wide and double-long liner, made of Chrome – Molybdenum (Cr – Mo) alloy steel, for large mills. Cr – Mo alloy provides better impact resistance and longer wear life in SAG mills. White iron, high carbon versions of Cr – Mo alloys, was shown to be superior for improved abrasion

resistance while a metal-faced rubber Polymet type product was introduced as the liner type offering high resistance to damage through the ball impacts.

Cleary and Morrison (2009) modeled the charge motion, the slurry motion within the charge, discharge through the grate and pulp lifter assembly, and the breakage process via particulate models such as DEM and SPH. Dynamics of real particle motion were simulated by using DEM code for the coarse fraction while using SPH code for the fine fraction. It was concluded that three-dimensional DEM simulations captured the particle motion accurately while two-dimensional DEM simulations only provided qualitative information on the particle motion. Stating that the behavior of mill charge was not like that of a partially filled tank, the authors indicated that a slurry pool only formed given that the mill charge was completely full with slurry. The authors also presented the analyses of banana screens, generally used for high capacity separation of iron ore, coal, and aggregates into different size fractions. The advantageous characteristics of the particulate models were stated with strong emphasis on the use for further understanding of unit processes in mineral processing.

2.3. Full Process Simulation Studies

Song et al. (2001) introduced the MILLSTAT software package for statistical analysis of mill databases. The package made use of various statistical principles, such as analysis of variance, linear and nonlinear regression analyses, and so forth, with the aim of forming a sound mill performance comparison basis for future designs as well as for modification of the current ones. Ultimately, PBM and DEM codes were included in the package to be utilized for material transport and particle size distribution calculations. Screening all the available data by the package tools, it was shown that it was possible to

obtain comprehensive information about the status of the current operations, and also to propose ideas for further improvement.

In 2004, Herbst described use of a high fidelity simulation tool to scale up tumbling mills. The HFS tool, as introduced by Metso Minerals Optimization services, involves use of DEM, CFD, DGB, and PBM codes. Characterizing breakage and wear properties in laboratory by ultra fast load cell measurements, the author demonstrated that it was viable to obtain consistent information on product particle size distribution, mill dimensions, and operating variables. Specifically, a scale up study for a mill of diameter 4.11 m and of length 2 m was presented, for which data from a batch mill of diameter 0.25 m and length 0.29 m were used as a basis.

Morrell (2004) proposed means of quantifying mill throughput, power draft, product size distribution, load size distribution, and slurry hold up in AG and SAG mills by empirical models.

The particular objective in the study was to show how well the models, which were developed with laboratory scale data, predicted plant scale milling performance. The models identified for each specific process were successfully validated by use of twenty-one sets of data from AG and SAG mill circuits.

Remarking on the necessity of fundamental modeling, Powell and Morrison (2007) gave a detailed review of comminution modeling studies in mineral processing. The authors emphasized the importance of advances in measurement techniques as well as the improvements in computational power, addressing the weaknesses and strengths of current modeling tools. Specifically, studies on liberation modeling were given focus. The authors annotated the concept of a virtual comminution machine as proposed by

Morrison. The progress towards developing a full process simulation tool, namely VCM, for all stages of grinding was reported by Morrison and Cleary (2008). Discussing the characteristics of DEM codes, the authors suggested alternatives for improvements as well as essential expansions to include certain variables of importance to the overall process. Some specific conclusions based on the progress were presented, informing on the new objectives in the study.

2.4. Summary

The grinding process consists of breakage, classification, and discharge stages. The modeling studies in the literature cover all aspects of the grinding process, identifying important variables affecting the process.

Those studies have revealed beneficial data on process specifics, proving adequate understanding of the grinding process. Particularly, some of the aspects such as charge motion and power draft have been studied in detail while discharge dynamics studies have received partial attention. The discharge performance is affected by the design of the grate, the pulp lifter channels, and the discharge trunnion. The models regarding discharge dynamics, with the exception of particulate models, have been developed based on experimental data, and therefore have limited usage. Substantially, the design of the grate is emphasized in most of the studies rather than the design of pulp lifter channels. On the other hand, the function of the pulp lifter channel is crucial as it transports the ore slurry to the discharge trunnion. Therefore, the study of pulp flow dynamics in the pulp lifter channels is essential.

CHAPTER 3

METHODS AND MATERIALS

The experimental system set-up and the experimental procedures for data collection are outlined in the current chapter. Additionally, the plant scale mill survey data are presented. The chapter concludes with a brief discussion of modeling theory.

The experimentally studied ranges of the mill rotational speed and the solution properties are given along with explanations of the methodology both for dynamic free surface profile experiments and dynamic discharge profile experiments.

The computational aspects and the mathematical principles employed for the proposed model are introduced, with specific reference to the multiphase flow model and turbulence model. The assumptions made in the proposed model are summarized.

The experiments were performed both for dynamic free surface profiles and dynamic discharge profiles, using only colorless fluid.

It would have been impossible to carry out the photographic studies shown here with slurry since the slurry would smear on the walls and obscure the free surface. Therefore, an alternate was sought. In this regard, the work of Shi and Napier-Munn (2002) on the effect of slurry rheology on grinding performance of industrial grinding mills was beneficial. The authors pointed to the dependence of slurry rheology on slurry density and particle size. The data collected, in terms of grinding index, mill throughput, slurry density, slurry viscosity, and feed fines content, was further statistically analyzed.

The survey results indicated the highly non-Newtonian nature of slurry while the results from statistical analyses confirmed the dependence of industrial grinding performance on slurry rheology. Referencing the survey results (Shi & Napier-Munn 2002), the effect of solid percentage in the slurry is readily mimicked by use of the glycerol solutions prepared at different volumetric concentrations.

The experimental pulp lifter channel used in the study is made up of Plexiglass and has a volume of 1300 cm^3. It is 40 cm in height, 21 cm wide at the top, 5 cm wide at the bottom and has a depth of 3 cm, as shown by Figure 3.1.

In addition to the experimental analyses, the published data on plant scale mills (Powell & Valery 2006) are utilized as well as a set of data on the ArcelorMittal Mont-Wright AG mill.

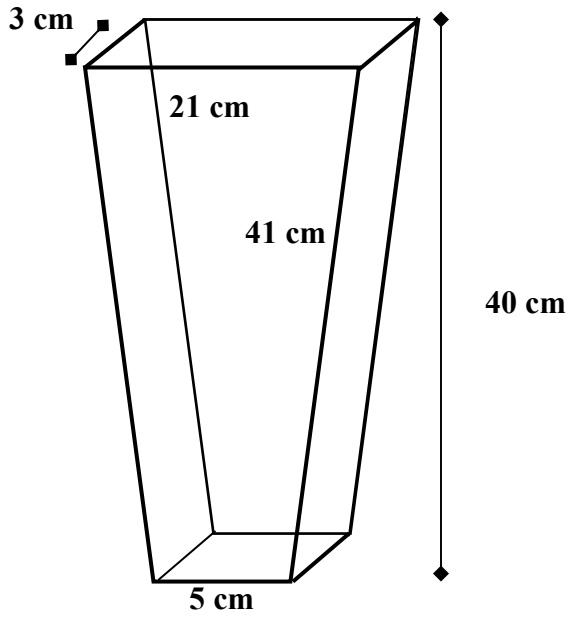

Figure 3.1 – The dimensions of the experimental pulp lifter channel of volume 1300 cm^3

3.1. Experimental Procedure

3.1.1 – Dynamic Free Surface Profile Experiments

The objective in the dynamic free surface profile experiments is to capture free surface profiles of a fluid body on a rotating system. The mill used (Figure 3.2) for the dynamic free surface profile experiments has an aspect ratio of 4.6, having a diameter of 92 cm and length of 20 cm. The critical mill speed is 44 revolutions per minute. The experiments are run at four different mill rotational speeds with four different volume fillings of glycerol solutions at three different concentrations, as shown in Table 3.1. The pulp lifter channel is affixed to the mill as shown in Figure 3.2.

The mill rotation is clockwise in the dynamic free surface profile experiments. The clock circle shown in Figure 3.3, superimposed on the mill circle, is referenced in the discussions to refer to locations of the channel as the mill rotates.

The filled pulp lifter channel is kept at the 12 o'clock region and the mill is started at the desired speed. There is no inflow to or outflow from the pulp lifter channel in these experiments. The free surface profiles are recorded for one single revolution of the mill.

The video records with high speed photography of the flow scenes therefore make up the experimental data collection strategy. A Fastec InLine high speed camera is used for capturing the images in monochrome mode. Fastec InLine cameras have various high speed digital image recording capabilities using a wide range of recording rates, sensor resolutions, and on board memory options. The camera is shown in Figure 3.4. A typical snapshot of a free surface profile is shown in Figure 3.5.

The viscosity measurements are done by using an Utube kinematic viscometer (Figure 3.6).

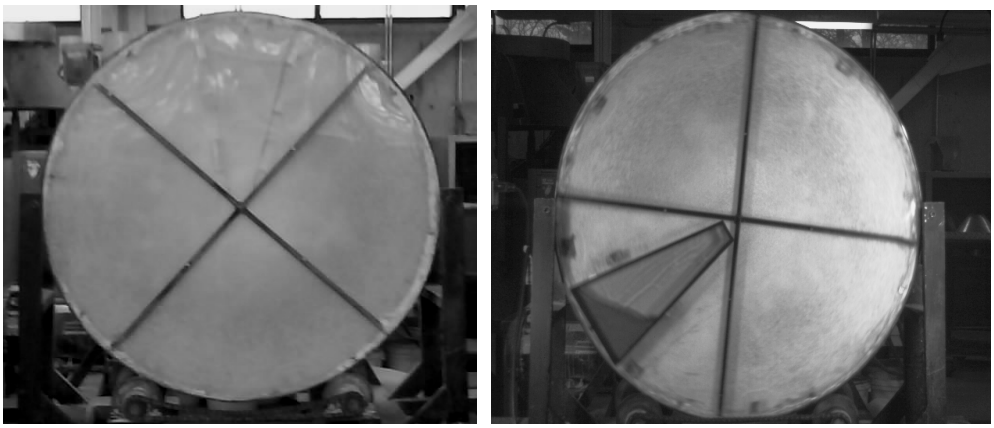

(a) (b)

Figure 3.2 – Pilot scale system set-up used for dynamic free surface profile experiments: (a) Mill (b) Mill and tank assembly

Table 3.1 – The experimentally studied ranges in terms of rotational speed, volume fillings of glycerol solutions, and glycerol solution concentrations

Mill rotational speeds (rpm)			
11.7	18.4	26.2	34
Percent critical speed (%)			
26.6	41.8	59.5	77.3
Volume fillings of glycerol solutions (cm^3)			
350	500	650	800
Glycerol concentrations by volume (%)			
65%	70%	75%	

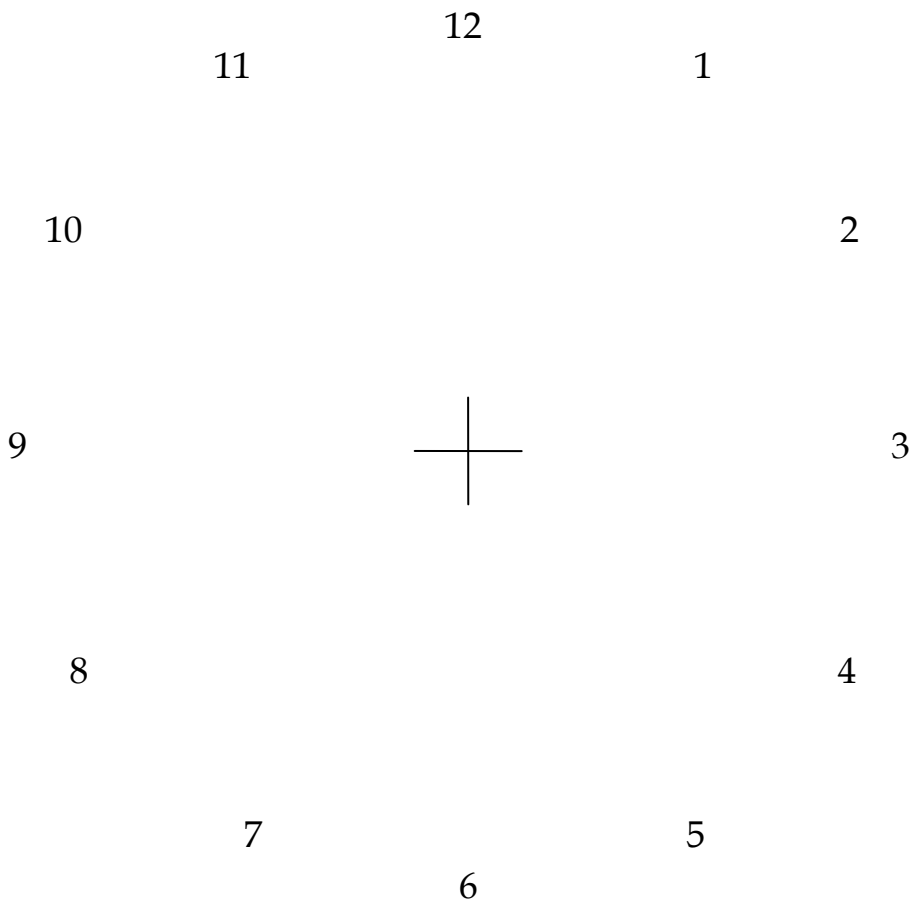

Figure 3.3 – Mill – Clock circle analogy

Figure 3.4 – Fastec InLine high speed camera

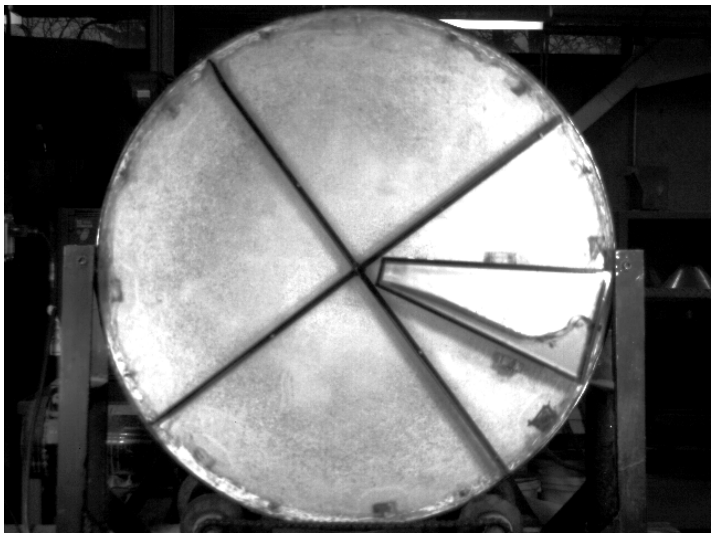

Figure 3.5 – A typical snapshot of free surface profile

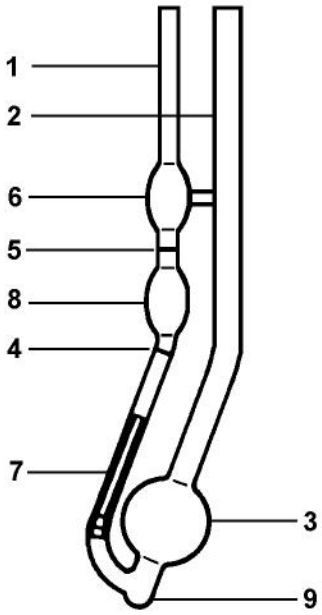

1. Tube with capillary
2. Venting Tube
3. Reservoir
4. Lower timing mark
5. Upper timing mark
6. Pre-run sphere
7. Capillary
8. Measuring sphere
9. Tube expanding

Figure 3.6 – Utube kinematic viscometer

The Utube kinematic viscometer works based on the principle of mechanical energy balance. In this method, the time that the fluid takes in moving through mark 5 and mark 4 is recorded, and the kinematic viscosity ($m^2.s^{-1}$) is calculated by multiplying the recorded value in seconds with the device constant. Table 3.2 gives the measured viscosity values of the glycerol solutions along with the solution density values.

In this method, the time that the fluid takes in moving through mark 5 and mark 4 is recorded, and the kinematic viscosity ($m^2.s^{-1}$) is calculated by multiplying the recorded value in seconds with the device constant. Table 3.2 gives the measured viscosity values of the glycerol solutions along with the solution density values.

3.1.2 – Dynamic Discharge Profile Experiments

The objective in the dynamic discharge profile experiments is to determine the amount of fluid flowing out of the channel during a single revolution of the mill as well as capturing the free surface profiles during the runs.

These experiments have been carried out for the current study at Universidad Autónoma de San Luis Potosí, Mexico under the guidance of Dr. Jose A. Delgadillo. These experiments have been carried out expressly for inclusion in this study.

Table 3.2 – The properties of the glycerol solutions: Viscosity and density

	Viscosity (mPa.s)	Density ($kg.m^{-3}$)
Glycerol by volume (%)		
65	28	1169
70	40	1183
75	70	1196

The mill rotation is counterclockwise in the dynamic discharge profile experiments. Two holes of 1 cm in diameter are drilled on the experimental pulp lifter channel for recording the volume discharged. In these experiments, the filled channel is kept at 6 o'clock, as seen in Figure 3.7 and the mill is started at the desired speed. The flow is collected exactly for one single revolution of the mill.

The first set of dynamic discharge experiments is conducted at volume fillings of 650 cm^3 and 350 cm^3 while keeping the mill rotational speed at 26.2 and 34 rpm. To investigate the effects of mill rotational speed in detail, a second set and third set of the experiments are run with volume fillings of 350 cm^3 and 500 cm^3 at mill rotational speeds of 26, 29, 32, and 35 rpm, covering a range of approximately 60 – 80% of the critical mill speed. In the third set of experiments, an additional hole of 1 cm diameter is drilled, completing the total number to three holes. The glycerol solution is prepared at the same concentration (85% by volume) for all the sets; however, due to temperature change in the laboratory, the glycerol solution in the second and the third sets of experiments has a different viscosity in comparison to the one used in the first set.

The experimental combinations tested in dynamic discharge experiments are as tabulated in Table 3.3. The glycerol solutions used for dynamic discharge profile experiments have a viscosity of 61 mPa.s and a density of 1220 $kg.m^{-3}$ for the first set, at a temperature of 30 ˚C and a viscosity of 83.5 mPa.s and a density of 1220 $kg.m^{-3}$ for the second and third sets, at a temperature of 23 ˚C.

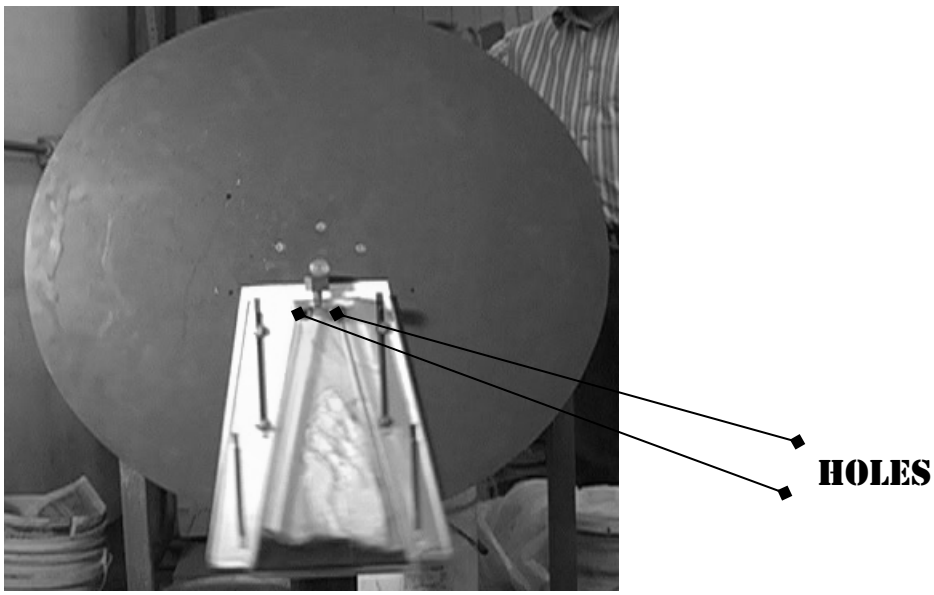

Figure 3.7 – Pilot scale system set-up used for dynamic discharge profile experiments (Mill and tank assembly)

Table 3.3 – The experimentally studied ranges in terms of rotational speed, volume fillings of glycerol solution of 85% by volume

Mill rotational speeds (rpm)					
26	26.2	29	32	34	35
Percent critical speed (%)					
59.0	59.5	65.9	72.7	77.3	79.5
Volume fillings of glycerol solutions (cm^3)					
	350	500	650		

3.2. Plant Scale Analyses

The plant scale data have been used as means of model validation. The published data sets along with the data collected at the ArcelorMittal Mont-Wright AG mill (Fermont, Quebec, Canada) are referenced. Table 3.4 shows the details of each mill design and operating variables. The survey data present the slurry density and percent solids in regards to the slurry properties, yet there is no information on the slurry viscosity which is one of the input variables for the case set-up. Therefore, the slurry density values as per survey data are directly referenced in the case set-up for simulations while the slurry viscosity values are estimated on the basis of the percent solids in consistency with literature data available (Shi & Napier-Munn 2002). The estimated slurry viscosity values, which have been used as an input in the simulations, are given in tables of plant scale data. The ArcelorMittal Mont-Wright AG mill, having a diameter of 9.76 m and length of 3.5 m, is fitted with 72 high-low lifters. Iron ore grinding is performed in the mill. There are 36 curved pulp lifter channels converging to 18 channels making up the pulp lifter assembly. The pulp lifter channel has a depth of 419 mm everywhere except at the outer circumference where it narrows to 150 mm in depth. The radial length of this narrow section is 370 mm. The depth change is due to a vertical grate at the outer periphery instead of the 15 degree inclination adopted in the inner grates. The pulp lifter channel depth refers to the distance between the grate plate and mill discharge head (interior dimension). Since the discharge head is inclined at 15 degrees, the depth is larger at the location where the channel connects to the mill trunnion.

Table 3.4 - Plant scale data, (Powell & Valery 2006)

	Los Bronces	**Los Bronces**	**Morila OC**	**Morila OC**
Diameter (m)	8.26	10.12	7.8	7.8
Length (m)	4.189	4.722	5.47	5.47
Trunnion Diameter (m)	2.0	2.2	2.17	2.17
Mill Rotational Speed (rpm)	11	10	11.35	11.35
Percent Critical Speed (%)	76.9	74.4	74.9	74.9
Pulp Lifter Channel Depth (mm)	375	464	270	270
Pulp Lifter Channel Volume (m^3)	0.625	1.1	0.912	0.912
Number of Pulp Lifters	30	32	13	13
Grate Open Area (m^2)	5.44	11.17	5.2	5.2
Slurry Density ($kg.m^{-3}$)	1670	1700	1722	2000
Solids %	65.4	67	66	79
Slurry Viscosity (mPa.s)	100	100	100	100

Table 3.4 Continued

	Gold ore	**Navachab**	**UG2 AG mill**	**Pb and Zn and Ag AG mill**
Diameter (m)	10.81	4.72	5.92	8.37
Length (m)	4.95	9.49	7.1	4.03
Trunnion Diameter (m)	2.2	1.195	1.45	2.170
Mill Rotational Speed (rpm)	8.8	17.3	13.2	11
Percent Critical Speed (%)	68.4	88.9	75.9	75.2
Pulp Lifter Channel Depth (mm)	430	300	200	300
Pulp Lifter Channel Volume (m^3)	2.092	0.61	0.265	1.1
Number of Pulp Lifters	18	8	20	14
Grate Open Area (m^2)	6.9	2.45	1.45	3.8
Slurry Density ($kg.m^{-3}$)	1869	1900	2280	2401
Solids %	72.3	73.1	79.6	82.6
Slurry Viscosity (mPa.s)	150	150	200	200

The details of the design and operating variables are summarized in Table 3.5. The dimensions of a single channel of the pulp lifter assembly for the mills are determined from mill diameter, trunnion diameter, number of pulp lifter channels, and channel depth. The volume of slurry held in the pulp lifter channel at the 6 o'clock location is set in accordance with the charge profile predictions by DEM simulations. Table 3.6 gives the channel dimensions and the initial volume filling of slurry for each of the plant scale mills studied.

Table 3.5 - ArcelorMittal Mont-Wright AG mill data

	Mont-Wright AG mill
Diameter (m)	9.76
Length (m)	3.5
Trunnion Diameter (m)	2.13
Mill Rotational Speed (rpm)	10
Percent Critical Speed (%)	74
Pulp Lifter Channel Depth (mm)	419
Pulp Lifter Channel Volume (m^3)	0.825
Number of Pulp Lifters	36
Grate Open Area (m^2)	7.5
Slurry Density ($kg.m^{-3}$)	1530
Solids %	51
Slurry Viscosity (mPa.s)	75

Table 3.6 – The single pulp lifter channel dimensions and the initial volume of slurry for plant scale simulations

Mill	Diameter × length (m)	Trunnion diameter (m)	Number of pulp lifter channels	Volume filling of slurry (m^3)
Los Bronces	8.26 × 4.189	2.0	30	0.1875
Los Bronces	10.12 × 4.772	2.2	32	0.44
Navachab	4.72 × 9.49	1.195	8	0.180
Morila OC	7.8 × 5.47	2.17	13	0.38
Morila OC	7.8 × 5.47	2.17	13	0.4
Gold Ore	10.81 × 4.95	2.2	18	0.554
Lead/ Zinc/ Silver AG Mill	8.37 × 4.03	2.0	14	0.374
UG2 AG Mill	5.92 × 7.1	1.45	20	0.085
Mont-Wright AG Mill	9.76 × 3.5	2.13	18	0.475

	Channel cross section (depth × length (m))		Cone angle (degrees)
	At circumference	At trunnion	
Los Bronces	0.375 × 0.865	0.375 × 0.209	12
Los Bronces	0.464 × 0.994	0.464 × 0.216	12
Navachab	0.300 × 1.854	0.300 × 0.470	0
Morila OC	0.270 × 1.885	0.270 × 0.360	0
Morila OC	0.270 × 1.885	0.270 × 0.360	0
Gold Ore	0.430 × 1.887	0.430 × 0.384	15
Lead/ Zinc/ Silver AG Mill	0.300 × 1.880	0.300 × 0.450	17
UG2 AG Mill	0.200 × 0.930	0.200 × 0.225	22.5
Mont-Wright AG Mill	0.419 × 1.703	0.150 × 0.370	15

3.3. Modeling Theory

Equations describing the fluid motion are the subject of fluid dynamics in which the conservation equations are defined mathematically. Numerical solution of the equations of motion, momentum and mass balance equations, lends itself to the study known as computational fluid dynamics.

In the current study, modeling of pulp flow in the pulp lifter channel by CFD is carried out. The transient multiphase turbulent flow simulations being the primary focus, the flow is simulated using commercial CFD packages, GAMBIT, version 2.4.4, and FLUENT, version 6.3.26. The volume of fluid model is used as the multiphase flow model while the standard k – ε model is used as the turbulence model.

The VOF method is employed for determination of location of the interface between the air and glycerol solution and slurry phases. The VOF formulation applies to models involving two or more immiscible fluids, representing each phase by a volume fraction in the computational cell. In each control volume, the volume fractions of all phases sum to unity.

Momentum transfer by turbulence is modeled by the standard k – ε turbulence model, which solves for the turbulent kinetic energy, k, and the dissipated energy, ε.

The simulation basically consists of preprocessing, processing, and postprocessing stages. First of all, the fluid domain to be studied is described by geometrical operations, called Boolean operations in the top down approach, followed by the geometrical discretization process, referred to meshing in the preprocessing stage.

The case is configured by assigning the models, the material properties, the initial conditions, the boundary conditions, the operating conditions, and the solution controls in

the processing stage; the actual solution is also the part of the processing stage. Finally, the simulation results are viewed and reported via postprocessing tools.

Simulating a large number of pulp lifter channels in the mill would require formidable computational time. Therefore, a simplified yet effective approach is taken up here. It is assumed that a single pulp lifter channel would fill up with slurry nearly to the height of mill charge level as the channel sweeps from the 8 o'clock to 6 o'clock region. Both in radial and curved pulp lifter channels, there is no interaction between adjacent channels. In other words, each channel fills up to a specific volume when it sweeps through the 6 o'clock region and discharges its content as it sweeps through the 3 o'clock to 9 o'clock region. It is also assumed that the flow back volume via grate slots is a small percentage of the total flow out of the channel. To date, there is no theoretical or experimental study conducted on flow back. That being the case, in the current study this flow is neglected and is presumed to be small.

The only flow restriction is the rectangular opening at the central end of the channel as the channel discharges into the discharge trunnion. Thus, the CFD problem becomes one of computing the discharge of an initial volume of fluid in the channel, as the channel makes one single revolution.

The pulp lifter channel receives the inflow of the pulp via grate openings and the pulp outflows from the channel. That means the physical description of the system is to include inflow and outflow boundaries. Practically, there is nothing in the pulp lifter channel as the grinding process commences. However, the proposed model assumes that the pulp flow in the pulp lifter channel can be simulated with only one outlet, specifically pressure outlet, and initial volume filling of the pulp. Further, the fluid is assigned

properties such that it resembles Newtonian characteristics. In the preprocessing stage of the plant scale simulations, utilization of the discrete element method for charge profiles, resulting from the set of design and operating variables characterizing the process specifics, is made. The charge profiles complement the configuration stage, providing the initial pulp depth within the ball and rock mass. In the configuration for the plant scale simulations, the single pulp lifter channel, cut from the original whole mill circle, is located at the 6 o'clock region, and filled to a depth in accordance with the data from DEM code.

Having assigned the material properties, the initial conditions, the boundary conditions, and the solution controls, the simulations are performed for one full revolution, in counterclockwise or clockwise direction. The recorded data files keep track of the slurry free surface profiles and the volume discharged.

3.4. Summary

The data collection strategies both for the dynamic free surface profile experiments and the dynamic discharge profile experiments are explained. The experimental set-ups are introduced, and the experimental procedures as well as the methods utilized, such as solution preparation and viscosity measurements, are explained.

The data on the plant scale mills with details on the design and operating variables are put forward, inclusive of the available literature data and the data for the ArcelorMittal Mont-Wright AG mill. The computational methodology and the CFD packages, namely GAMBIT (version 2.4.4) and FLUENT (version 6.3.26), are introduced. The specifics of the proposed model are stated along with the CFD models and the mathematical principles.

CHAPTER 4

MODELING SLURRY FLOW DYNAMICS IN PULP LIFTER CHANNEL

Chapter 4 comprises an analysis of the mathematical background relating to description of pulp flow in the pulp lifter channel.

The details of the proposed model are introduced, addressing the specific aspects of the computational fluid dynamics methodology. Theoretical discussion of the CFD models, namely the multiphase flow model and turbulence model, is made by way of introducing the governing equations for each.

CFD methodology is illustrated by way of discussing one example case for all the simulations, namely the Dynamic Free Surface Profile simulation, Dynamic Discharge Profile simulation, and Plant Scale simulation.

The fluid pulp rotating inside the mill is mainly subject to gravitational force, centrifugal force, pressure force, and viscous forces. The gravitational force and the centrifugal force are the predominant forces. The force balance is expressed by using Newton's second law of motion, as indicated by Figure 4.1. Newton's second law specifies the force balance on any system in terms of the mass of the system and the net acceleration. The theoretical force balance on the fluid motion as depicted in Figure 4.1 is described by the Navier Stokes equations.

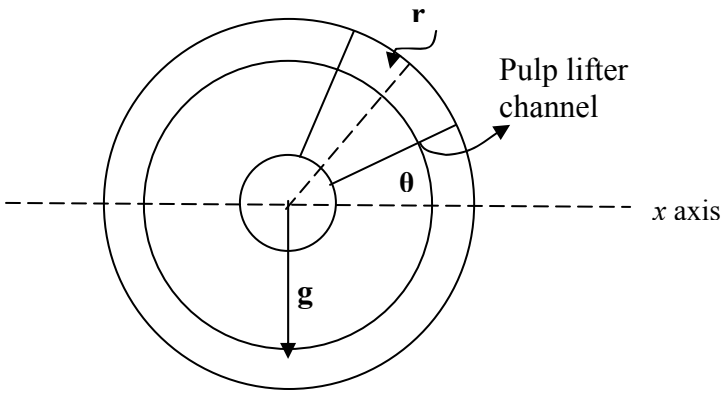

$$F_{NET} = F_{GRAVITATIONAL} + F_{CENTRIFUGAL} + F_{PRESSURE} + F_{VISCOUS}$$

$$\sum F = m \times a_{NET}$$

Figure 4.1 – Theoretical force balance on pulp lifter channel

The Navier Stokes equations are nonlinear partial differential equations, for which the analytical solution is obtained for only simple cases. Therefore, almost always, numerical solution techniques are employed. The set of Navier Stokes equations in the Cartesian coordinate system is given by Equation 4.1 through Equation 4.3 (Bird, Stewart & Lightfoot 2007). The left-hand side of the equations expresses the transient term and the advection terms, which describe the interaction amongst fluid elements, while the right-hand side stands for the pressure term, the diffusion term, and the body forces term.

$$\rho\frac{\partial u}{\partial t} + \rho u\frac{\partial u}{\partial x} + \rho v\frac{\partial u}{\partial y} + \rho w\frac{\partial u}{\partial z} = -\frac{\partial P}{\partial x} + \frac{\partial \tau_{xx}}{\partial x} + \frac{\partial \tau_{xy}}{\partial y} + \frac{\partial \tau_{xz}}{\partial z} \qquad (4.1)$$

$$\rho\frac{\partial v}{\partial t} + \rho u\frac{\partial v}{\partial x} + \rho v\frac{\partial v}{\partial y} + \rho w\frac{\partial v}{\partial z} = -\frac{\partial P}{\partial y} + \frac{\partial \tau_{yx}}{\partial x} + \frac{\partial \tau_{yy}}{\partial y} + \frac{\partial \tau_{yz}}{\partial z} + \rho g \qquad (4.2)$$

$$\rho\frac{\partial w}{\partial t} + \rho u\frac{\partial w}{\partial x} + \rho v\frac{\partial w}{\partial y} + \rho w\frac{\partial w}{\partial z} = -\frac{\partial P}{\partial z} + \frac{\partial \tau_{zx}}{\partial x} + \frac{\partial \tau_{zy}}{\partial y} + \frac{\partial \tau_{zz}}{\partial z} \qquad (4.3)$$

where the shear stresses are given by

$$\tau_{xy} = \tau_{yx} = \mu\left[\frac{\partial u}{\partial y} + \frac{\partial v}{\partial x}\right] \quad \tau_{yz} = \tau_{zy} = \mu\left[\frac{\partial v}{\partial z} + \frac{\partial w}{\partial y}\right] \quad \tau_{xz} = \tau_{zx} = \mu\left[\frac{\partial u}{\partial z} + \frac{\partial w}{\partial x}\right]$$

$$\tau_{xx} = \mu\left[2\frac{\partial u}{\partial y} - \frac{2}{3}\left(\nabla.\vec{\mathrm{v}}\right)\right] \quad \tau_{yy} = \mu\left[2\frac{\partial v}{\partial y} - \frac{2}{3}\left(\nabla.\vec{\mathrm{v}}\right)\right] \quad \tau_{zz} = \mu\left[2\frac{\partial w}{\partial z} - \frac{2}{3}\left(\nabla.\vec{\mathrm{v}}\right)\right]$$

$$\vec{\mathrm{v}} = u\,\vec{i} + v\,\vec{j} + w\,\vec{k}$$

The mass balance for the incompressible fluid is solved for by the continuity equation, given by Equation 4.4.

$$\frac{\partial(u)}{\partial x} + \frac{\partial(v)}{\partial y} + \frac{\partial(w)}{\partial z} = 0 \qquad (4.4)$$

or

$$\nabla.\vec{\mathrm{v}} = 0$$

Considering the equations of motion, represented by the Navier Stokes equations and the continuity equation, the flow dynamics in a rotating channel is studied by numerically solving these equations, characterizing the pulp flow in the pulp lifter channel. The inherent transient multiphase turbulent flow, which is possibly of non-Newtonian nature, is analyzed computationally**.** The computational power required for such computations is challenging, requiring supercomputers.

Therefore, the multiprocessor computing is applied for the computations; moreover, the superposition principle is made use of to integrate over all channels of the system. The superposition principle states that the responses from each independent unit of the system formulate the net response of the system.

The partitioning schemes in FLUENT use bisection algorithms to create the partitions. Creation of equal number of cells for each processor is the main objective (Fluent 6.3 user's guide 2006).

The domain is partitioned into subdomains; the important factors affecting the partitioning are the load balance, the efficient communication among the compute nodes, and the speed. The elements should be evenly distributed so that each processor has equal load. Reducing the time required for the computations has been the primary objective, in the study, in using the multiprocessor computing. The speed-up of calculations is dependent on the efficiency of communication, which in turn is determined by the distribution of original and ghost vertices. In consideration of the stated points, the *Principal Axes* algorithm, which bisects the domain based on a coordinate frame aligned with the principal axes of the domain, has been used in this study.

FLUENT CFD code is employed for the simulations. The computational model uses a typical unstructured mesh of 100,000 volume elements, consisting of hexahedral and quadrilateral cells, for the experimental dynamic free surface profile and dynamic discharge profile simulations (Figure 4.2). The fluid domain is set as moving mesh while moving wall boundary conditions are assigned to walls. Pressure-velocity coupling is handled by Semi implicit for pressure linked equations (SIMPLE) algorithm. Finite volume discretization schemes are used for pressure, volume fraction,

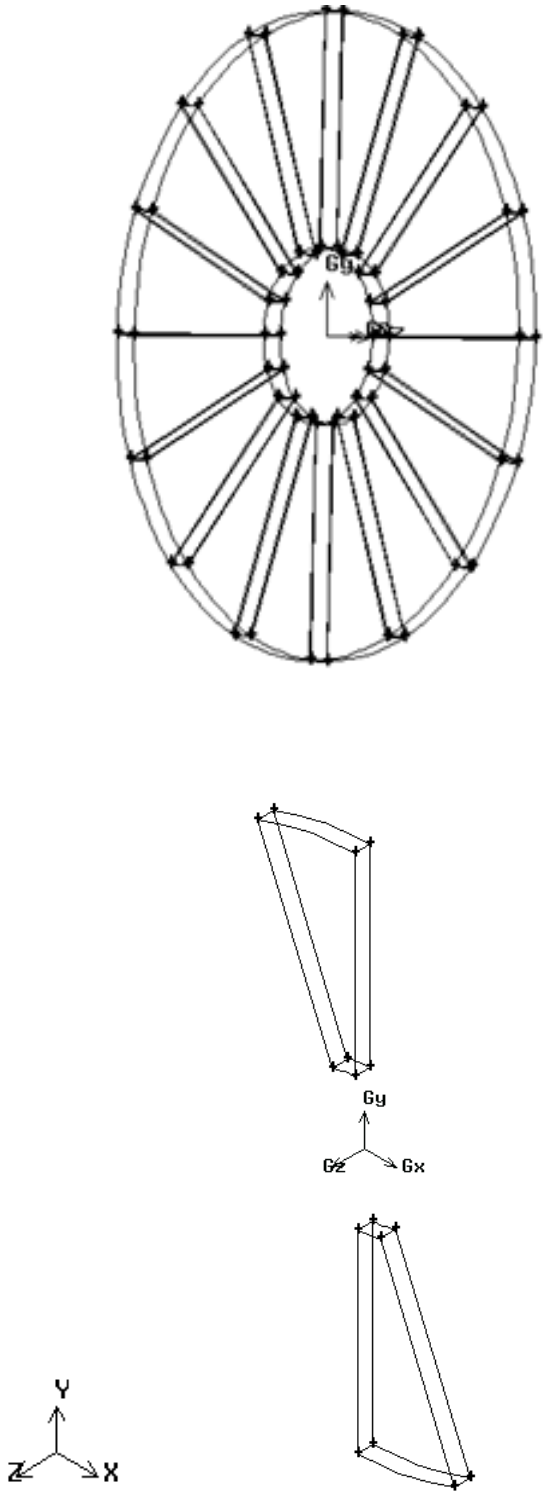

Figure 4.2 – The model geometry of a pair pulp lifter channels

momentum – turbulence. The respective algorithms are (PREssure STaggering Option) PRESTO!, geometric reconstruction (Geo-Reconstruct), and First Order Upwind. The model parameters used for the set-up and solution control parameters, for the experimental dynamic free surface profile and dynamic discharge profile simulations, are given in Table 4.1.

The solution control parameters are set by assigning the discretization algorithms for pressure, pressure-velocity coupling, momentum, volume fraction, turbulence kinetic energy, and turbulence dissipation energy, as given in Table 4.1. The solution is also controlled by underrelaxation parameters which are needed to be set for pressure, momentum, body forces, volume fraction, turbulence kinetic energy, and turbulence dissipation energy.

The underrelaxation parameters stabilize the solution by reducing the oscillations caused by numerical errors. The underrelaxation parameters facilitate updating the values of the variables in the solution, advancing to the next step on the basis of the old values and newly predicted values. In simple terms, the new state of the solution is determined by taking the weighted average of the old values and newly predicted values via underrelaxation parameters. The underrelaxation parameters take values in the range from 0 to 1. Equation 4.5 illustrates the use of underrelaxation parameters for the updated pressure, P, with the value for pressure from the previous step, P^*, the new calculated value of pressure in the current step, P^θ, and the underrelaxation parameter, η.

$$P = P^* + \eta\left(P^\theta - P^*\right) \qquad (4.5)$$

Table 4.1 – Simulation parameters for experimental dynamic free surface profile and dynamic discharge profile

Dynamic Free Surface Profile Experiments			
Multiphase model	Turbulence model	Discretization	Boundary conditions
Volume of Fluid model	k – ε model	Pressure: PRESTO! Pressure-velocity coupling: SIMPLE Momentum: First order upwind Volume fraction: Geo-Reconstruct Turbulence kinetic energy: First order upwind Turbulence dissipation energy: First order upwind	Fluid: Moving mesh Walls: Moving wall (rotational)
Dynamic Discharge Profile Experiments			
Multiphase model	Turbulence model	Discretization	Boundary conditions
Volume of Fluid model	k – ε model	Pressure: PRESTO! Pressure-velocity coupling: SIMPLE Momentum: First order upwind Volume fraction: Geo-Reconstruct Turbulence kinetic energy: First order upwind Turbulence dissipation energy: First order upwind	Fluid: Moving mesh Pressure outlet: Absolute pressure (Pa): 0 Turbulence intensity (%): 5 Turbulence length scale (m): 1×10^{-3} Walls: Moving wall (rotational)

4.1. Theory of Free Surface Flow Modeling

Free surface flow refers to a multiphase flow where the phases are separated by a distinct interface. Specifically, the interface between the gas and liquid phases is designated to move freely due to large density differences between the phases. In other words, there is no constraint on the movement of the gas-liquid interface. Currently, there are two approaches for the numerical calculation of such multiphase flows: Euler-Lagrange approach and Euler-Euler approach.

The Euler-Lagrange approach classifies the phases as continuous and dispersed. Navier Stokes equations are solved for the continuous phase and the calculations on the dispersed phase are performed via force balance. In the Euler-Euler approach, the different phases are treated mathematically as an interpenetrating continuum. The concept of volume fraction of each phase, describing the volume of each single phase in the cell, is introduced. These volume fractions are assumed to be continuous functions of space and time and their sum is equal to 1. Theoretically, in the Eulerian coordinate system, one keeps record of the flowing material with respect to a fixed position while in the Lagrangian coordinate system, one moves with the flowing material.

The volume of fluid model is designed for two or more immiscible fluids where the location of the interface between the fluids is of interest. In the VOF model, a single set of momentum equations is shared by the fluids, and the volume fraction of each of the fluids in each computational cell is traced throughout the domain, via solution of continuity equations for each phase (Fluent 6.3 user's guide 2006). The characteristic continuity equation solved for each phase is given by Equation 4.6.

$$\frac{1}{\rho_a}\left[\frac{\partial(\alpha_a \rho_a)}{\partial t} + \nabla.\left(\alpha_a \rho_a \vec{v}\right)\right] = \frac{1}{\rho_a}\left[S_{\alpha_a} + \sum_{a=1}^{n}\left(\dot{m}_{ab} - \dot{m}_{ba}\right)\right] \qquad (4.6)$$

where

α_a : The volume fraction of each phase, from 1 to n (·)

ρ_a : The density of each phase, from 1 to n ($kg.m^{-3}$)

S_{α_a} : The mass source term for each phase, from 1 to n ($kg.s^{-1}$)

$\dot{m}_{\alpha b}$: The mass transfer term from phase a to phase b ($kg.s^{-1}$)

The mathematical representation of sum of volume fractions resulting from the solution of corresponding continuity equations is given by Equation 4.7.

$$\sum_{a=1}^{n} \alpha_a = 1 \qquad (4.7)$$

The material properties are expressed as volume weighted averages in each cell. For instance, for any property φ, of fluid made up of two phases, is calculated using the volume fractions of each phase (α_1, α_2) in the cell (Equation 4.8).

$$\varphi = \alpha_1 \varphi_1 + \alpha_2 \varphi_2 \qquad (4.8)$$
$$\alpha_1 + \alpha_2 = 1$$

As the cell volume occupied by phases is recorded for each cell, the location of the phase is directly interpreted with reference to cell coordinates. That is, the orientation of the free surface is estimated based on the volume fraction of each phase, as given by Equation 4.6, and the cell volume coordinates.

FLUENT makes use of the Courant number in VOF calculations. The Courant number, *CFL*, is a dimensionless number that compares the incremental time step to the characteristic time it takes the fluid to empty the cell volume (Equation 4.9). The characteristic time is calculated in terms of the Global Courant number and ratio of volume of each cell to the sum of the outgoing fluxes.

$$CFL = \frac{\Delta t}{\Delta x_{cell} / v_{fluid}} \qquad (4.9)$$

The incremental time step used in the volume fraction calculations near the free surface is therefore different from the incremental time step assigned for the general solution. In other words, the incremental time step used in the volume fraction calculations near the free surface is continuously updated throughout the solution. The Courant number is specified as the VOF model is activated for the multiphase flow model. The Courant number used in this study is 0.25, meaning that the incremental time step used near the free surface in VOF calculations is 25% of the characteristic time. In the study, Geo-Reconstruct algorithm has been used for the discretization of volume fraction. The geometric reconstruction scheme specifies the fluid interface using a piecewise linear approach. The piecewise linear approach is one of the well known reconstruction algorithms (Rider and Kothe 1998). FLUENT identifies the piecewise linear approach as accurately applicable for unstructured meshes. The advection of fluid through the cell faces is calculated by the linear slope marking the fluid interface within each cell (Fluent 6.3 user's guide 2006).

Hirt and Nichols (1981) stated that even though both Lagrangian and Eulerian coordinate systems found application in fluid dynamics, Eulerian formulations were better suited to perform calculations involving free surfaces. The VOF model, being an Eulerian formulation, was shown to be simple, yet efficient for treating free boundaries. The relevant literature for a thorough discussion of VOF model includes publications by Sussman and Puckett (2000) and Marek et al. (2008).

4.2. Theory of Turbulence Modeling

Turbulence is characterized by eddies or instabilities; from a fixed reference frame, instabilities are measured as velocity fluctuations about the mean velocity. These fluctuations are represented by Reynolds stresses given by Equation 4.10.

$$\tau = -\rho \overline{u_i' u_j'} \qquad (4.10)$$

The Reynolds stresses are formulated in terms of time average of multiplication of velocity fluctuations, relying on the fact that the time average of multiplied velocity fluctuations is not zero even though the time average of velocity fluctuations is zero. The fluctuations in velocity are denoted by prime notation while the time average is shown by bar notation in Equation 4.10.

The Boussinesq approach, which is the basis of the Reynolds averaged Navier Stokes model, proposes that the transport of momentum by turbulence is a diffusive process and thus that the Reynolds stresses can be modeled using an eddy viscosity which is similar to dynamic viscosity, as given by Equation 4.11.

$$\tau = -\rho \overline{u_i' u_j'} = \mu_T \left(\frac{\partial \bar{u}_i'}{\partial x_j} + \frac{\partial \bar{u}_j'}{\partial x_i} \right) - \frac{2}{3} \left(\rho k + \mu_T \frac{\partial \bar{u}_i'}{\partial x_j} \right) \delta_{ij} \qquad (4.11)$$

The RANS equations govern the transport of the averaged flow quantities, with the whole range of the scales of turbulence being modeled. The equations of motion are averaged in time. The RANS based modeling approach therefore greatly reduces the required computational effort and resources, and is widely adopted for practical engineering applications.

As in the case of single phase flows, the multiphase flow, in other words the free surface flow with a distinct interface between the phases, turbulence is characterized by high Reynolds numbers. The Reynolds number is a dimensionless number quantifying the ratio of inertial forces to viscous forces. Turbulent flows have unsteady and irregular features. The influence of inertia is significant on large eddies as they move through the flow, interacting with other eddies. The viscous effects are dominant on small eddies, being the means of dissipation of turbulent kinetic energy into heat under the effect of viscous resistance.

The standard k – ε model is from the family of RANS model equations. The model introduces two additional transport equations to account for the turbulent properties of the flow. The turbulent kinetic energy is denoted by k and the transport equation for k is as given by Equation 4.12 while Equation 4.13 stands for the transport equation for ε, characterizing the scale of turbulence (Fluent 6.3 user's guide 2006).

$$\rho\frac{\partial k}{\partial t}+\rho(u.\nabla k)=\nabla.\left((\mu+{\mu_T}/{\sigma_k})\nabla k\right)+P_k-\rho\times\varepsilon \qquad (4.12)$$

$$\rho\frac{\partial \varepsilon}{\partial t}+\rho(u.\nabla \varepsilon)=\nabla.\left((\mu+{\mu_T}/{\sigma_\varepsilon})\nabla \varepsilon\right)+C_{1\varepsilon}{\varepsilon}/{k}P_k-C_{2\varepsilon}\rho{\varepsilon^2}/{k} \qquad (4.13)$$

where

$$P_k=-\rho\overline{u_i'u_j'}\frac{\partial u_j}{\partial x_i}$$

The equation defining k is given in terms of turbulence intensity, I (Equation 4.14). The turbulence intensity, Equation 4.15, is defined as the ratio of the root-mean-square of the velocity fluctuations to the mean flow velocity (Fluent 6.3 user's guide 2006). The ratio is expressed in percentages; the turbulence intensity of 1% or less signifies low turbulence while the turbulence intensity of 10% or more is considered high.

$$k=\frac{3}{2}\left(u_{avg}\right)^2 I^2 \qquad (4.14)$$

$$I=\frac{u'}{u_{avg}} \qquad (4.15)$$

The turbulence length scale, *l*, and k are included in the formulation of ε, as given by Equation 4.16. The turbulence length scale gives information about the size of the large eddies which has energy. The equation representing *l* is based on the characteristic length *L* (Equation 4.17).

$$\varepsilon = C_{\mu}^{3/4}\left(k^{1.5}/l\right) \qquad (4.16)$$

$$l = 0.07 \times L \qquad (4.17)$$

The Prandtl number, symbolized by the constants σ_k and σ_ε, defines the ratio of momentum diffusivity to thermal diffusivity for k and ε, respectively. The turbulent viscosity given by Equation 4.18 is formulated in terms of k and ε.

$$\mu_T = \rho C_{\mu} \frac{k^2}{\varepsilon} \qquad (4.18)$$

The default model constants are $C_{1\varepsilon}$ = 1.44, $C_{2\varepsilon}$ = 1.92, C_{μ} = 0.09, σ_k = 1.0, and σ_ε = 1.3. Those constants have been used in the pulp lifter channel flow calculations. The fundamentals of turbulence modeling were covered comprehensively in many publications, some of which include books by Pope (2000), and Fergizer and Peric (2001) explaining the RANS equations and the k – ε model equations in detail. In particular, Wilcox (1998) gave an overview of turbulence modeling in the context of CFD, with particular focus on k – ε model.

4.3. Computational Methodology

In this section, the computational methodology is illustrated with regards to preprocessing, processing, and postprocessing stages. Particularly, the basic procedure for dynamic free surface profile simulations, dynamic discharge profile, with free surface

profiles, simulations, and plant scale simulations are outlined by one example for each. All the simulations are carried out in three dimensions.

The computational geometry used in the simulations of dynamic free surface profile experiments and dynamic discharge profile experiments references the exact pulp lifter channel used in the experiments, as shown in Figure 3.1.

For the plant scale simulations, the computational geometry is a single pulp lifter channel cut from the pulp lifter assembly of the mill, which is based on the information regarding the mill diameter, the trunnion diameter, the pulp lifter channel depth, and the number of pulp lifter channels.

The computations are run using multiprocessors, and due to the fact that the partitioning is case dependent, the case set-up with appropriate models, boundary conditions has been performed on single processor first, and then the saved case file is read into multiprocessors. Then the computational geometry is partitioned using the *Principal Axes* algorithm.

4.3.1 – Dynamic Free Surface Profile Simulations

The preprocessing stage involves use of GAMBIT for the construction and the meshing of the fluid domain. The procedure for dynamic free surface profile simulation for glycerol solution, 75% by volume, of volume filling of 350 cm^3 as the channel rotates at a mill rotational speed of 34 rpm is explained stepwise, as given below:

1. Create the volume resembling the pulp lifter assembly by using cylinder elements centered on the z-axis (Cylinder element (1): Height – 0.03 m, Radius1 – 0.46 m, Cylinder element (2): Height – 0.03 m, Radius1 – 0.125 m). And then subtract Cylinder element (2) from Cylinder element 1.

2. Create a plane intersecting the original volume perpendicularly by using the brick element (Width – 0.0025 m, Depth – 1.25 m, Height – 1.25 m).
3. Copy the created brick element by using the rotate option under *copy/move*. Specify the rotation angle as 22.5˚, and create four copies in the counterclockwise direction. Then select the same brick element again and repeat the copy operation with an angle of -22.5˚ in the clockwise direction.
4. Subtract the resulting volumes from the volume representing the pulp lifter assembly so that the assembly is distinctly divided into sixteen pulp lifter channels (Figure 4.3).
5. Delete the fourteen pulp lifter channel volumes, leaving a vertical symmetric pair around the x-axis. The reason for using a pair of pulp lifter channels for Dynamic Free Surface Profile simulations is the fact the domain is rotating. So as to align the coordinate axes with the moving channel, two symmetric pulp lifter channels around the x-axis are required. Two channels are especially necessary for Dynamic Free Surface Profile simulations since animation is used for postprocessing the results.
6. Under the *Zones* menu, assign the boundary conditions: select all the faces and set the boundary condition as WALL.
7. Under *Mesh* menu, select volume 2 corresponding to the pulp lifter channel above the x-axis, and mesh the volume with mapped mesh of size 0.0015 m. Following that, select volume 1, mesh it with mapped mesh of size 0.004 m.
8. Export the mesh.

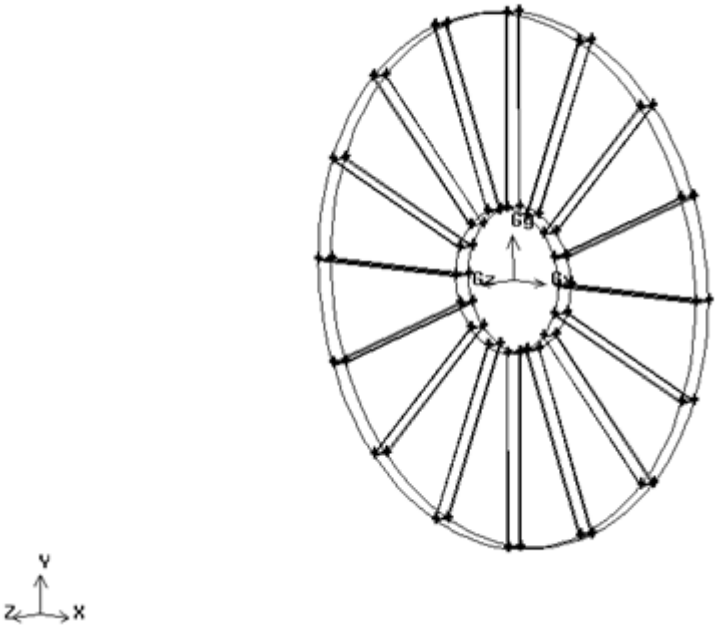

Figure 4.3 – The computational geometric model for pulp lifter assembly with sixteen pulp lifter channels

The processing and postprocessing stages are both performed via use of FLUENT. The case set-up with appropriate models, boundary conditions, solution control parameters, and initiation of the solution are covered in the processing stage.

The procedure in the processing stage for dynamic free surface profile simulation for glycerol solution, 75% by volume, of volume filling of 350 cm^3 as the channel rotates at mill rotational speed of 34 rpm is detailed below:

1. Read the mesh file, check the grid.
2. Define the multiphase flow model as VOF model with two phases. Check the Implicit Force option under Body Force Formulation.

Activating the multiphase flow model sets the solver as unsteady in time automatically.

3. Define the viscous model as k – ε model with default parameters.

4. Define the material properties for the phases: Air with density of 1.225 $kg.m^{-3}$, viscosity of 0.000018 Pa.s. Create a new fluid named "Glycerolsoln" with density of 1183 $kg.m^{-3}$, viscosity of 0.04 Pa.s.
5. Specify Air as the primary phase, and the Glycerolsoln as the secondary phase.
6. Set the component of gravitational acceleration in the y-direction as -9.81 $m.s^{-2}$, under *Operating Conditions*, also check the Specified Operating Density option under Variable-Density Parameters.
7. Define the fluid boundary condition as **"**Moving Mesh**"** with the corresponding mill rotational speed of 34 rpm (3.54 $rad.s^{-1}$).
8. Define the wall boundary condition as **"**Moving Wall**"** on rotational axes.
9. Set the residual monitors and activate plotting. The convergence is determined based on the history of residuals, and the requirement is that the scaled residuals decrease to a certain value. The convergence criterion for continuity, x-velocity, y-velocity, z-velocity, turbulent kinetic energy (k), and turbulent dissipated energy (ε), is set at 0.001 which is the default.
10. Initialize the solution.

Once the solution is initialized, the menus *Adapt* and *Report* are activated.

11. Check the volume of the fluid by using the *Volume Integrals* submenu under the *Report* menu.
12. Mark a fluid volume equivalent to 350 cm^3 by using the *Region* submenu under the *Adapt* menu, on the upper pulp lifter channel.

13. Patch the marked volume with glycerol solution (75% by volume). The patched volume is checked via the *Report* menu using the volume integral option for phases (Air and Glycerolsoln) in the *Volume Integrals* submenu.
14. Check the set-up via the *Case Check* submenu under the *Solve* menu.
15. Assign the incremental time step as 0.00025 s.

The underrelaxation parameters for pressure, density, body forces, momentum, turbulent kinetic energy (k), turbulent dissipated energy (ε), and turbulent viscosity, respectively, are 0.3, 1, 1, 0.7, 0.8, 0.8, and 1.

16. Save the case file and close the program.
17. Start FLUENT in three dimensions with two processors by using *File* menu.
18. Read the case file, and then initialize the solution.

Figure 4.4 shows the partitioning of the pulp lifter channel volume above the x-axis, where the phase Glycerolsoln is patched.

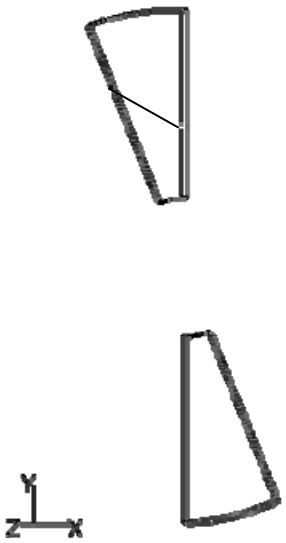

Figure 4.4 – The partitioned pulp lifter channel volume in the Dynamic Free Surface Profile Computations

19. Mark a fluid volume equivalent to 350 cm^3 again, and patch the volume with Glycerolsoln.
20. Set the animation for the volume fraction of the Glycerolsoln phase, which is used as means of postprocessing the results for dynamic free surface simulations. Define the animation sequences using the time steps option for contours of volume fraction of Glycerolsoln phase on a new window, through the *Animation* submenu under the *Solve* menu.
21. Run the iterations for 7100 time steps, corresponding to one full revolution of the pulp lifter channel rotating at 34 rpm.

Figure 4.5 presents a sample contour plot for volume fractions of air, shown by blue, and glycerol solution, shown by red, at the 3 o'clock region. For this particular sample scene, the glycerol solution used is at a concentration of 75% by volume and the volume filling of the glycerol solution is 350 cm^3. That is to say, the volumes occupied by glycerol solution and air phases are 350 cm^3 and 950 cm^3 respectively; these volumes remain constant throughout the simulation as there is no inflow or outflow from the channel. The free surface profiles demonstrate the resulting shape profile of the glycerol solution in the channel as a result of the effective force field.

The free surface profile at the particular location, 3 o'clock region, is obtained as the mill rotates at 34 rpm in the clockwise direction.

The results are qualitative in nature; the comparison of the free surface profiles on a one-on-one basis is the tool for assessing the conformity of the simulation results to that of experimental results. The CPU time required for the simulation is approximately 30 hours in comparison to 15 hours in wall clock time.

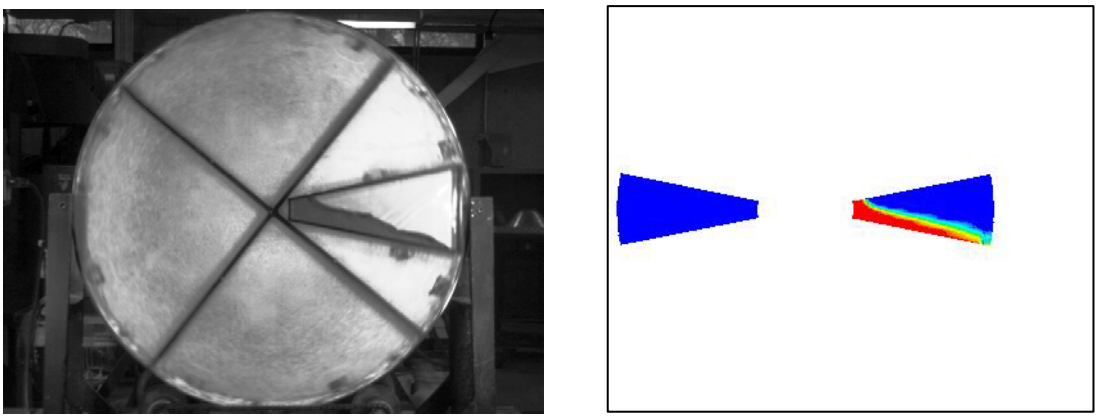

Figure 4.5 – The sample contour plot of volume fractions of glycerol solution and air at 3 o'clock region, displaying the alignment of the volume of glycerol solution in the channel

The animation is recorded on files with .cxa, .hmf extensions. Once the simulation is completed, the file with extension .cxa is read through *Animation* menu; it is played by using the FLUENT player, and also the successive views are recorded on the files with extension .hmf. These files can be hardcopied in JPEG format.

4.3.2 – Dynamic Discharge Profiles Simulations

The procedure for the dynamic discharge profile simulation for glycerol solution, 85% by volume, of volume filling of 350 cm^3 as the channel rotates at a mill rotational speed of 26.2 rpm is explained stepwise, as given below:

1. Create the volume resembling the pulp lifter assembly by using cylinder elements centered on the z-axis (Cylinder element (1): Height – 0.03 m, Radius1 – 0.46 m, Cylinder element (2): Height – 0.03 m, Radius1 – 0.125 m). And then subtract Cylinder element (2) from Cylinder element 1.
2. Create a plane intersecting the original volume perpendicularly by using a brick element (Width – 0.0025 m, Depth – 1.25 m, Height – 1.25 m).

3. Copy the created brick element by using the rotate option under *copy/move*. Specify the rotation angle as 22.5˚, and create four copies in the counterclockwise direction. Then select the same brick element again and repeat the copy operation with an angle of -22.5˚ in the clockwise direction.
4. Subtract the resulting volumes from the volume representing the pulp lifter assembly so that the assembly is distinctly divided into sixteen pulp lifter channels.
5. Delete the fourteen pulp lifter channel volumes, leaving a vertical symmetric pair around x-axis. The reason for using a pair of pulp lifter channels for Dynamic Free Surface Profile simulations is the fact the domain is rotating. So as to align the coordinate axes with the channel changing location, two symmetric pulp lifter channels around the x-axis are required.
6. Split the frontal face of the lower pulp lifter channel such that an area of 0.00016 m^2, corresponding to area covered by two-1 cm holes, is marked.
7. Under the *Zones* menu, assign the boundary conditions: select the frontal face area marked and set the boundary condition as PRESSURE OUTLET. The boundary condition for all the other faces is set as WALL.
8. Under the *Mesh* menu, select volume 1 corresponding to the pulp lifter channel below the x-axis, and mesh the volume with mapped mesh of size 0.00225 m. Following that, select volume 2, and mesh it with mapped mesh of size 0.0025 m.
9. Export the mesh.

The procedure in the processing stage for the dynamic discharge profile simulation for glycerol solution, 85% by volume, of volume filling of 350 cm^3 as the channel rotates at mill rotational speed of 26.2 rpm is detailed below:

10. Read the mesh file, check the grid.
11. Define the multiphase flow model as VOF model with two phases. Check the Implicit Force option under Body Force Formulation.

Activating the multiphase flow model sets the solver as unsteady in time automatically.

12. Define the viscous model as k – ε model with default parameters.
13. Define material properties for the phases: Air with density of 1.225 $kg.m^{-3}$, viscosity of 0.000018 Pa.s. Create a new fluid named "Glycerolsoln" with density of 1220 $kg.m^{-3}$, viscosity of 0.061 Pa.s.
14. Specify Air as the primary phase, and the Glycerolsoln as the secondary phase.
15. Set the component of gravitational acceleration in the y-direction as -9.81 $m.s^{-2}$, under *Operating Conditions*, also check Specified Operating Density under Variable-Density Parameters.
16. Define the fluid boundary condition as **"**Moving Mesh**"** with the corresponding mill rotational speed of 26.2 rpm (2.725 $rad.s^{-1}$).
17. Set the absolute pressure to 0 Pa at the pressure outlet boundary as means of satisfying the free surface boundary condition. Specify the turbulence parameters at outlet boundary condition using turbulence intensity (5%) and turbulence length scale (0.001 m).
18. Define the wall boundary condition as **"**Moving Wall**"** on rotational axes.

19. Set the residual monitors and activate plotting. The convergence is determined based on the history of residuals, and the requirement is that the scaled residuals behave the same for the last 30,000 time steps of the solution. The convergence criterion for continuity, x-velocity, y-velocity, z-velocity, turbulent kinetic energy (k), and turbulent dissipated energy (ε), is set at 0.001 which is the default.
20. Initialize the solution.

Once the solution is initialized, the menus *Adapt* and *Report* are activated.

21. Check the volume of the fluid by using the *Volume Integrals* submenu under the *Report* menu; also check the area of the outlet through the *Surface Integrals* submenu under the *Report* menu.
22. Mark a fluid volume equivalent to 350 cm^3 by using the *Region* submenu under the *Adapt* menu.
23. Patch the marked volume with glycerol solution (85% by volume). The patched volume is checked via the *Report* menu using the volume integral option for phases (Air and Glycerolsoln) in the *Volume Integrals* submenu.
24. Check the set-up via the *Case Check* submenu under the *Solve* menu.
25. Assign the incremental time step as 0.00001 s.

The underrelaxation parameters for pressure, density, body forces, momentum, turbulent kinetic energy (k), turbulent dissipated energy (ε), and turbulent viscosity, respectively, are 0.3, 1, 1, 0.7, 0.8, 0.8, and 1. The underrelaxation parameter for pressure is reduced to 0.2 for 10,000 – 12,000 time steps around the 12 o'clock region, as judged by the behavior of residuals.

26. Save the case file and close the program.

27. Start FLUENT in three dimensions with two processors by using *File* menu.
28. Read the case file, and then initialize the solution.

Figure 4.6 shows the partitioning of the pulp lifter channel volume below the x-axis, where the phase Glycerolsoln is patched.

29. Under File menu, set the number of time steps for autosave as 14,300 so that the case and data files are saved every 14,300 time steps. The number of time steps specified for autosave corresponds to each sweep of the pulp lifter channel volume, and is determined by taking into consideration the mill rotational speed and number of pulp lifter channels.
30. Mark a fluid volume equivalent to 350 cm^3 again, and patch the volume with Glycerolsoln.
31. Run the iterations for 229,000 time steps, corresponding to one full revolution of the pulp lifter channel rotating at 26.2 rpm.

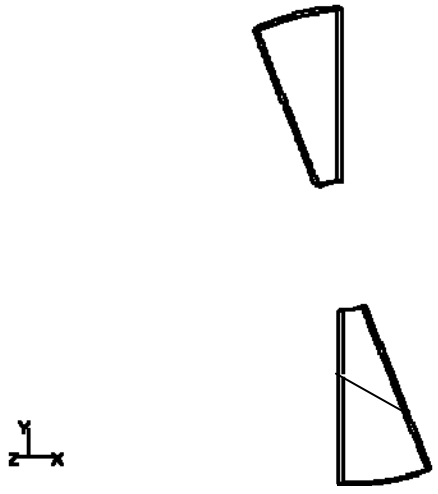

Figure 4.6 - The partitioned pulp lifter channel volume in the Dynamic Discharge Profile Computations

Once the pulp lifter channel passes over the horizontal line at the 9 o'clock location, the discharge from the pulp lifter channel stops. That is, the iterations beyond the horizontal line are conducted to ensure the convergence of the solution as well as to record the free surface profiles in the 9 o'clock – 6 o'clock region.

32. Once the simulation is complete, postprocess the results using volume fraction contour plots by the *Contours* submenu under the *Display* menu and record the remaining volume of glycerol solution for every 0.143 seconds. The volume reports are obtained via the *Report* menu using the volume integral option for Glycerolsoln phase in the *Volume Integrals* submenu.

Figure 4.7 presents a sample free surface profile at the 9 o'clock region as the volume of glycerol solution discharges from the channel rotating at 26.2 rpm. The volume fractions of air, shown by blue, and glycerol solution, shown by red, at the 9 o'clock region are illustrated. The initial volume filling of glycerol solution is 350 cm^3 (85% by volume), and the mill rotates at 26.2 rpm in the counterclockwise direction.

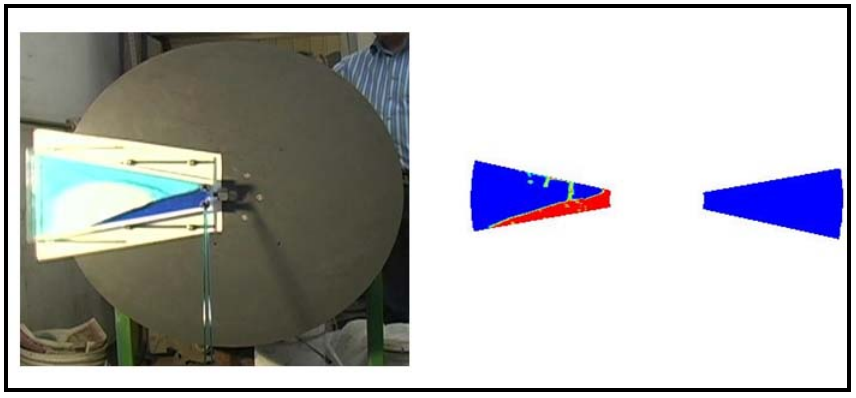

Figure 4.7 - The sample contour plot of volume fractions of glycerol solution and air at 9 o'clock region, displaying the alignment of the volume of glycerol solution in the channel

The results are both qualitative and quantitative in nature. Qualitatively, the free surface profiles obtained by the simulations are compared to that of the experimental results. The results for volume discharged are also analyzed quantitatively as the volume reports obtained from the simulations are compared with the values recorded in the experiments. For instance, the volume report of the simulation for the case shown in Figure 4.7 indicates a volume discharge of 64 cm^3, at the 9 o'clock region, while the experimental record indicates a volume discharge of 65 cm^3. The CPU time required for the simulation is approximately 96 hours in comparison to 48 hours in wall clock time.

The detailed variations of the discharge experiments along with accompanying simulations are presented in Chapter 5, under section 5.2 titled *Dynamic Discharge Experiments*. Specifically, there are twenty sets of results for which the mill rotational speed, the volume filling of glycerol solution, and solution viscosity have been varied.

4.3.3 – Plant Scale Simulations

The procedure for plant scale simulation for the Los Bronces SAG mill, in which a single pulp lifter channel has a volume of 1.1 m^3, with volume filling of 0.44 m^3, as the mill rotates at 10 rpm is explained stepwise, as given below:

1. Create the volume resembling the pulp lifter assembly by using cylinder elements centered on the z-axis (Cylinder element (1): Height – 0.464 m, Radius1 – 5.06 m, Cylinder element (2): Height – 0.464 m, Radius1 – 1.1 m). And then subtract Cylinder element (2) from Cylinder element 1.
2. Create a plane intersecting the original volume perpendicularly by using a brick element (Width – 0.0025 m, Depth – 12 m, Height – 12 m).

3. Copy the created brick element by using the rotate option under *copy/move*. Specify the rotation angle as 11.25˚, and create eight copies in the counterclockwise direction. Then select the same brick element again and repeat the copy operation with an angle of -11.25˚ in the clockwise direction.
4. Subtract the resulting volumes from the volume representing the pulp lifter assembly so that the assembly is distinctly divided into thirty-two pulp lifter channels (Figure 4.8).

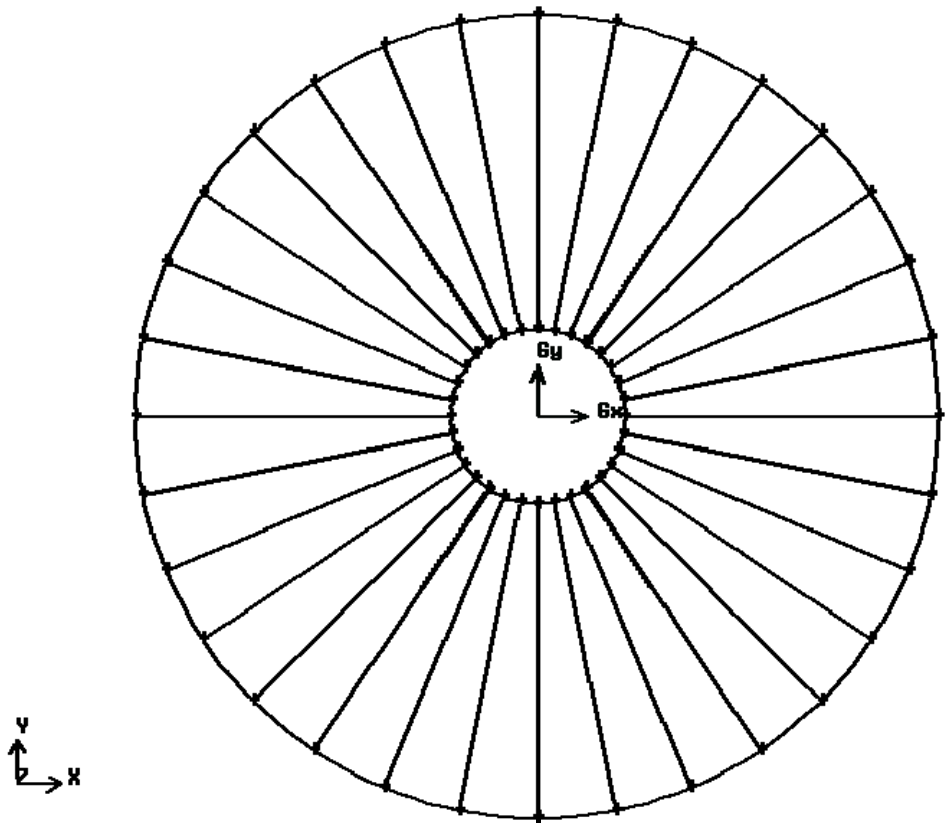

Figure 4.8 – The computational geometric model for the Los Bronces SAG mill with thirty-two pulp lifter channels (Diameter 10.12 m and length 4.722 m)

5. Overlay the DEM charge profile and circle representing the pulp lifter assembly, as seen in Figure 4.9. By that way, approximate volume filling of slurry is estimated.
6. Delete the thirty-one pulp lifter channel volumes, leaving only one channel at around the 7 o'clock location to be filled up to approximately 40% of the pulp lifter channel volume with slurry.
7. Under the *Zones* menu, assign the boundary conditions, select the face, marked red in Figure 4.10, and set the boundary condition as PRESSURE OUTLET. The boundary condition for all the other faces is set as WALL.

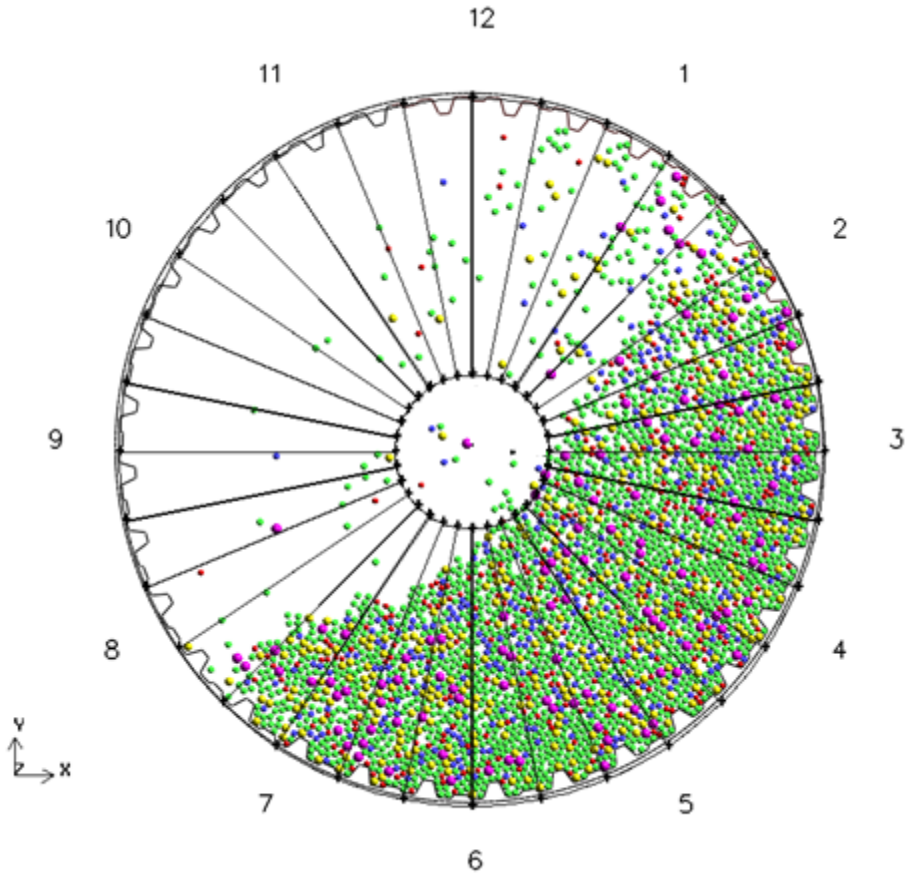

Figure 4.9 – The mill circle overlaid on DEM charge profile, Los Bronces SAG mill (Diameter 10.12 m and length 4.722 m)

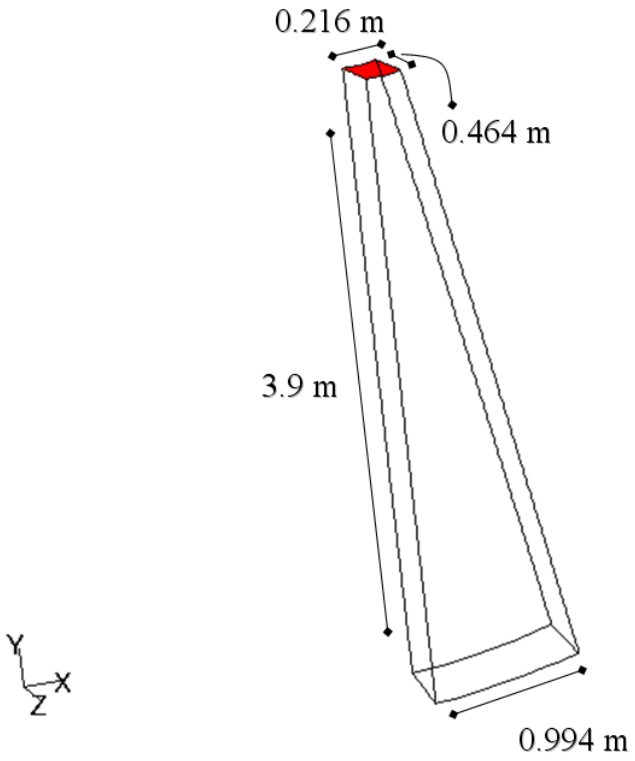

Figure 4.10 – The computational geometry for single pulp lifter channel of the Los Bronces SAG mill, with outlet boundary marked in red

8. Under the *Mesh* menu, mesh the volume with mapped mesh of size 0.01 m. Export the mesh.

The procedure employed in the processing stage for the Los Bronces SAG mill simulation is detailed below:

1. Read the mesh file, check the grid.
2. Define the multiphase flow model as VOF model with two phases. Check the Implicit Force option under Body Force Formulation
3. Define the viscous model as k – ε model with default parameters.

4. Define material properties for the phases: Air with density of 1.225 $kg.m^{-3}$, viscosity of 0.000018 Pa.s. Create a new fluid named "Slurry" with density of 1700 $kg.m^{-3}$, viscosity of 0.1Pa.s.
5. Specify Air as the primary phase, and the Slurry as the secondary phase.
6. Set the component of gravitational acceleration in the y-direction as -9.81 $m.s^{-2}$, under *Operating Conditions*, also check Specified Operating Density under Variable-Density Parameters.
7. Define the fluid boundary condition as "Moving Mesh" with the corresponding mill rotational speed of 10 rpm (1.04 $rad.s^{-1}$).
8. Set the absolute pressure to 0 Pa at the pressure outlet boundary as means of satisfying the free surface boundary condition. Specify the turbulence parameters at outlet boundary condition using turbulence intensity (5%) and turbulence length scale (0.03 m).
9. Define the wall boundary condition as **"**Moving Wall**"** on rotational axes.
10. Set the residual monitors and activate plotting. The convergence is determined based on the history of residuals, and the requirement is that the scaled residuals behave the same for the last 50,000 time steps of the solution. The convergence criterion for continuity, x-velocity, y-velocity, z-velocity, turbulent kinetic energy (k), and turbulent dissipated energy (ε), is set at 0.001 which is the default.
11. Initialize the solution.

12. Check the volume of the fluid by using the *Volume Integrals* submenu under the *Report* menu; also check the area of the outlet through the *Surface Integrals* submenu under the *Report* menu.
13. Mark a fluid volume equivalent to 0.44 m^3 by using the *Region* submenu under the *Adapt* menu.
14. Patch the marked volume with slurry. The patched volume is checked via the *Report* menu using the volume integral option for phases (Air and Slurry) in the *Volume Integrals* submenu.
15. Check the set-up via the *Case Check* submenu under the *Solve* menu.
16. Assign the incremental time step as 0.00001 s.

The underrelaxation parameters for pressure, density, body forces, momentum, turbulent kinetic energy (k), turbulent dissipated energy (ε), and turbulent viscosity, respectively, are 0.3, 1, 1, 0.7, 0.8, 0.8, and 1. The underrelaxation parameter for pressure is reduced to 0.2 for 10,000 – 20,000 time steps around the 12 o'clock region, as judged by the behavior of residuals.

17. Save the case file and close the program.
18. Start FLUENT in three dimensions with four processors by using *File* menu.
19. Read the case file, and then initialize the solution.
20. Under the *File* menu, set the number of time steps for autosave as 18,750 so that the case and data files are saved every 18,750 time steps. The number of time steps specified for autosave corresponds to each sweep of the pulp lifter channel volume, and is determined by taking into consideration the mill rotational speed and number of pulp lifter channels.

Figure 4.11 shows the partitioning of the pulp lifter channel volume for the Los Bronces SAG mill.

21. Mark a fluid volume equivalent to 0.44 m^3 again, and patch the volume with Slurry.
22. Run the iterations for 600,000 time steps, corresponding to one full revolution of the pulp lifter channel rotating at 10 rpm. Once the pulp lifter channel passes over the horizontal line at the 9 o'clock location, the discharge from the pulp lifter channel stops. That is, the iterations beyond the horizontal line are conducted to ensure the convergence of the solution as well as to record the free surface profiles in the 9 o'clock – 6 o'clock region.
23. Once the simulation is complete, postprocess the results using volume fraction contour plots by the *Contours* submenu under the *Display* menu and record the remaining volume of glycerol solution for every 0.1875 seconds.

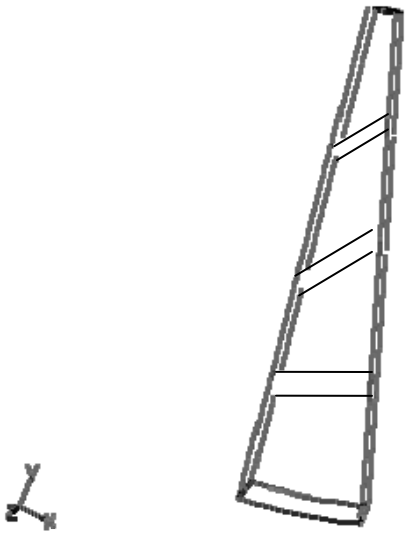

Figure 4.11 - The partitioned pulp lifter channel volume of the Los Bronces SAG mill

The volume reports are obtained via *Report* menu using the volume integral option for Slurry phase in the *Volume Integrals* submenu.

Figure 4.12 presents the free surface profiles of slurry on the mill circle as the volume of slurry discharges from the channel rotating at 10 rpm. The volume fractions of air, shown by blue, and slurry, shown by red, are illustrated. The initial volume filling slurry is 0.44 m^3, and the mill rotates at 10 rpm in the counterclockwise direction. The percent readings on the circle indicate the percent volume of the slurry remaining in the pulp lifter channel as the slurry discharges from the channel. The CPU time required for the simulation is 288 – 384 hours in comparison to 72 – 96 hours in wall clock time.

The results are quantitative in nature in the sense that the volumetric flow rates calculated based on the simulation results are compared to volumetric flow rates given by the survey data (Powell & Valery 2006). For the case shown in Figure 4.12, the volumetric flow rate is 1152 $m^3.h^{-1}$ based on the simulation results as compared to 1322 $m^3.h^{-1}$ on basis of the survey data. The CPU time required for the simulation is approximately 96 hours in comparison to 48 hours in wall clock time.

Chapter 6 presents the results for plant scale simulations, providing the comparisons of volumetric flow rates and solids flow rates in a tabular format. Specifically, there are nine sets of results for which the design and operating conditions are dictated by the survey data as given in Table 3.4 (Powell & Valery 2006).

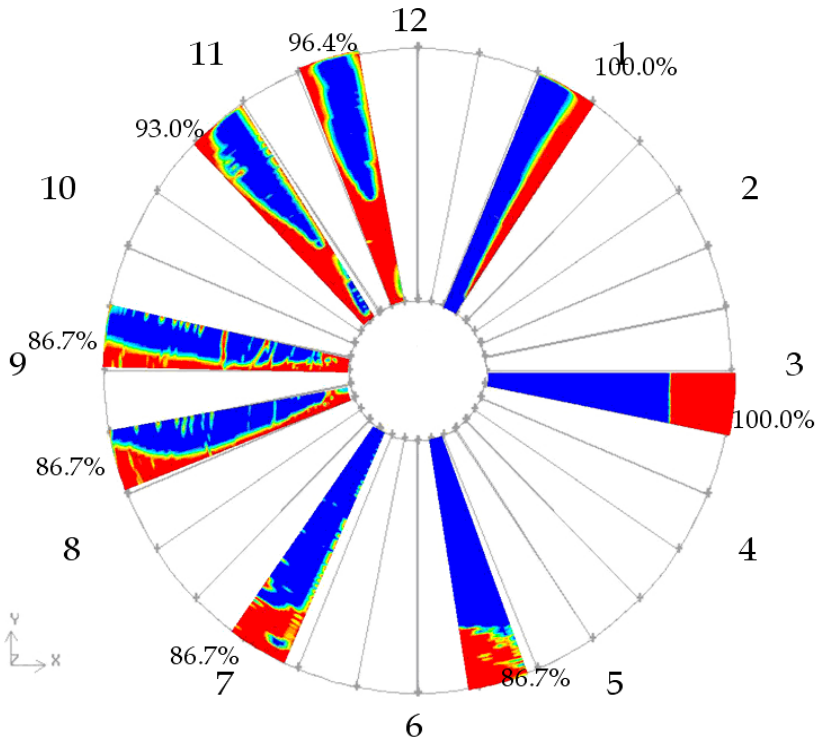

Figure 4.12 – The CFD prediction of free surface profiles, Los Bronces SAG mill (Diameter 10.12 m and length 4.722 m)

4.4. Summary

The mathematical background for governing equations describing the pulp flow in the pulp lifter channel has been provided in the current chapter. The computational methodology is introduced. The principle CFD models employed have been discussed theoretically.

The VOF model is presented as the multiphase flow model in the context of free surface modeling while the standard k – ε model is presented as the turbulence model. The model equations solved for the volume fraction in order to determine the location of the interface between the phases are explained. The standard k – ε model, from RANS family models, is delineated by giving the formulations for the turbulent kinetic energy and the dissipated energy.

Moreover, the computational methodology for dynamic free surface profile simulations, dynamic discharge profile simulations, and plant scale simulations are outlined by one example for each.

The simulation results concerning the experimental part of the study are both qualitative and quantitative. The results for the free surface profiles are qualitative in the sense that the free surface profiles obtained by the simulations are compared to that of the experimental results. The results for the discharge profiles are both qualitative and quantitative. The free surface profiles obtained by the simulations are compared to that of experimental profiles, as the channel discharges. The results for volume discharged are also analyzed quantitatively as the volume reports obtained from the simulations are compared to the values recorded by the experimental results.

The plant scale simulation results are quantitative in nature in the sense that the volumetric flow rates calculated based on the simulation results are compared to volumetric flow rates given by survey data (Powell & Valery 2006).

CHAPTER 5

RESULTS AND DISCUSSION

In the current chapter, the experimental results and computational fluid dynamics simulation results obtained for the dynamic free surface profiles and the dynamic discharge profiles are compared while the variables mill rotational speed, volume filling, and solution viscosity are changed. The accuracy of the model predictions is examined based on the conformity of the simulation results to the experimental results. The objective is to assess whether the model predicts the experimental results reasonably well.

5.1. Dynamic Free Surface Profile Experiments

There are forty-eight sets of experiments for dynamic free surface profiles along with the corresponding simulation results for each. Out of those, only twelve sets of the results are presented here in order to illustrate the effects of mill rotational speeds and glycerol solution concentrations on flow dynamics. More of the results are provided in Appendix A. The colormap in FLUENT signifies the maximum by red, and the minimum by blue. Other values, covered in the range between the maximum and the minimum, are interpolated and shown by different colors. The number of colors selected determines the size of the colormap (Fluent 6.3 user's guide 2006).

Figure 5.1 shows the contours of volume fraction of glycerol solution with only two colors selected in the colormap and with twenty colors selected in the colormap, for glycerol solution 85% by volume. As seen from Figure 5.1, there is no variation in color on the profile with only two colors selected in the colormap; that is, the color variation observed when twenty colors are selected in the colormap is due to the interpolation FLUENT applies. Therefore, red and blue colors used in the presentation of results solely signify the maximum and the minimum values, specifically 1 for the glycerol solution phase and the slurry phase and 0 for the air phase.

The clock circle overlaid on the mill circle, referred to in the discussions and the color legend representing the contours of volume fraction, are shown in Figure 5.2.

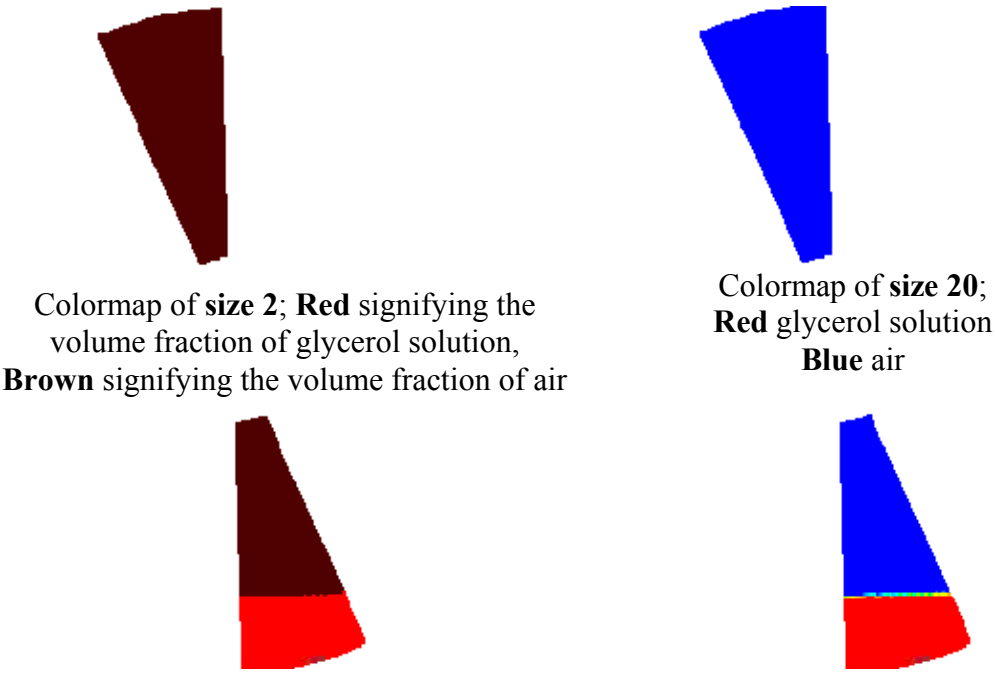

Figure 5.1 – The designation of effect of colormap size, the contours of volume fraction of glycerol solution (85% by volume) with volume filling of 500 cm^3 at 29 rpm

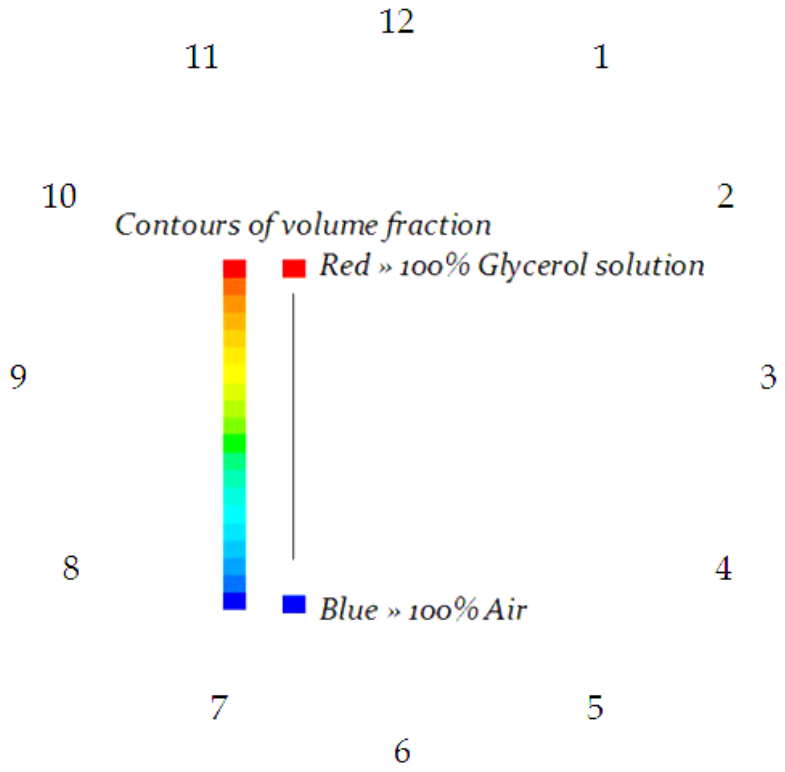

Figure 5.2 – Mill – Clock circle analogy and color legend representing the volume fraction of phases

Figure 5.3 through Figure 5.6 show the captured dynamic free surface profiles of glycerol solution at different mill rotational speeds expressed in revolutions per minute, respectively, as 11.7 rpm, 18.4 rpm, 26.2 rpm, and 34 rpm. The free surface profiles are well captured by CFD predictions. The forces acting on the fluid are centrifugal force, gravitational force, viscous forces, and pressure force. However, the centrifugal force and gravitational force have more significance on the flow behavior.

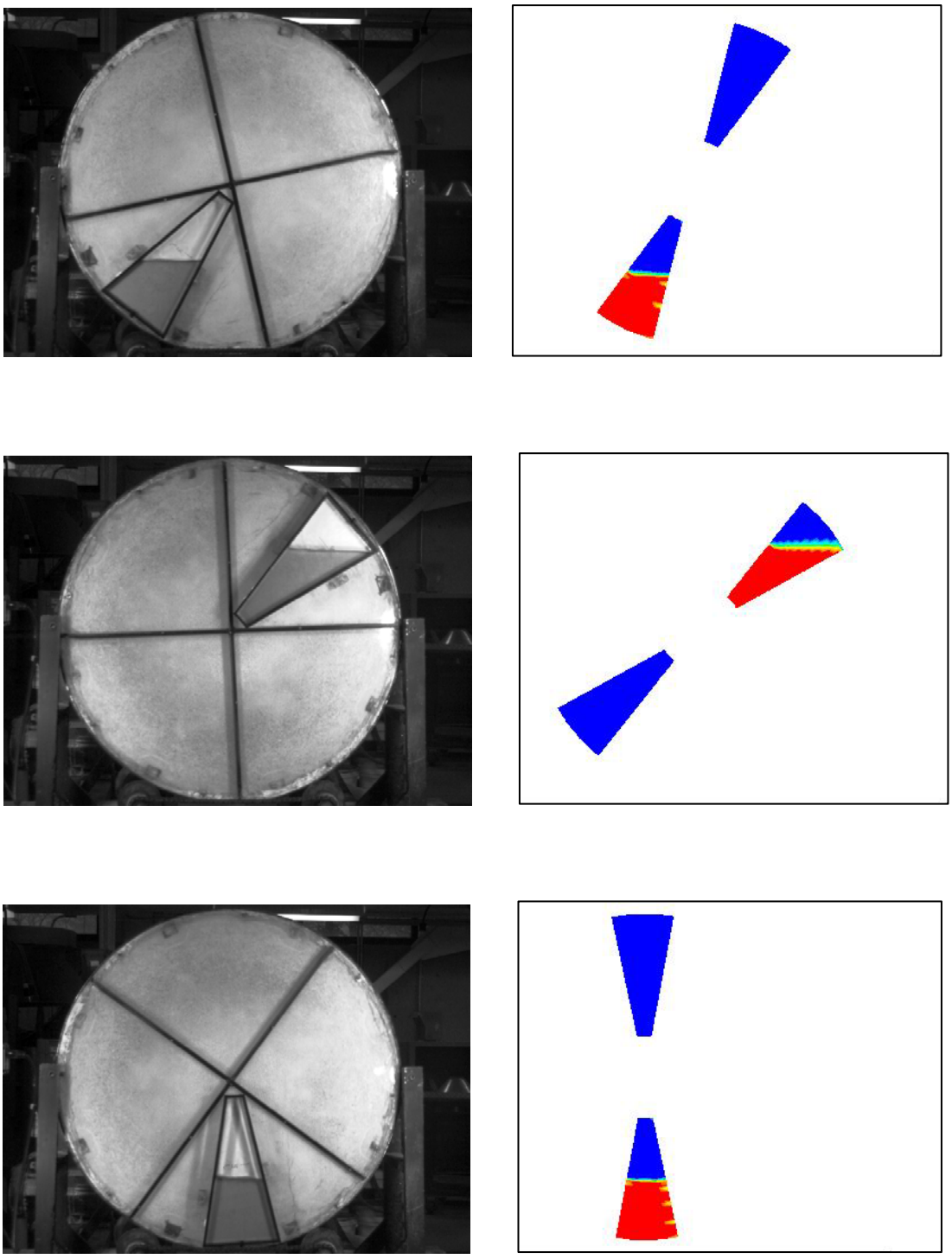

Figure 5.3 – Experimental and CFD free surface profiles glycerol solution (65% by volume) with volume filling of 800 cm^3 (61.5% of channel volume) at 11.7 rpm

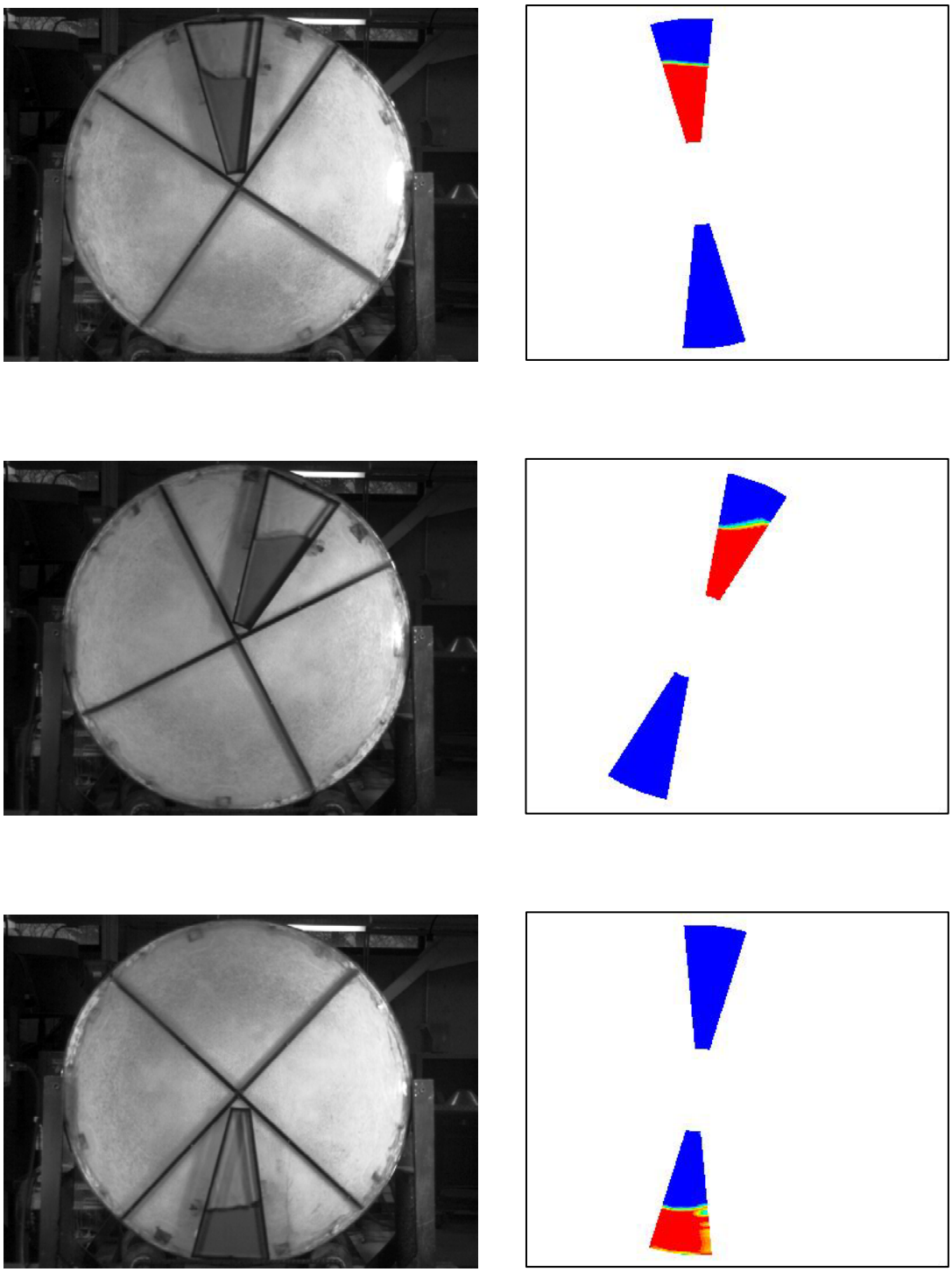

Figure 5.4 – Experimental and CFD free surface profiles for glycerol solution (75% by volume) with volume filling of 650 cm^3 (50% of channel volume) at 18.4 rpm

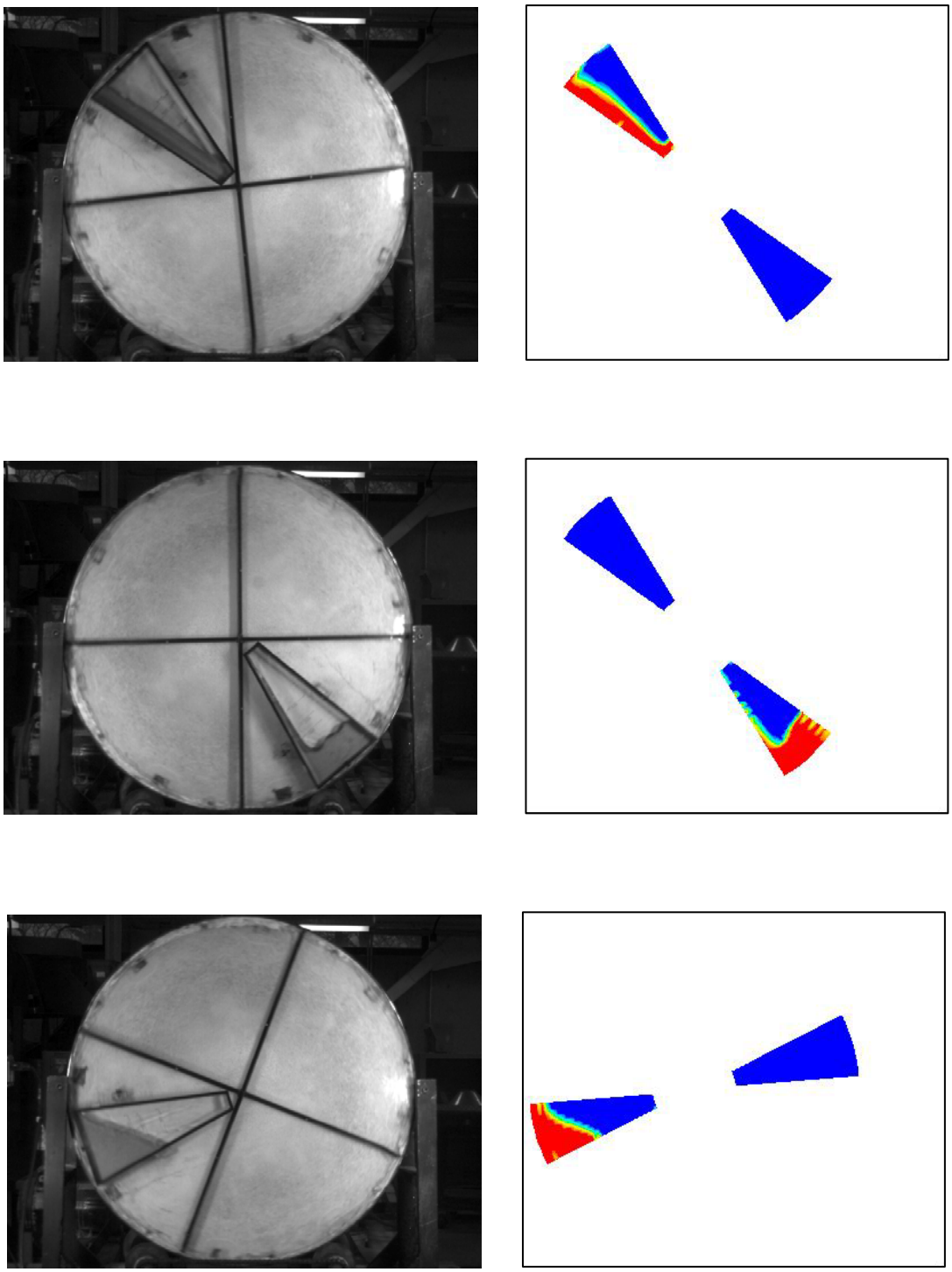

Figure 5.5 – Experimental and CFD free surface profiles for glycerol solution (70% by volume) with volume filling of 500 cm^3 (38.5% of channel volume) at 26.2 rpm

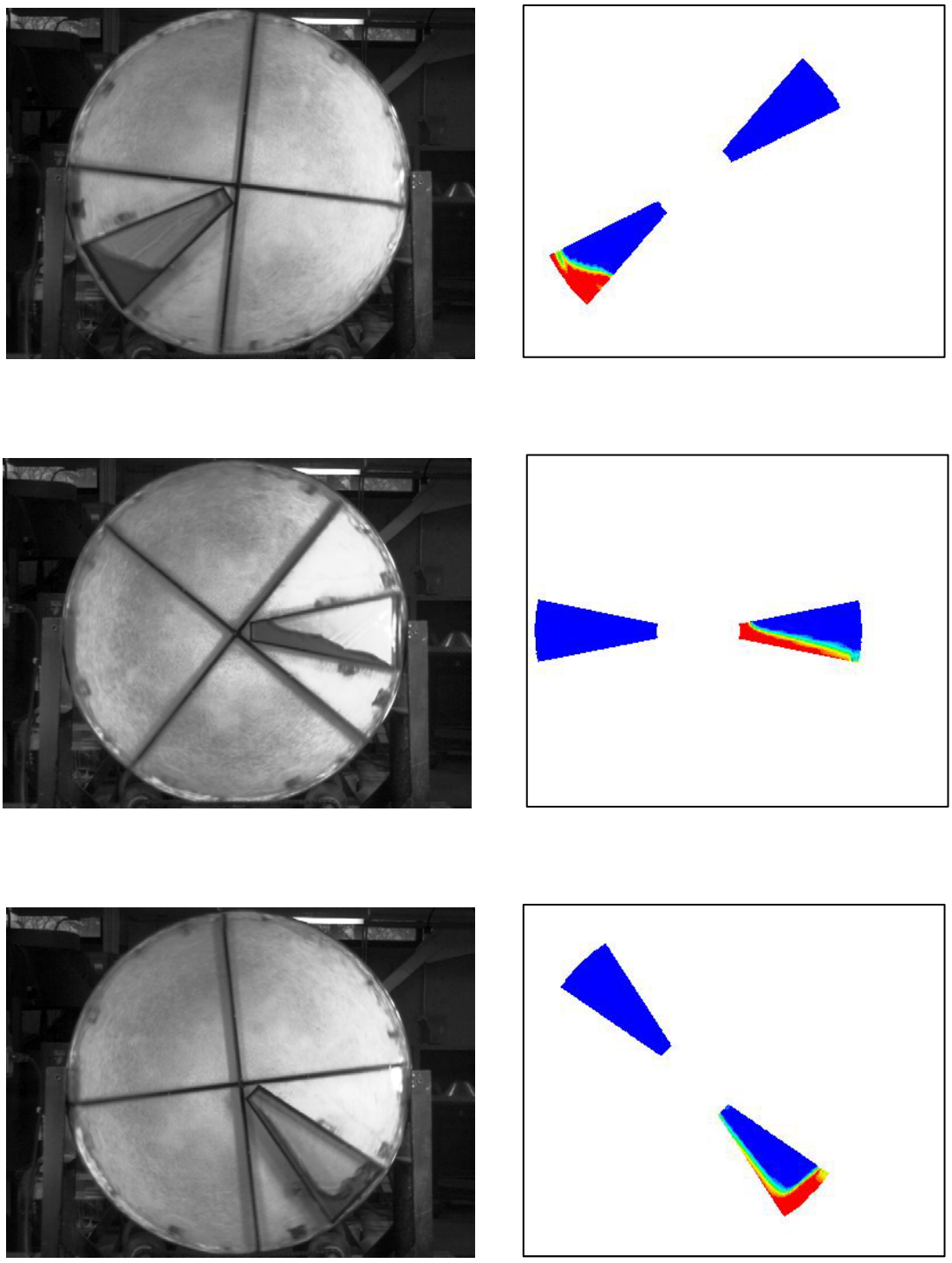

Figure 5.6 – Experimental and CFD free surface profiles for glycerol solution (75% by volume) with volume filling of 350 cm^3 (27% of channel volume) at 34 rpm

Generally, the free surface profiles at 6 o'clock and 12 o'clock regions are flat, under the effect of centrifugal and gravitational force and centrifugal force, respectively. On the upper half of the mill circle, the centrifugal force draws the fluid outwards while the gravitational force acts in the inward direction, resulting in a net force either centrifuge or gravity dominant, whereas both centrifugal force and gravitational force act in the same direction on the lower half of the mill circle, pushing the fluid outward. Hence, at around the 4 o'clock – 8 o'clock regions the fluid figuratively adheres to the channel walls. At the 3 o'clock and 9 o'clock regions, the gravitational force in the radial direction is zero and the free surface profile is predominantly controlled by the centrifugal force.

The effect of mill rotational speed is detailed in Figure 5.7 and Figure 5.8. It is readily seen that as the mill rotational speed increases, the centrifugal force increases, hence the fluid is pinned to channel walls.

Principally, the fluid takes the shape of the container in which it is enclosed. Therefore, the shape of the pulp lifter channel and the volume of the fluid relative to that of the pulp lifter channel determine the available flow space, the area through which the fluid can flow freely. The volume fillings of 800 cm^3 (61.5% of the channel volume) and 350 cm^3 (27% of the channel volume) are compared in Figure 5.9 and Figure 5.10, at the same mill rotational speed. The comparison shows that as the volume filling increases, the fluid becomes more restricted, particularly due to the shape of the channel. Moreover, the lesser volume filling has a counterbalancing effect on the force field, giving smoother profiles.

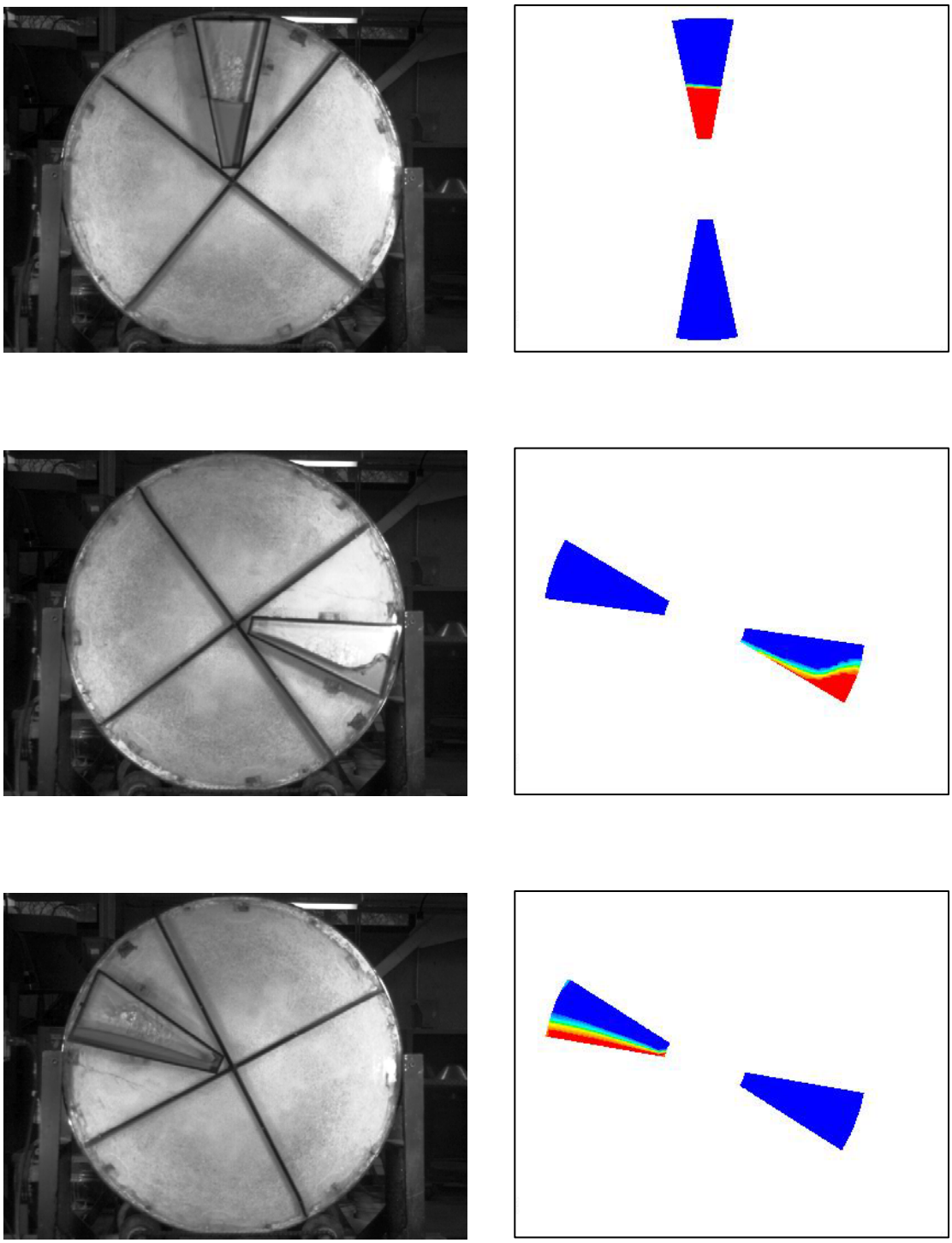

Figure 5.7 – Experimental and CFD free surface profiles for glycerol solution (70% by volume) with volume filling of 350 cm^3 (27% of channel volume) at 11.7 rpm

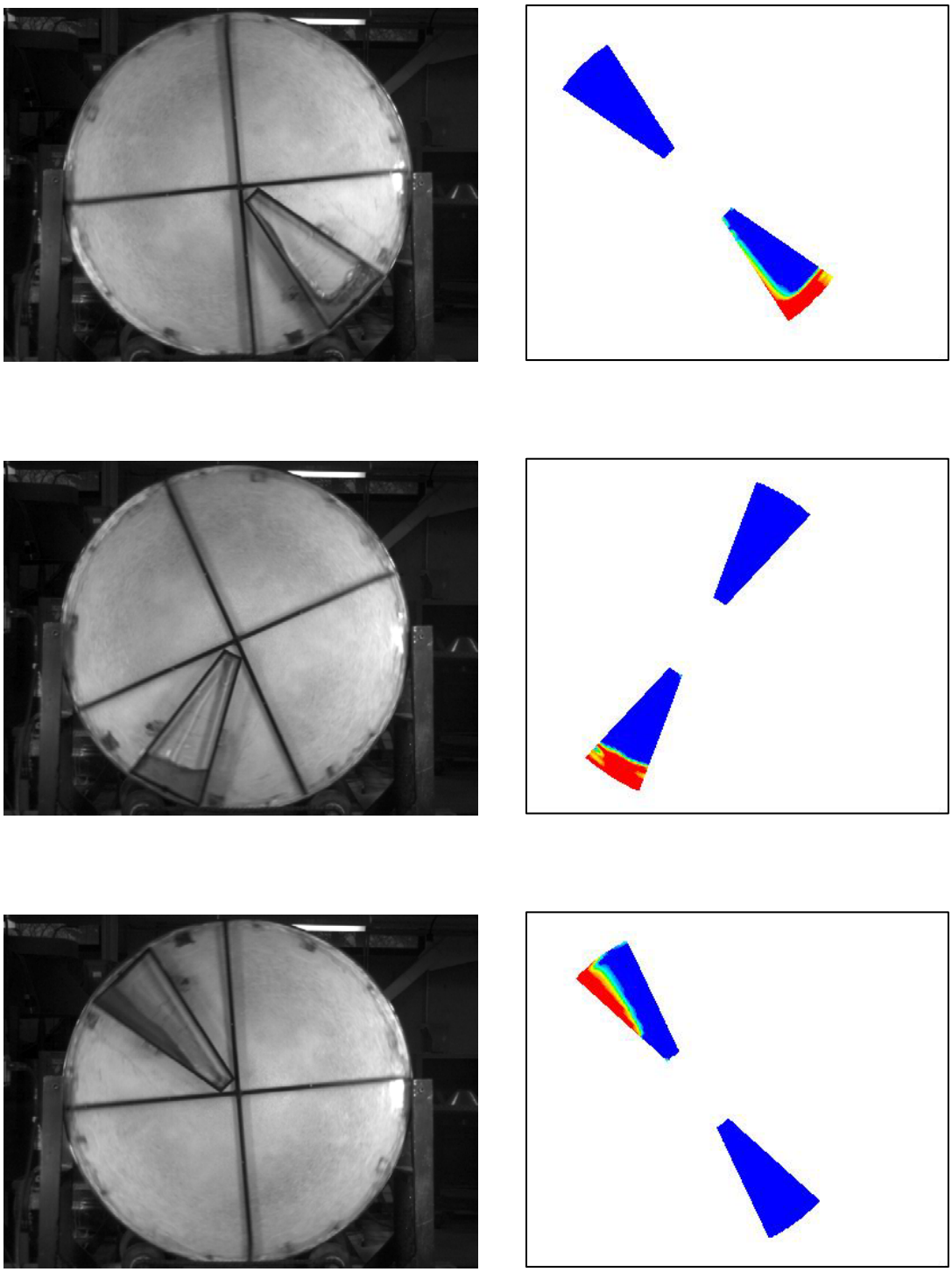

Figure 5.8 – Experimental and CFD free surface profiles for glycerol solution (70% by volume) with volume filling of 350 cm^3 (27% of channel volume) at 34 rpm

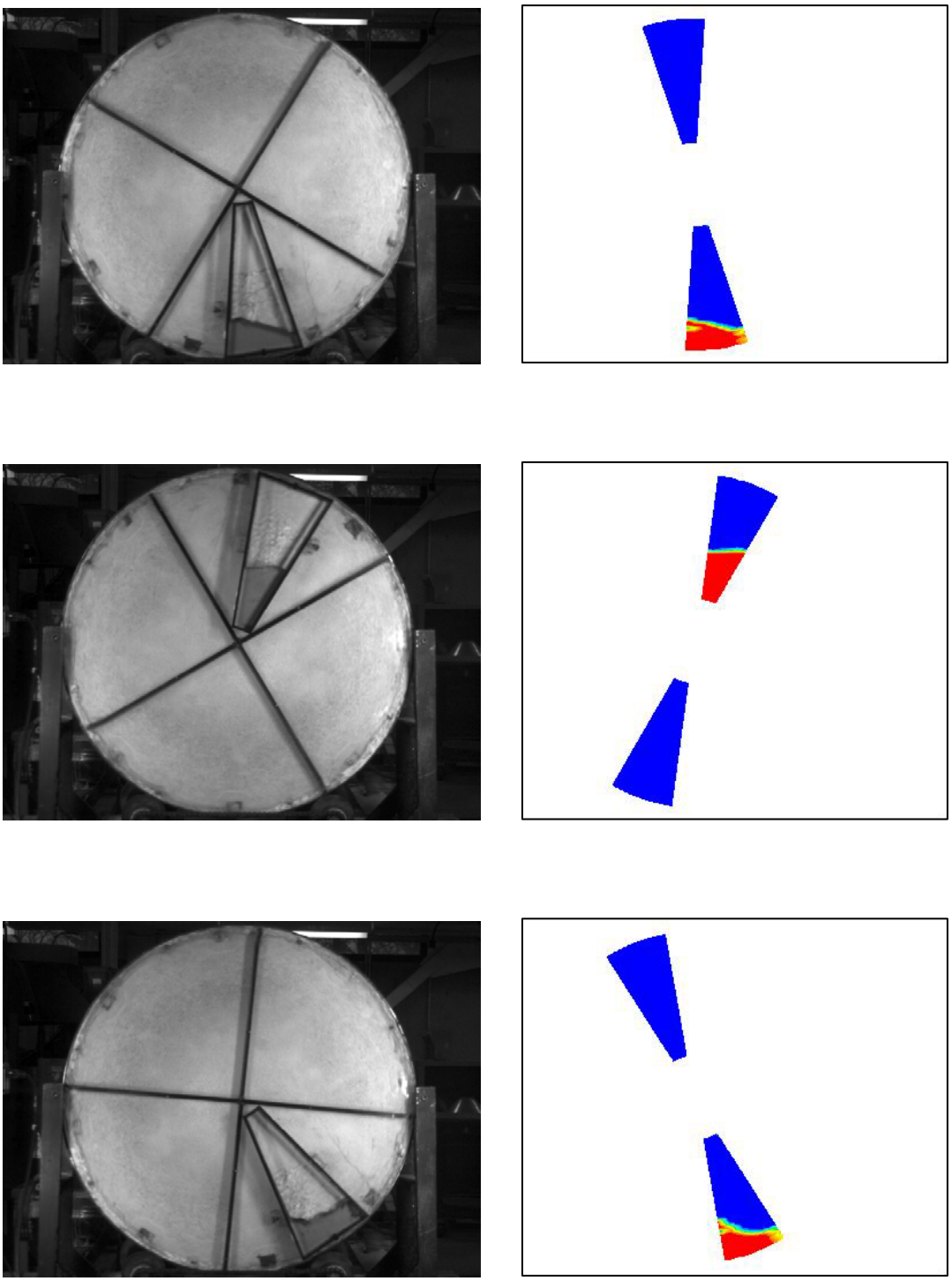

Figure 5.9 – Experimental and CFD free surface profiles for glycerol solution (70% by volume) with volume filling of 350 cm^3 (27% of channel volume) at 18.4 rpm

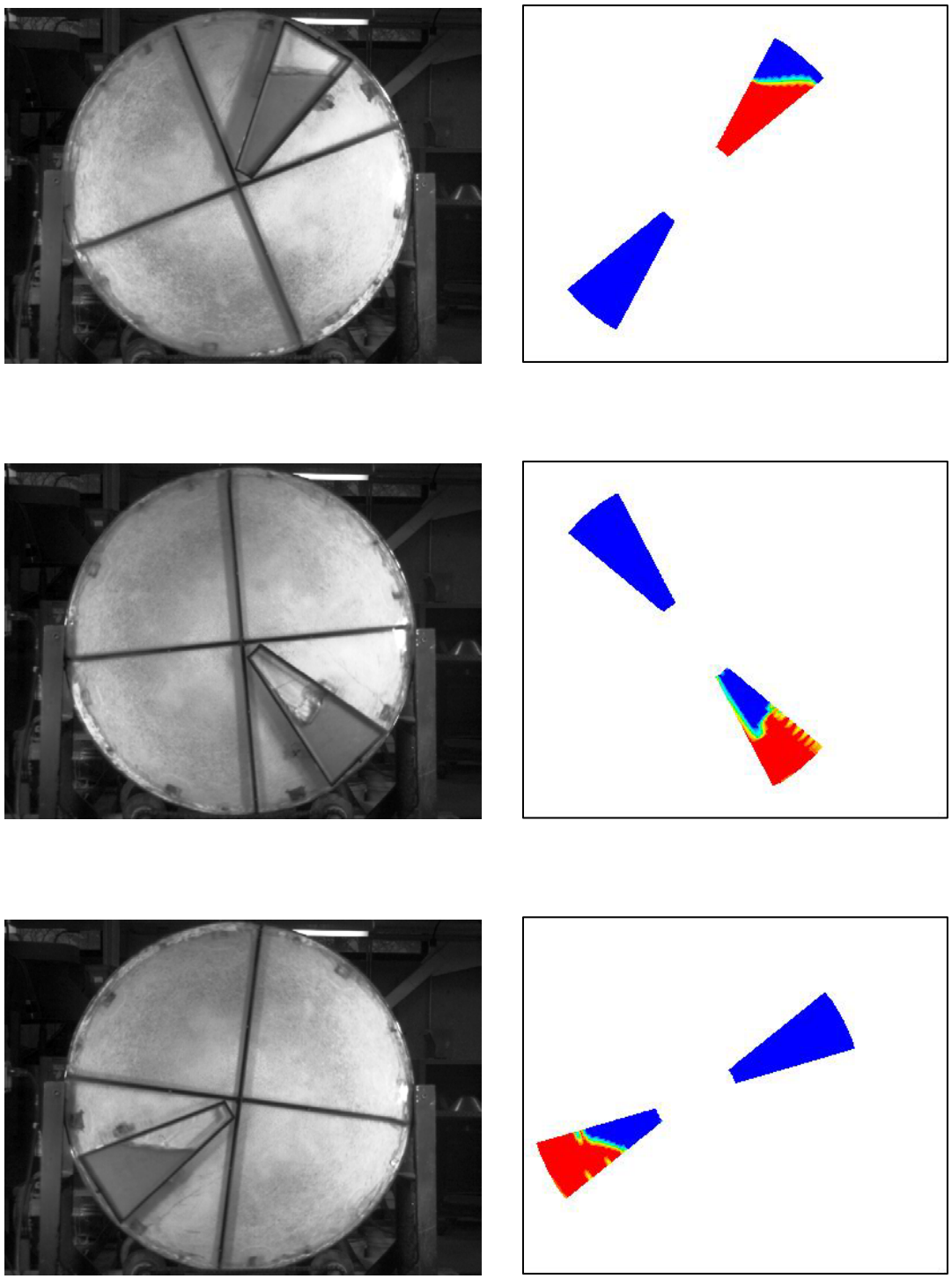

Figure 5.10 – Experimental and CFD free surface profiles for glycerol solution (70% by volume) with volume filling of 800 cm^3 (61.5% of channel volume) at 18.4 rpm

It has also been seen in the experimental runs that the effects of the solution density and the solution viscosity become more significant as the glycerol solution concentration increases. Figure 5.11 through 5.14 demonstrate the dynamic free surface profiles for various glycerol solution concentrations at different mill rotational speeds. The range covered for solution viscosity, in the dynamic free surface profile experiments, is between 30 mPa.s and 70 mPa.s. Even though the profiles only differ slightly, the physical examination of the solutions reveals the contrast. It should be noted that the scale of the experiments and the Newtonian nature of the solution contribute to the observed profiles.

The simulations on a hypothetical full pulp lifter assembly consisting of sixteen pulp lifter channels, for free surface profiles, have also been run apart from the single pulp lifter channel simulations. The mill embodying the pulp lifter channels has a diameter of 98 cm, and the trunnion diameter is 25 cm. There is no inflow to or outflow from the pulp lifter channel in these simulations. The simulation results for the full pulp lifter assembly are given in Appendix C.

The purpose of performing those simulations has been, on the first hand, to illustrate the free surface profiles developing in the system as the mill operates at specified conditions. Secondly, the profiles are meant to demonstrate the independence of each pulp lifter channel clearly.

The simulation results have shown that there is no interaction among the pulp lifter channels as the volume of fluid put in each channel only occupies the flow space available within the channel where it is enclosed.

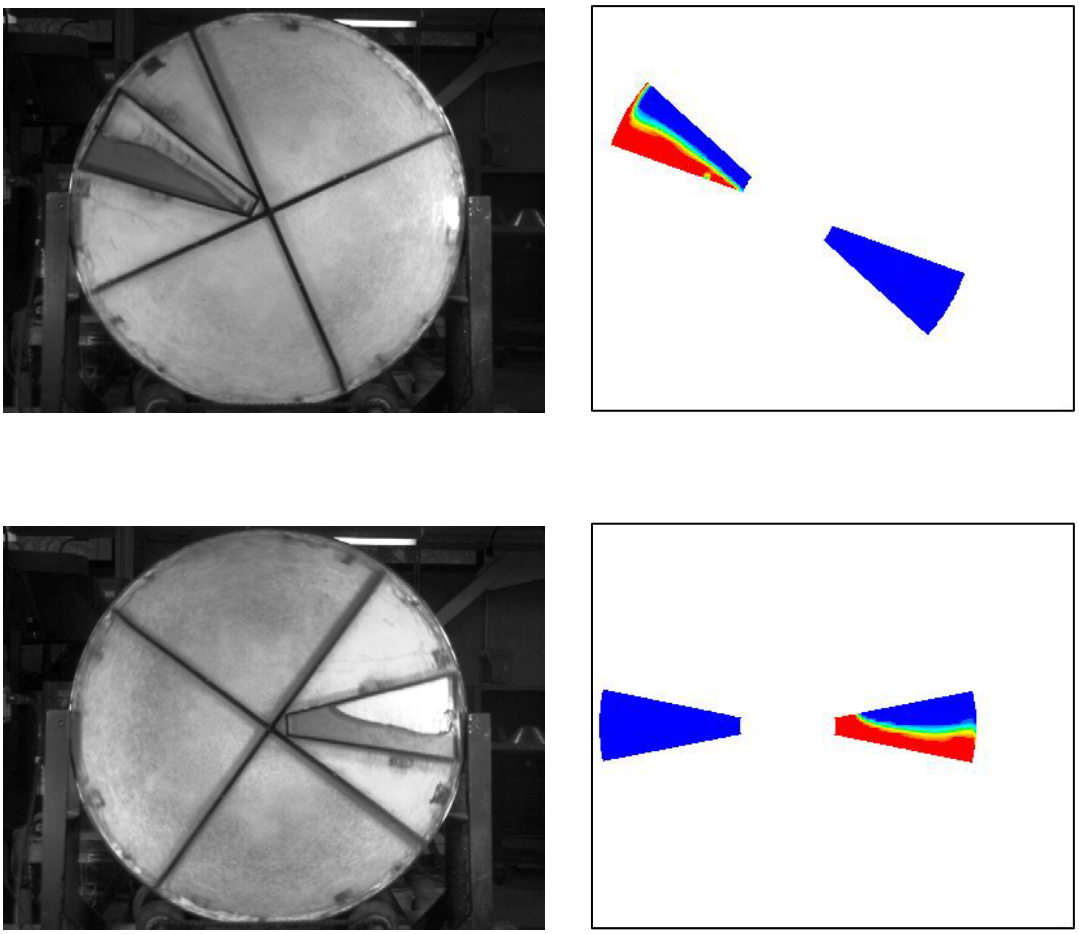

Figure 5.11 – Experimental and CFD free surface profiles for glycerol solution (65% by volume) with volume filling of 650 cm^3 (50% of channel volume) at 26.2 rpm

Likewise, the significance of initial volume filling and the volume of the fluid relative to that of the pulp lifter channel is emphasized. The influence of mill rotational speed has also been demonstrated by the simulation results, pointing out the fact that the mill rotational speed is one of the variables affecting the progression of free surface profiles.

Moreover, the simulation results prove that the flow in the full pulp lifter assembly for the pilot scale mill set-up such as the one described in the hypothetical case can entirely be simulated, given that the multiprocessor computing is available.

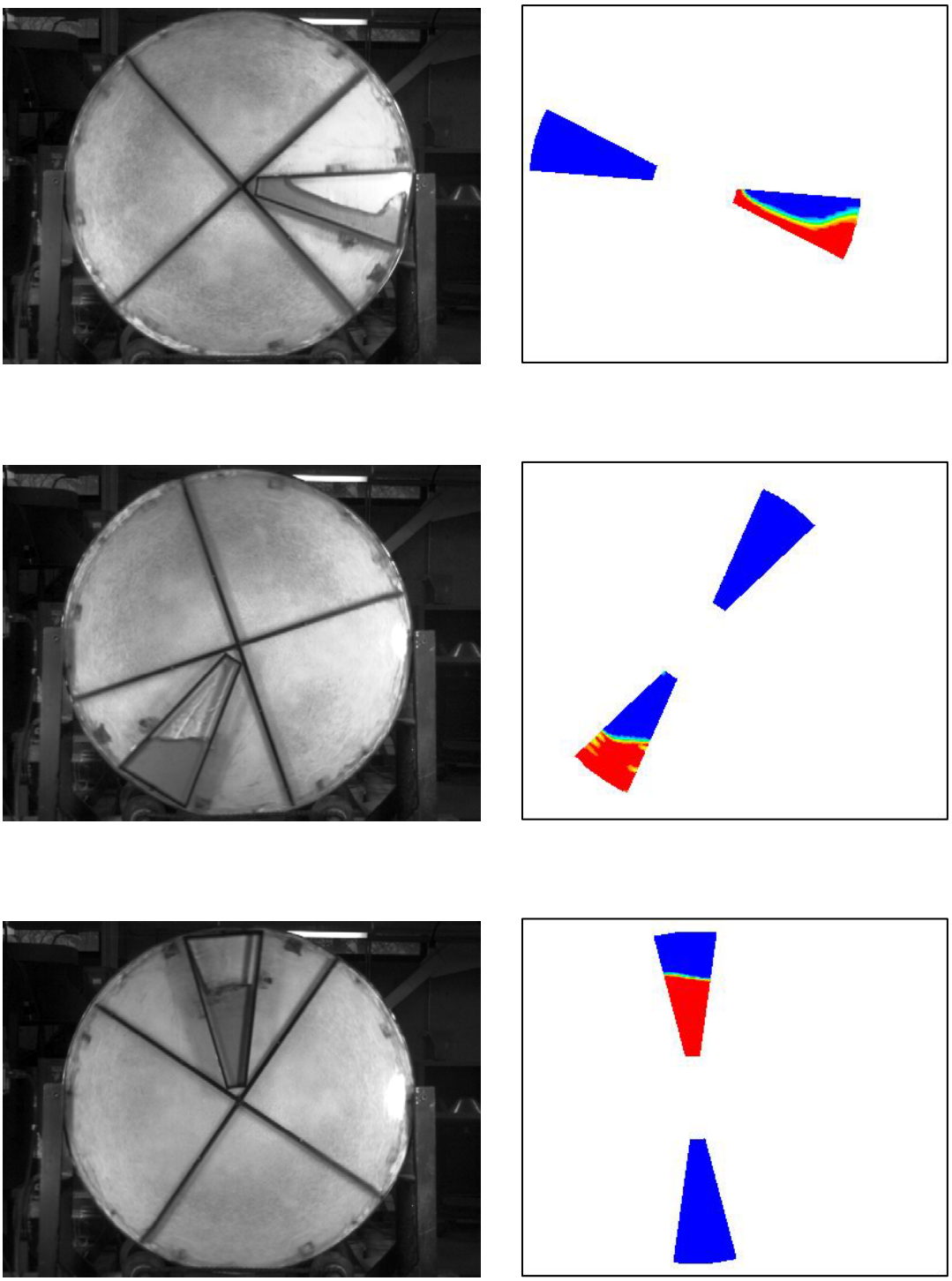

Figure 5.12 – Experimental and CFD free surface profiles for glycerol solution (70% by volume) with volume filling of 650 cm^3 (50% of channel volume) at 26.2 rpm

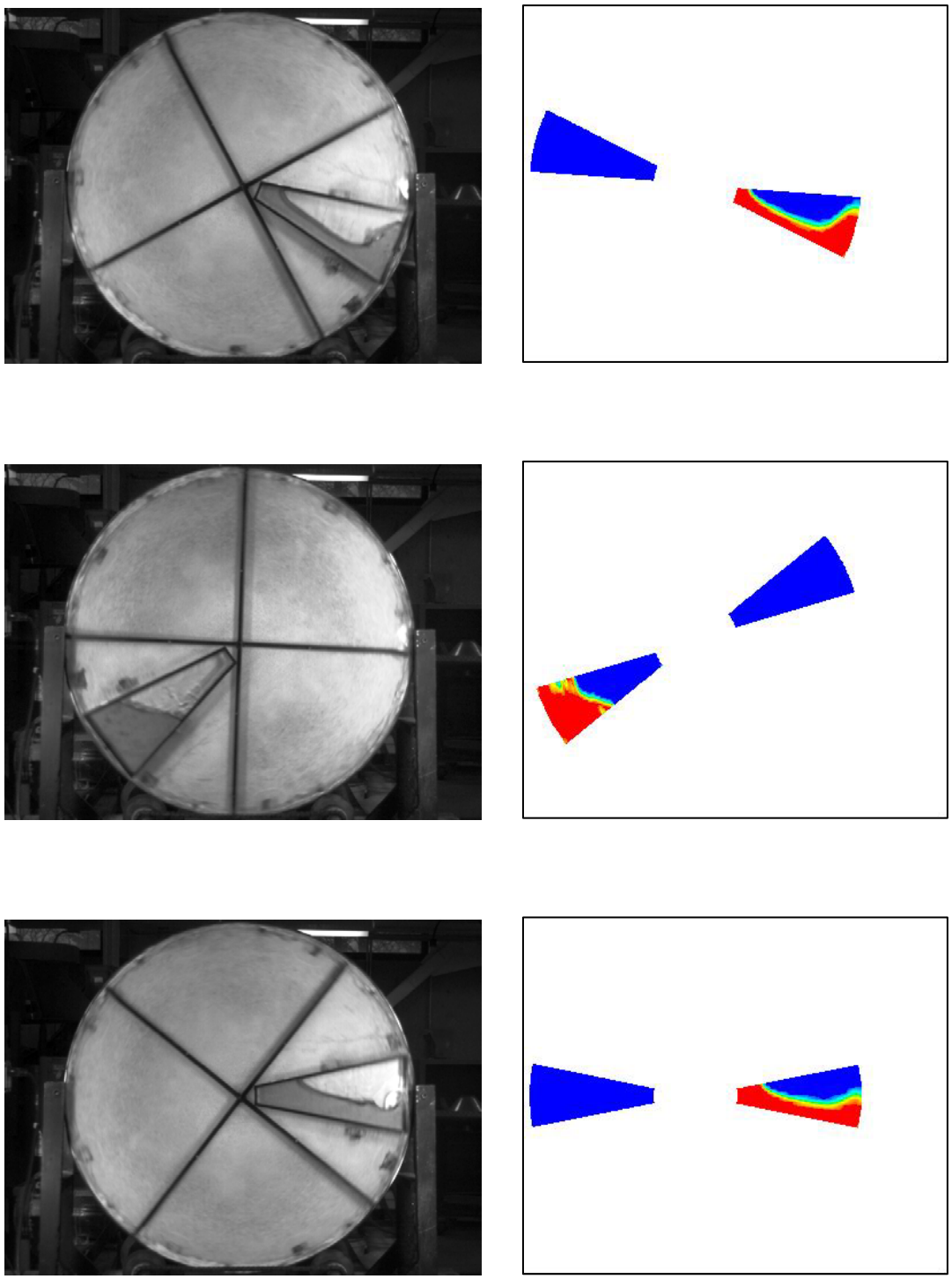

Figure 5.13 – Experimental and CFD free surface profiles for glycerol solution (70% by volume) with volume filling of 650 cm^3 (50% of channel volume) at 34 rpm

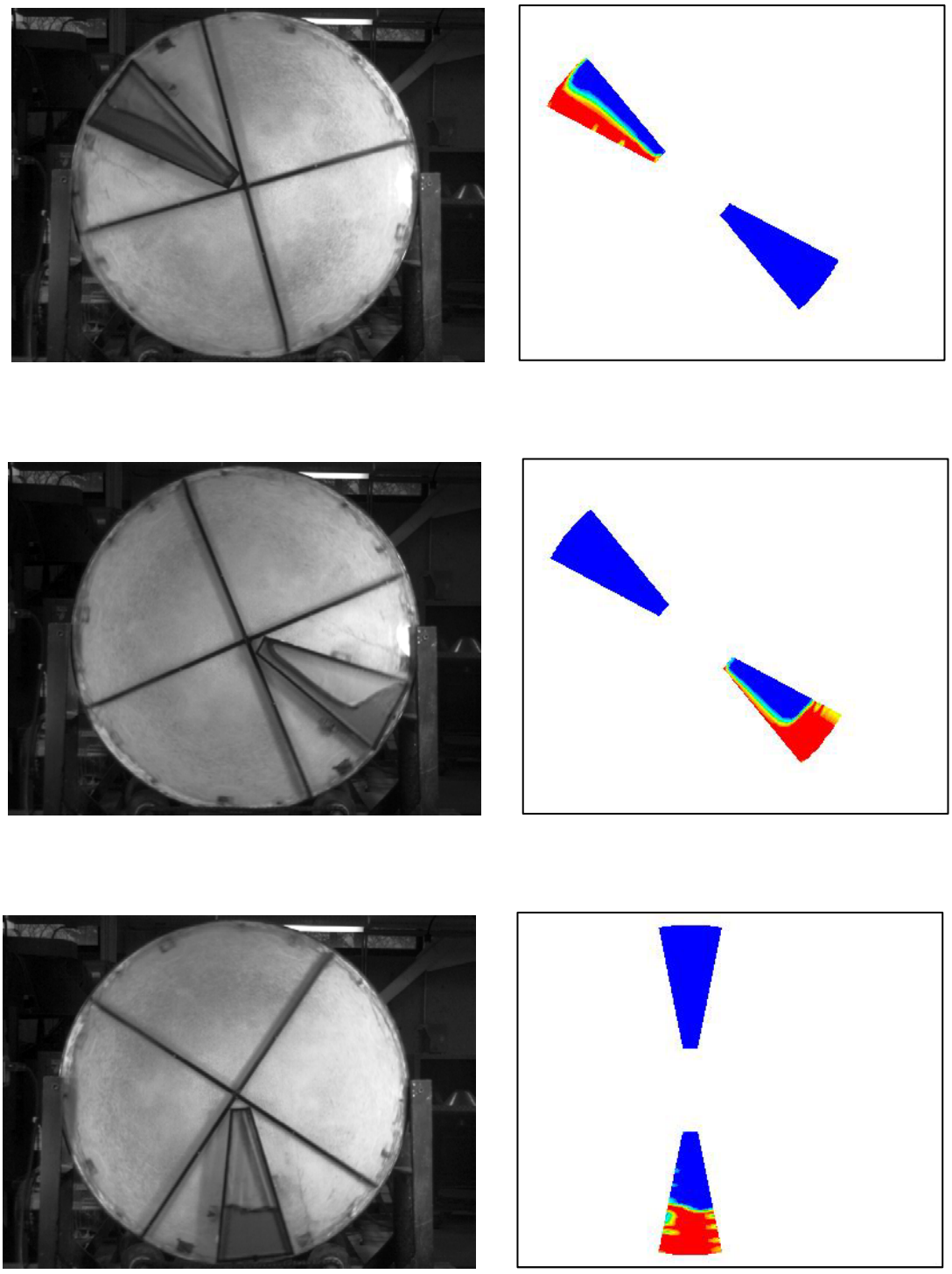

Figure 5.14 – Experimental and CFD free surface profiles for glycerol solution (75% by volume) with volume filling of 650 cm^3 (50% of channel volume) at 26.2 rpm

5.2. Dynamic Discharge Profile Experiments

These experiments have been carried out for the current study at Universidad Autónoma de San Luis Potosí, Mexico under the guidance of Dr. Jose A. Delgadillo. These experiments have been carried out expressly for inclusion in this study. Figure 5.15 and Figure 5.16 show a sample of free surface profile scenes of the dynamic discharge profile experiments along with the corresponding simulation results. It is noted once again that the free surface profiles obtained by CFD predictions show good match to the experimental results.

The CFD computations are run for one full revolution, and the results are in terms of volume discharged. The glycerol solutions used in the first set experiments, and the second and third sets of experiments have different viscosities. The particular reason for that is the temperature recorded at the time of solution preparation, specifically 30 ˚C for the first set versus 23 ˚C for the second and the third sets. In the first and the second sets of experiments, two holes of 1 cm in diameter have been used while three holes of 1 cm in diameter are used for the third set. Table 5.1 and Table 5.2 present the results of the discharge experiments by way of comparison of experimental and predicted volume of discharge. The experimental data for dynamic discharge profile experiments, consisting of five repetitions for each run, are provided in Appendix B.

The volumetric flow rate out of the channel is dictated by body forces exerted by the channel walls on the fluid. The flow behavior is nonlinear in the sense that the volume flowing out of the channel is not proportional to the initial volume. The nonlinear characteristics are intensified by the turbulent momentum transfer as a lot of energy is dissipated.

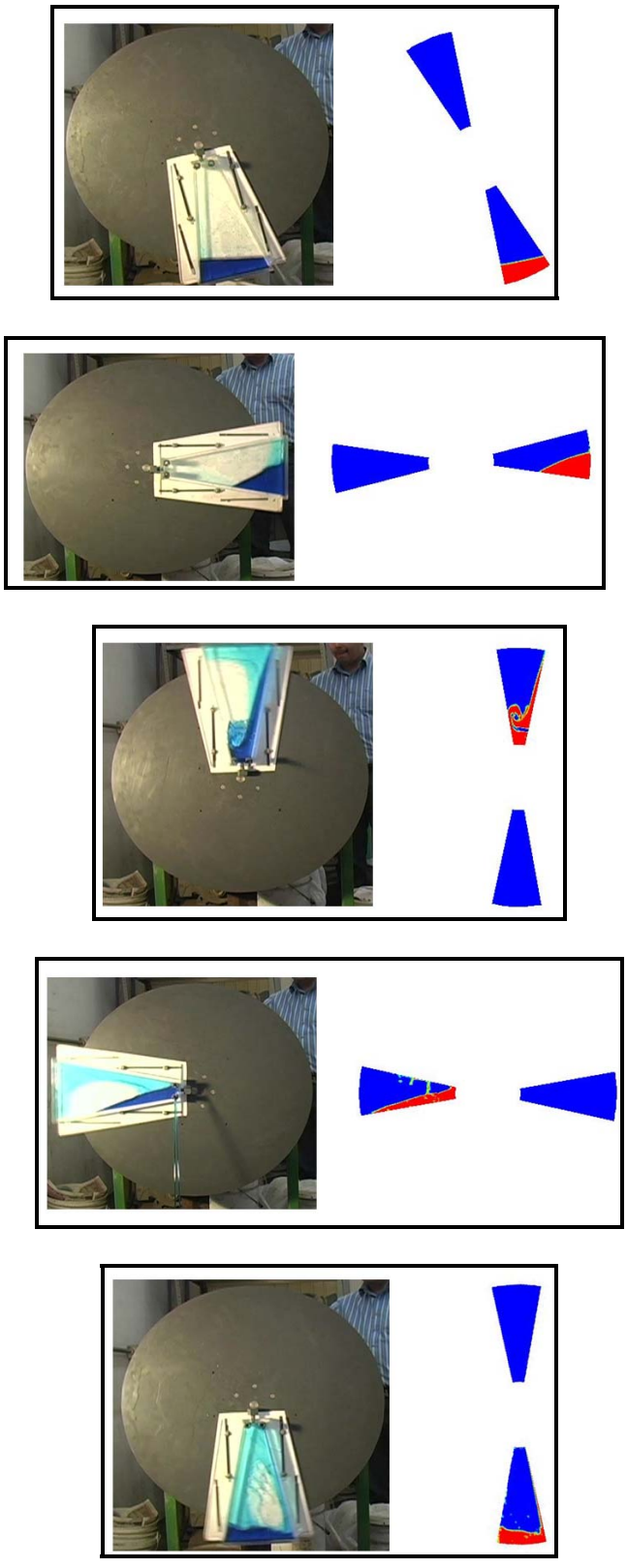

Figure 5.15 – Experimental and CFD discharge profiles for 85% by volume glycerol solution of 350 cm^3 volume filling (27% of channel volume) at 26.2 rpm

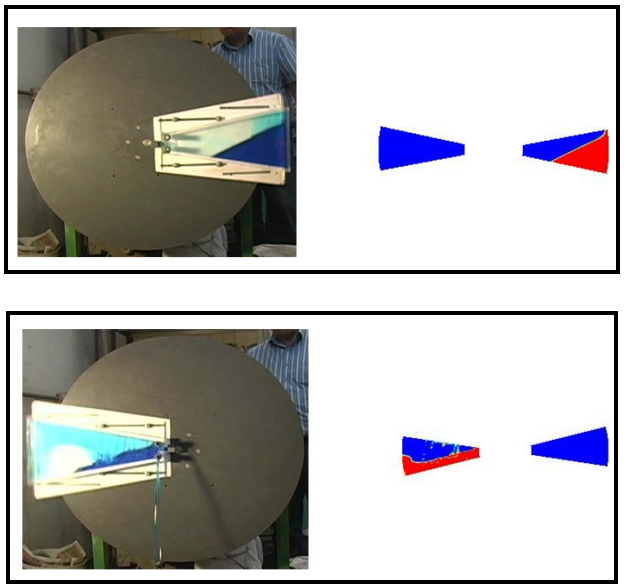

Glycerol Solution (85%), 650 cm^3 volume filling (50% of channel volume) at 26.2 rpm

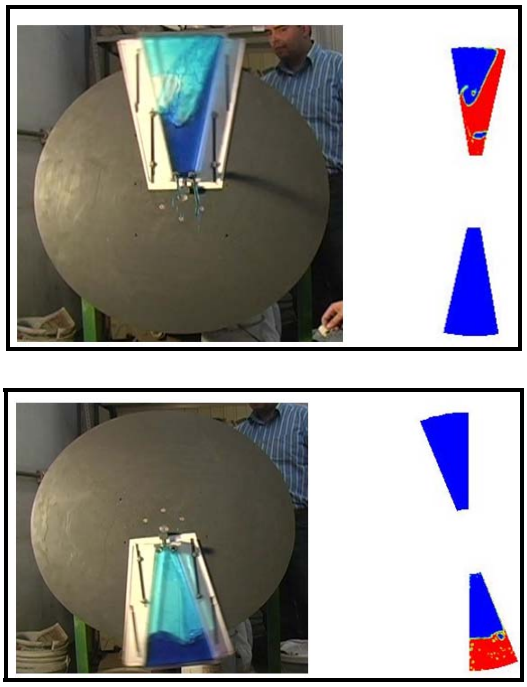

Glycerol Solution (85%), 650 cm^3 volume filling (50% of channel volume) at 34 rpm

Figure 5.16 – Experimental and CFD discharge profiles for 85% by volume glycerol solution

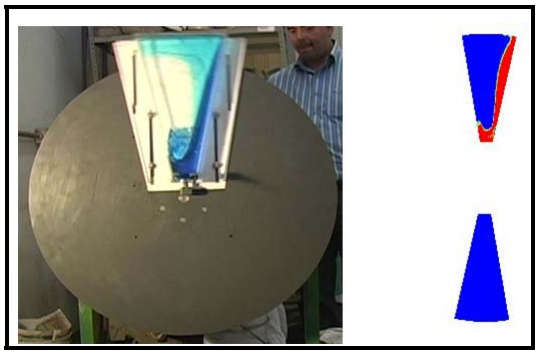

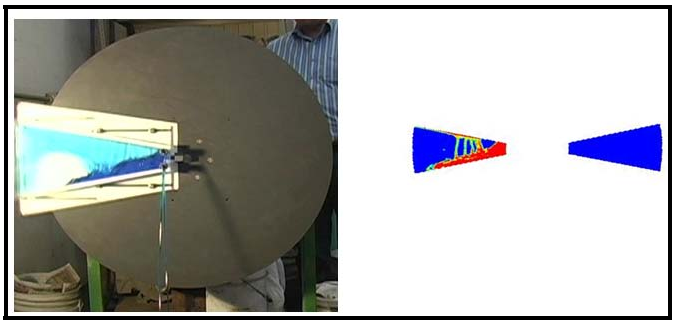

Glycerol Solution (85%), 350 cm^3 volume filling (27% of channel volume) at 34 rpm

Figure 5.16 Continued

Table 5.1 – The volume of discharge recorded for glycerol solution (85% by volume) (μ = 61 mPa.s) in experiments and CFD predictions

Test	Speed (rpm)	Initial volume (cm^3)	Volume discharged in one revolution (cm^3) **Experiment**	Volume discharged in one revolution (cm^3) **CFD prediction**
1	26.2	650	108	105
2	34.0	650	64.4	56
3	26.2	350	65	64
4	34.0	350	36.2	13

Table 5.2 – Experimental volume discharged and CFD predictions for (85% by volume glycerol solution) (μ = 83.5 mPa.s)

Test	Speed (rpm)	Initial volume (cm^3)	Volume discharged in one revolution (cm^3) **Experiment**	Volume discharged in one revolution (cm^3) **CFD prediction**
1	26	500	55.8	54.0
2	29	500	45.0	37.5
3	32	500	37.4	42.0
4	35	500	30.8	30.6
5	26	350	41.8	43.1
6	29	350	32.4	25.6
7	32	350	27.4	24.5
8	35	350	21.4	23.3
9	26	500	81.4	59.2
10	29	500	65.6	50.0
11	32	500	53.2	42.0
12	35	500	43.0	39.8
13	26	350	51.6	47.0
14	29	350	45.2	42.0
15	32	350	37.6	38.0
16	35	350	29.4	28.8

* Test 9 through test 16 corresponds to experimental results and CFD predictions obtained with three holes

The volumetric flow rate is obtained simply by dividing the resulting volume by the time required for a single revolution. The volumetric flow rates together with the percentage of volume discharged (with respect to initial volume fillings) are given in Table 5.3 and Table 5.4. The CFD predictions for volumetric flow agree fairly well with experimental results, capturing the experimental volume discharged by 87% on the average. However, the CFD prediction for test 4 in Table 5.1, volume filling of 350 cm^3 for the channel rotating at 34 rpm, is lower than the experimental volume recorded for the test. The predicted volume for test 4, in Table 5.1 and Table 5.4, is only 36% of the experimental volume. But again, the CFD predictions for all the other tests, as shown in Table 5.1 and Table 5.2, are reasonably consistent with the experimental results. Considering the 87%, on the average, match it is concluded that the poor predictional quality for test 4 in Table 5.1 is due to numerical errors in the specific simulation.

It is seen that the volume discharged as well as the resulting volumetric flow rate decrease as the mill rotational speed increases (Figure 5.17 and Figure 5.18). Obviously, more area available for discharge leads to more discharge, in turn increasing the volumetric flow rate, as seen by the results in Table 5.2, and Figure 5.19.

As the solution viscosity increases, the fluid resistance to flow increases, causing a decrease in the volume discharged as shown in Figure 5.20. The effect of viscosity change on the volume discharged is demonstrated by the experimental results for the first set of experiments with two holes and second set of experiments with two holes.

Table 5.3 – Experimental volumetric flow rate and the percentage discharge of glycerol solution (85% by volume) (μ = 61 mPa.s)

Test	Speed (rpm)	Initial volume (cm^3)	Volumetric flow rate ($cm^3.s^{-1}$)	Percentage of volume discharged
1	26.2	650	47.2	18.6
2	34	650	36.5	10.3
3	26.2	350	28.4	16.6
4	34	350	20.5	9.9

Table 5.4 – Experimental volumetric flow rate and the percentage discharge of glycerol solution (85% by volume) (μ = 83.5 mPa.s)

Test	Speed (rpm)	Initial volume (cm^3)	Volumetric flow rate ($cm^3.s^{-1}$)	Percentage of volume discharged
1	26	500	24.2	11.2
2	29	500	21.8	9.0
3	32	500	20.0	7.5
4	35	500	18.0	6.2
5	26	350	18.1	11.9
6	29	350	15.7	9.3
7	32	350	14.6	7.8
8	35	350	12.5	6.1
9	26	500	35.3	16.3
10	29	500	31.7	13.1
11	32	500	28.4	10.6
12	35	500	25.1	8.6
13	26	350	22.4	14.7
14	29	350	21.8	12.9
15	32	350	20.0	10.7
16	35	350	17.1	8.4

* Test 9 through test 16 corresponds to experimental results and CFD predictions obtained with three holes

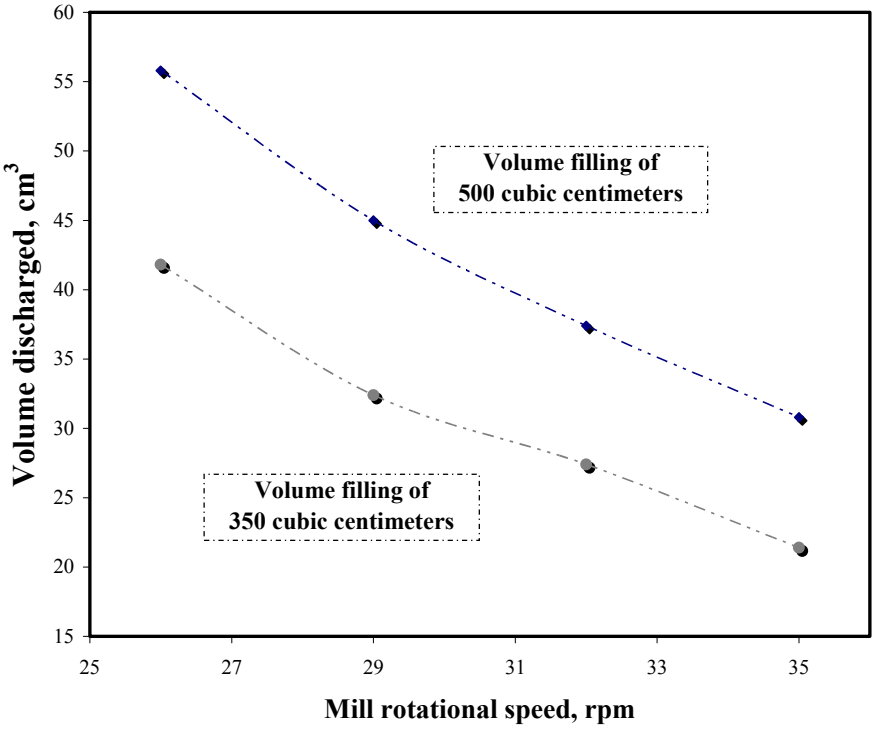

Figure 5.17 – The effect of mill rotational speed on the experimental volume discharged, illustrated with volume fillings of 500 cm^3 (38.5% of channel volume) and 350 cm^3 (27% of channel volume)

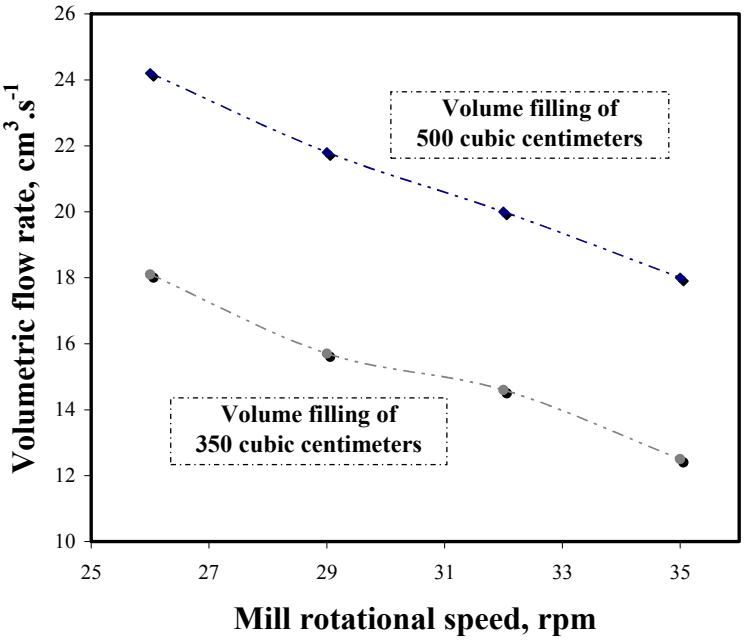

Figure 5.18 – The effect of mill rotational speed on the experimental volumetric flow rate, illustrated with volume fillings of 500 cm^3 (38.5% of channel volume) and 350 cm^3 (27% of channel volume)

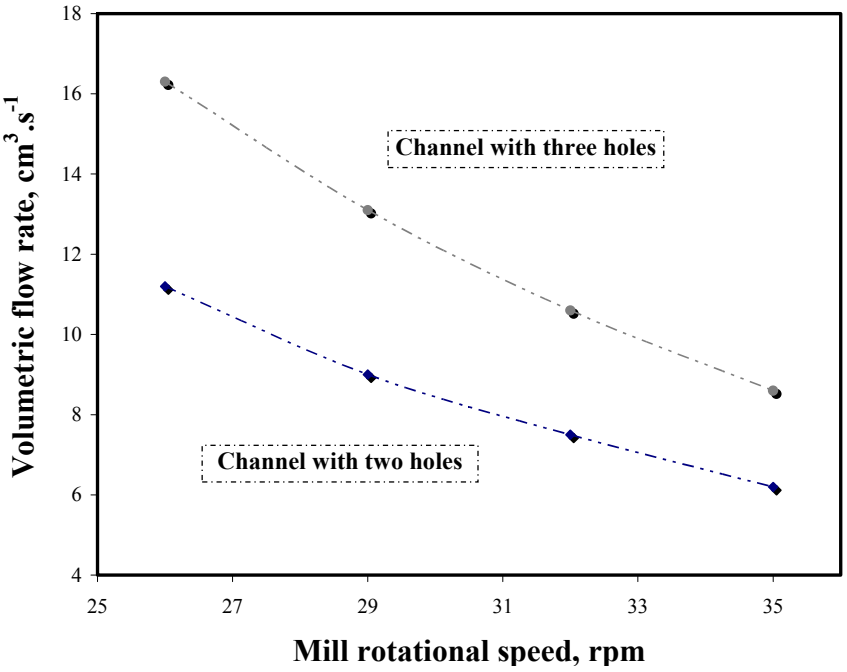

Figure 5.19 – The effect of discharge area on the volumetric flow rate at the volume filling of 500 cm^3 (38.5% of channel volume)

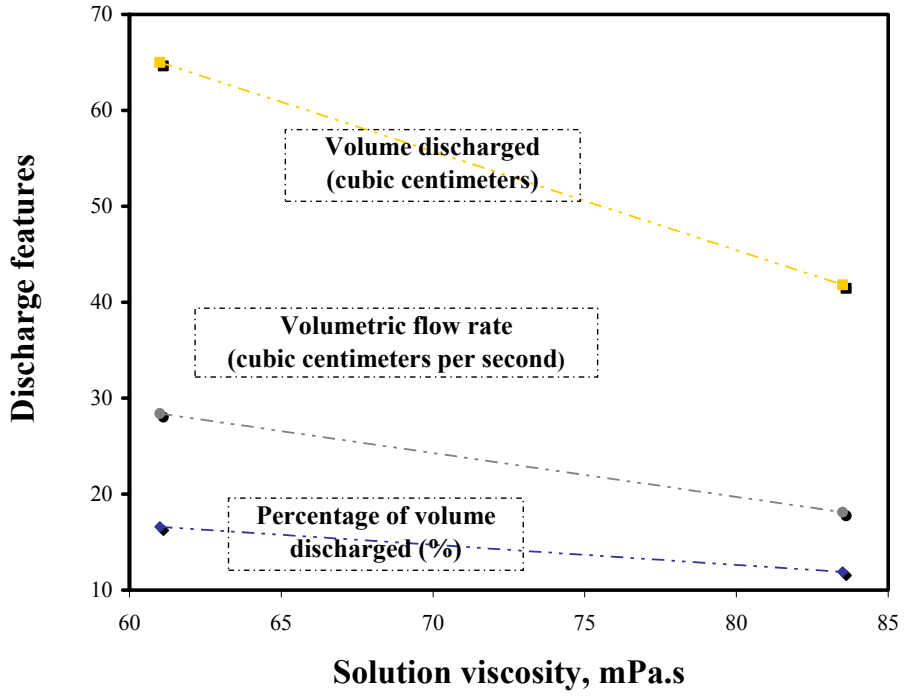

Figure 5.20 – The effect of solution properties on the experimental volumetric discharge, demonstrated by the profiles for glycerol solution (85% by volume) with volume filling of 350 cm^3 (27% of channel volume) at 26 rpm

For instance, in the first set, the experimental volume discharged out of the pulp lifter channel for an initial volume filling at 350 cm^3, as the channel rotates at 26 rpm is reported as 65 cm^3 (Table 5.1, test 3) while it is 41.8 cm^3 (Table 5.2, test 5) for the second set. Likewise, in the first set, the experimental volume discharged out of the pulp lifter channel for an initial volume filling at 350 cm^3, as the channel rotates at 34 rpm is reported as 36.2 cm^3 (Table 5.1, test 4) while it is 21.4 cm^3 (Table 5.2, test 8) for the second set. Furthermore, the results show that the ratio of volume discharged to that of initial volume filling is constant for each initial volume filling for the same pulp lifter channel volume, but the ratio decreases with increasing mill rotational speed and solution viscosity. The percentage of the volume discharged with respect to initial volume filling does not change even though the fluid level above the discharge opening increases as the volume of fluid increases in the channel (Figure 5.21). As seen in Table 5.4, for experimental runs with three holes, the percentages of the volume discharged for test 10 with an initial volume filling of 500 cm^3 and test 14 with an initial volume filling of 350 cm^3 are observed to be the same, 13.1% versus 12.9%. Thereby, the results prove the complexity of the calculations, and that there are multiple driving mechanisms in the system. In other words, the flow behavior can not be described by general rules defined via algebraic correlations. The set of nonlinear partial differential equations, Navier Stokes equations and continuity equation, characterize the behavior at best. Besides, the solution of those partial differential equations by numerical methods necessitates the correct configuration of the flow problem, with particular attention to mesh quality, incremental time step, and solution control parameters.

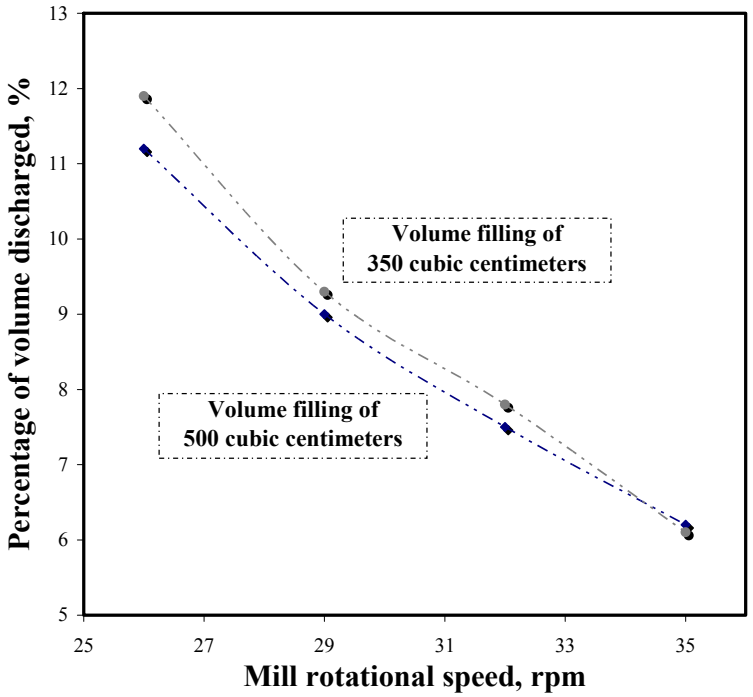

Figure 5.21 – The percentage volume discharged with respect to the initial volume filling versus the mill rotational speed

The calculations are based on simultaneous solution of the equations for the mass conservation, three components of velocity, turbulent kinetic energy (k), and dissipated energy (ε). The convergence of the overall solution depends on the correct calculation of each set of equations. The overall solution does not converge even when there is only one variable that does not meet the convergence criterion, carrying any numerical error forward by the subsequent iterations.

The flow behavior is influenced by the surface forces, pressure force and shear stress forces, body forces, gravitational force and centrifugal force, in the system. The time dependence of the flow behavior as well as the rotation of the domain results in continuously changing net force field on the fluid. Therefore, it is important that the flow behavior is modeled by appropriate set of equations, with the right initial and boundary conditions, defining behavior correctly, and that the numerical techniques employed provide accurate results.

With increasing mill rotational speed, the active discharge area, in other words the portion of the upper half of the mill circle where outflow takes place, decreases. Figure 5.22 illustrates the free surface profiles obtained at two different mill rotational speeds as the volume filling of 500 cm^3 of glycerol solution (85% by volume) discharges. The profiles have been recorded for each sweep of the pulp lifter channel during the rotation of the mill. The pulp lifter channel covers 22.5 degrees of 360 degree mill circle while the clock circle has tick marks for every 30 degrees. It is noted that the outflow begins around 1 o'clock in contrast to around 2 o'clock as the mill rotational speed increases to 35 rpm from 26 rpm. Also, the relative volume discharged at the locations on the mill circle from around 1 o'clock to 9 o'clock is less.

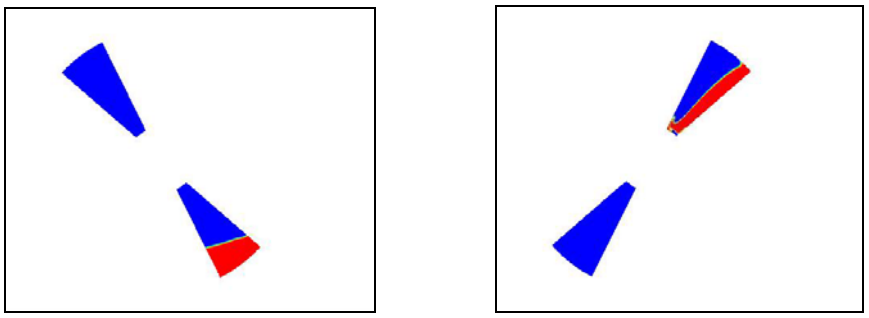

Pulp lifter channel at 26 rpm

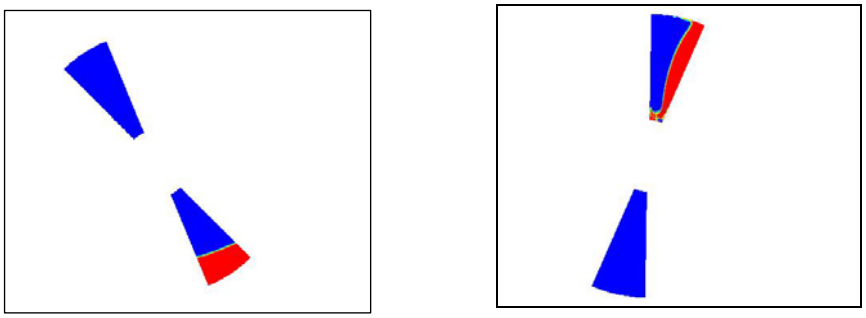

Pulp lifter channel at 35 rpm

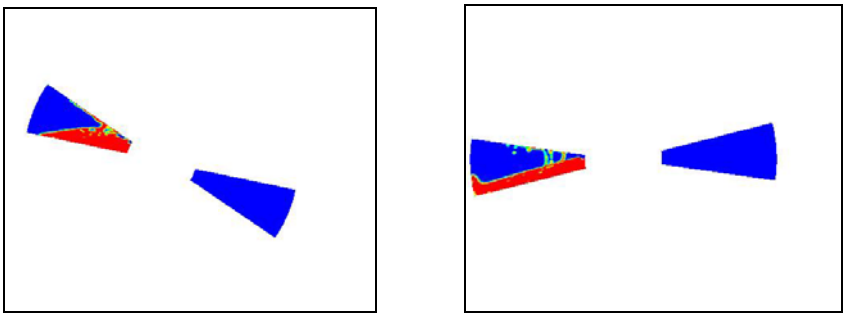

Pulp lifter channel at 26 rpm

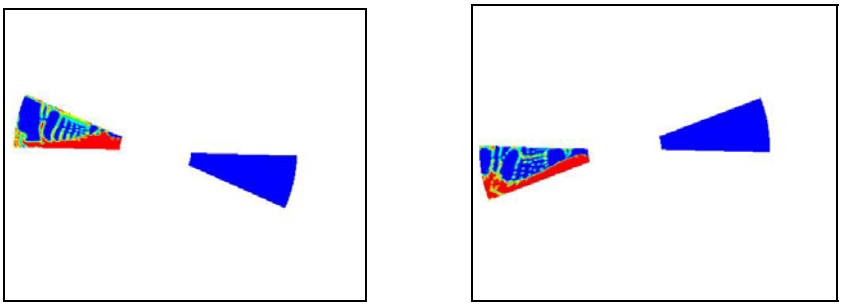

Pulp lifter channel at 35 rpm

Figure 5.22 – CFD discharge profiles for glycerol solution (85% by volume) of 500 cm^3 volume filling (38.5% of channel volume)

5.3. Summary

The comparisons of the experimental results and CFD simulation results are demonstrated in the current chapter, specifically for the dynamic free surface profiles and the dynamic discharge profiles.

The effects of mill rotational speed and glycerol solution concentrations are elaborated. The explanations of the force field effective in the system are given.

It is seen that the free surface profiles obtained by CFD predictions show good match with the experimental results, detailing the free surface profiles progressing in the channel as the channel rotates at the specified mill rotational speed. The predictions for the volume discharged also agree fairly well with experimental results, capturing the experimental volume discharged by 87% on the average.

With increasing mill rotational speed, the volume discharged as well as the resulting volumetric flow rate decreases. The volume discharged decreases as the solution viscosity increases. The glycerol solution used in the first set of experiments has a viscosity of 61 mPa.s while the glycerol solution used in the second set of experiments has a viscosity of 83.5 mPa.s. The tests for volume filling of 350 cm^3 have been conducted both in the first and the second sets of experiments. Comparing the results from the first set and second set, it is seen the volume discharged decreases by 36% as the channel rotates at 26 rpm, and the decrease is 41% as the channel rotates at 34 rpm.

Furthermore, the results, as demonstrated by twenty sets of experimental data which have five repetitions for each, indicate that the percentage of the volume discharged with respect to initial volume filling does not change as the initial volume filling is increased or decreased.

CHAPTER 6

MODEL VALIDATION WITH PLANT SCALE MILL DATA

The predictive quality of computational fluid dynamics results for the experimental data confirms that CFD methodology thoroughly explains the process dynamics. On that account, the same CFD methodology is employed to predict the performance plant scale mills. Published detailed sets of data in operating autogenous grinding and semiautogenous grinding mills are utilized (Powell & Valery 2006). Also, the methodology is used for predicting the data collected at the ArcelorMittal Mont-Wright AG mill (Fermont, Quebec, Canada). The mill - clock circle is provided here once again (Figure 6.1), for reference during the discussion. Red and blue colors used in the presentation of results solely signify the maximum and the minimum values, specifically 1 for the slurry phase and 0 for the air phase. The CFD computations are run for one full revolution, and the results are obtained in terms of volume discharged. Once the channel passes over the horizontal line (9 o'clock region – counterclockwise rotation or 3 o'clock region – clockwise rotation) the discharge stops. The difference between the initial volume and the recorded volume as the channel just passes the horizontal line is taken as the volume discharged.

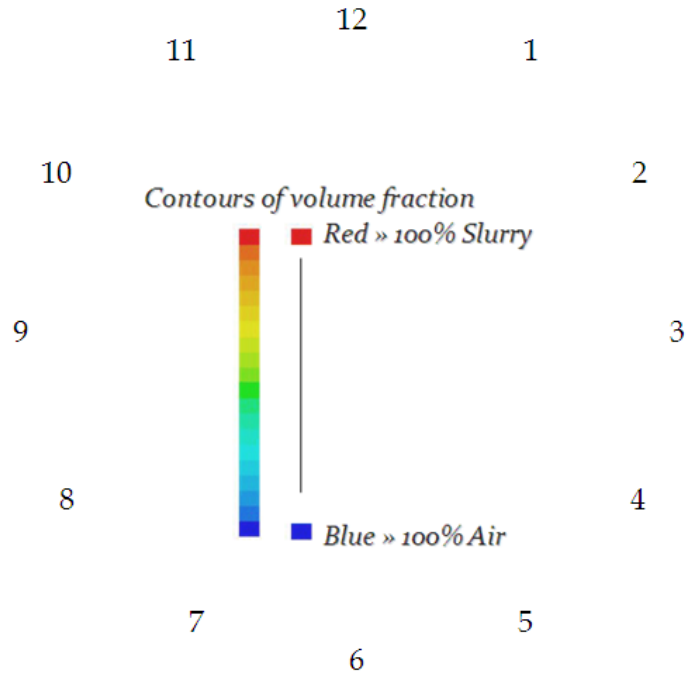

Figure 6.1 – Mill – Clock circle analogy and color legend representing the volume fraction of phases

Multiplying the volume discharged from a single channel in one revolution by the number of pulp lifter channels in the mill yields the overall volume discharged, as dictated by superposition principle. Then, the volumetric flow rate is obtained simply by dividing the resulting volume by the time for a single revolution.

The results for plant scale mills are presented with discrete element method charge profile predictions accompanied by CFD discharge profiles. Figures 6.2 through 6.9 demonstrate the DEM-CFD profiles for eight data sets of the published mill surveys (Powell & Valery 2006). The figures illustrate the free surface profiles in a single channel at different locations during the simulation, as shown with the clock circle superimposed on the mill circles. The percent readings, seen on the figures, correspond to the percentage of the fluid volume remaining in the pulp lifter channel with respect to the initial fluid volume in the pulp lifter channel.

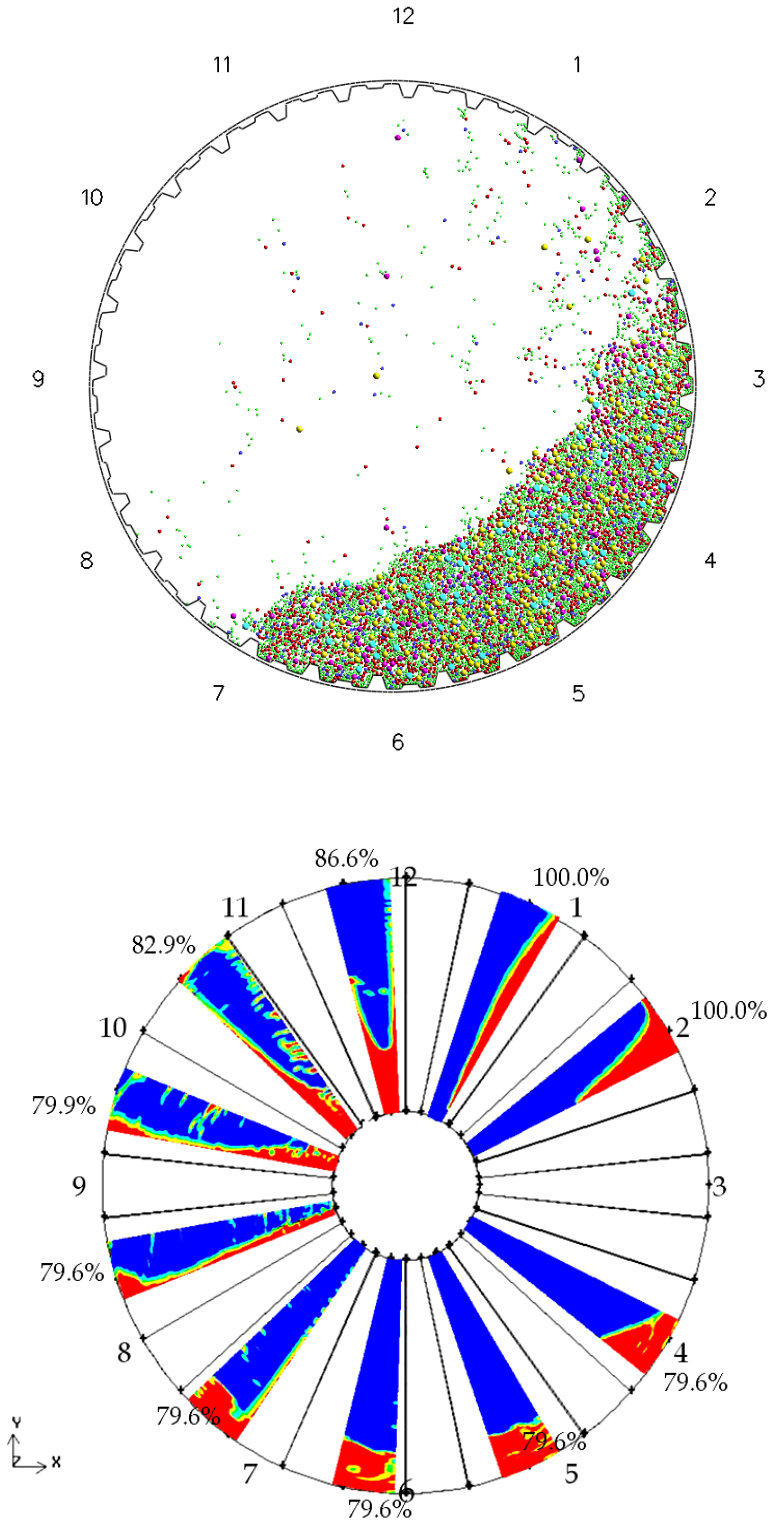

Figure 6.2 – DEM charge profile and CFD prediction of free surface profiles as the mill discharges, Los Bronces SAG mill (Diameter 8.26 m and length 4.189 m)

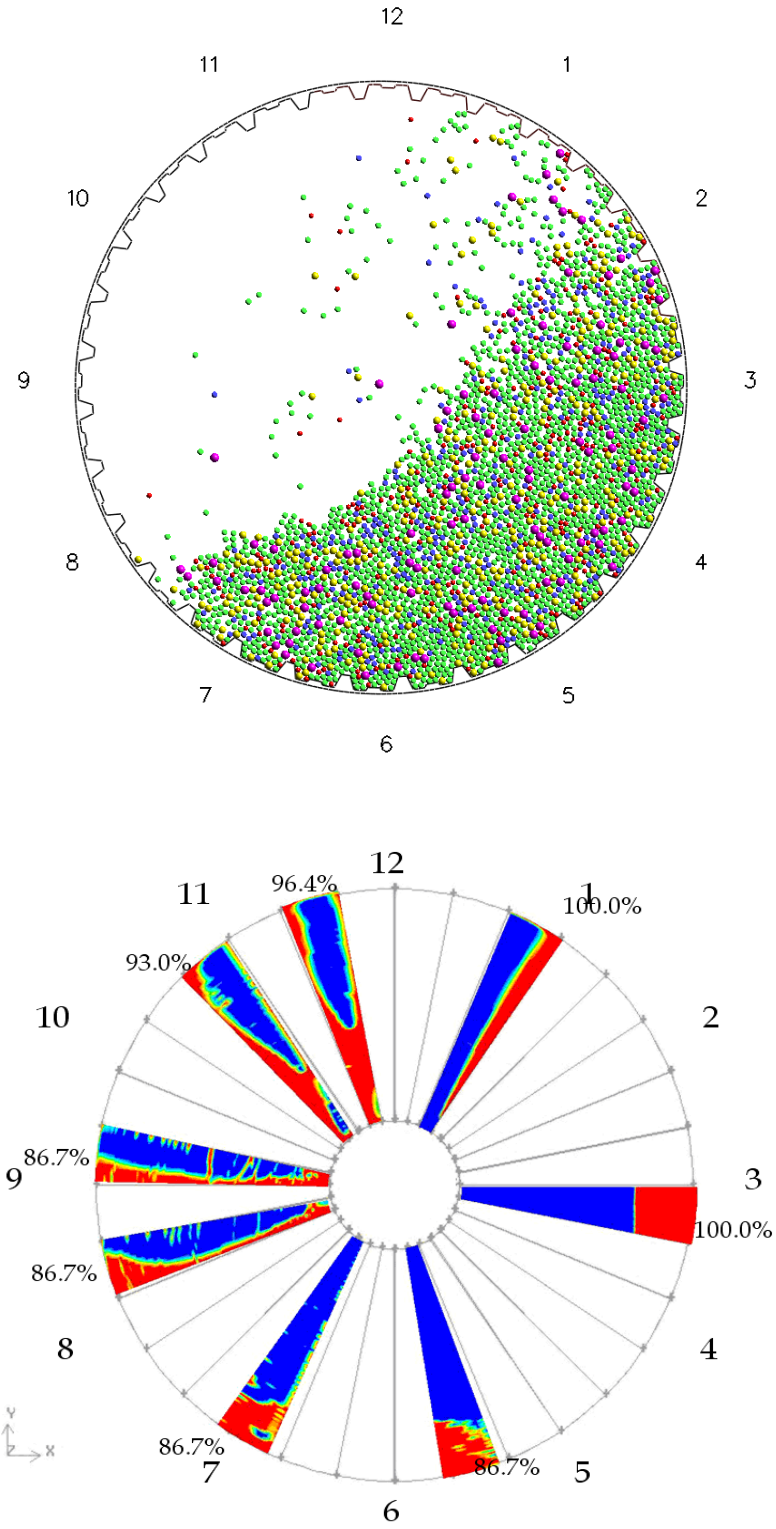

Figure 6.3 – DEM charge profile and CFD prediction of free surface profiles as the mill discharges, Los Bronces SAG mill (Diameter 10.12 m and length 4.722 m)

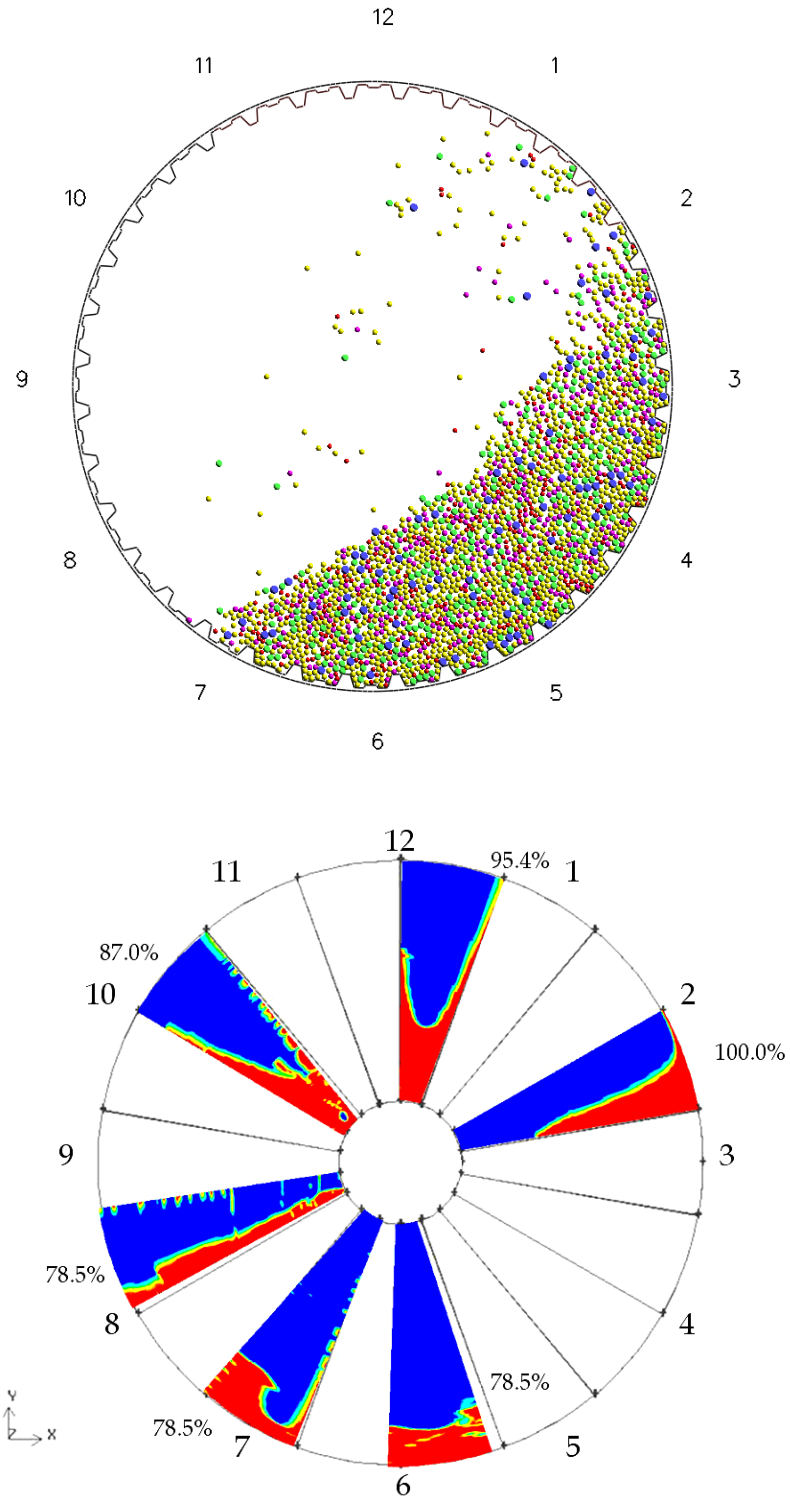

Figure 6.4 – DEM charge profile and CFD prediction of free surface profiles as the mill discharges, Gold ore SAG mill (Diameter 10.81 m and length 4.95 m)

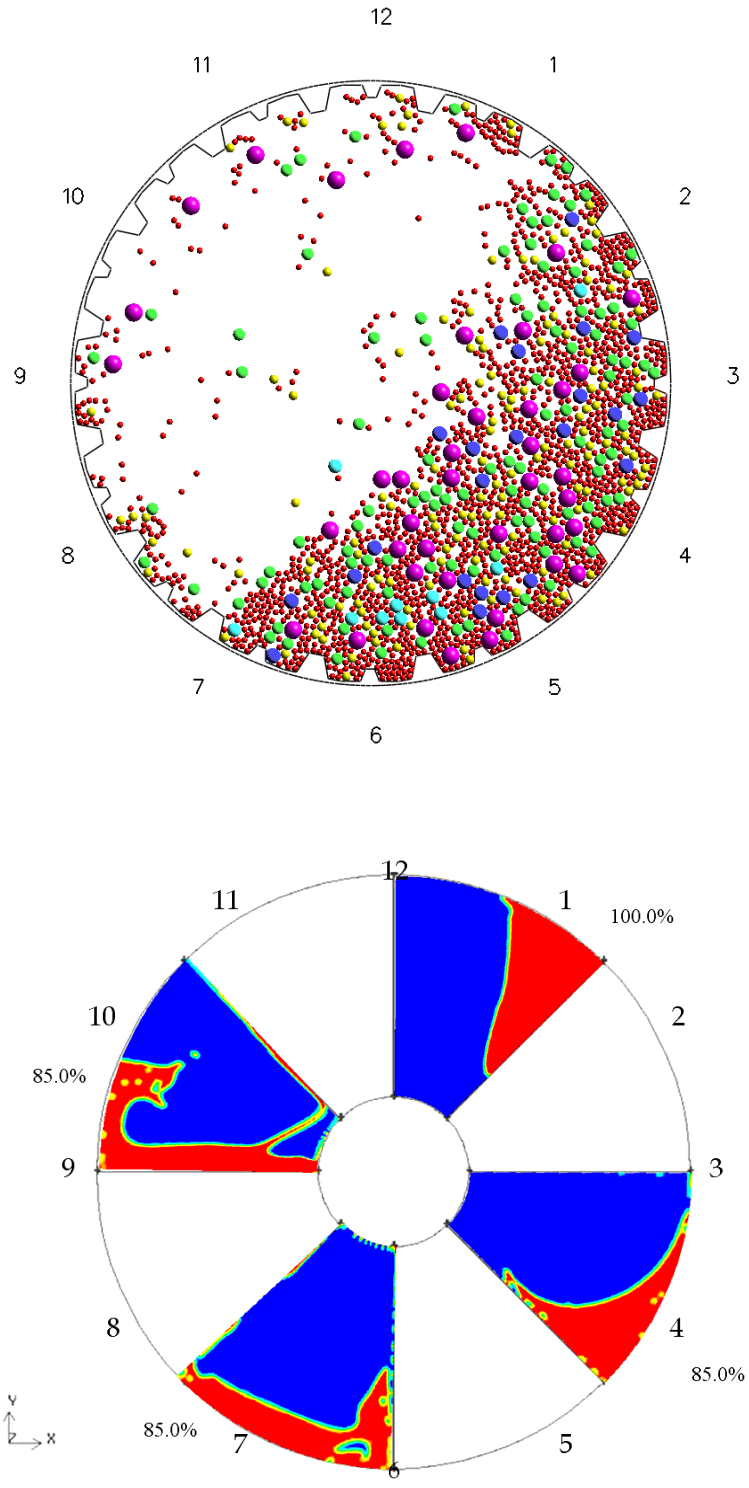

Figure 6.5 – DEM charge profile and CFD prediction of free surface profiles as the mill discharges, Navachab SAG mill (Diameter 4.72 m and length 9.49 m)

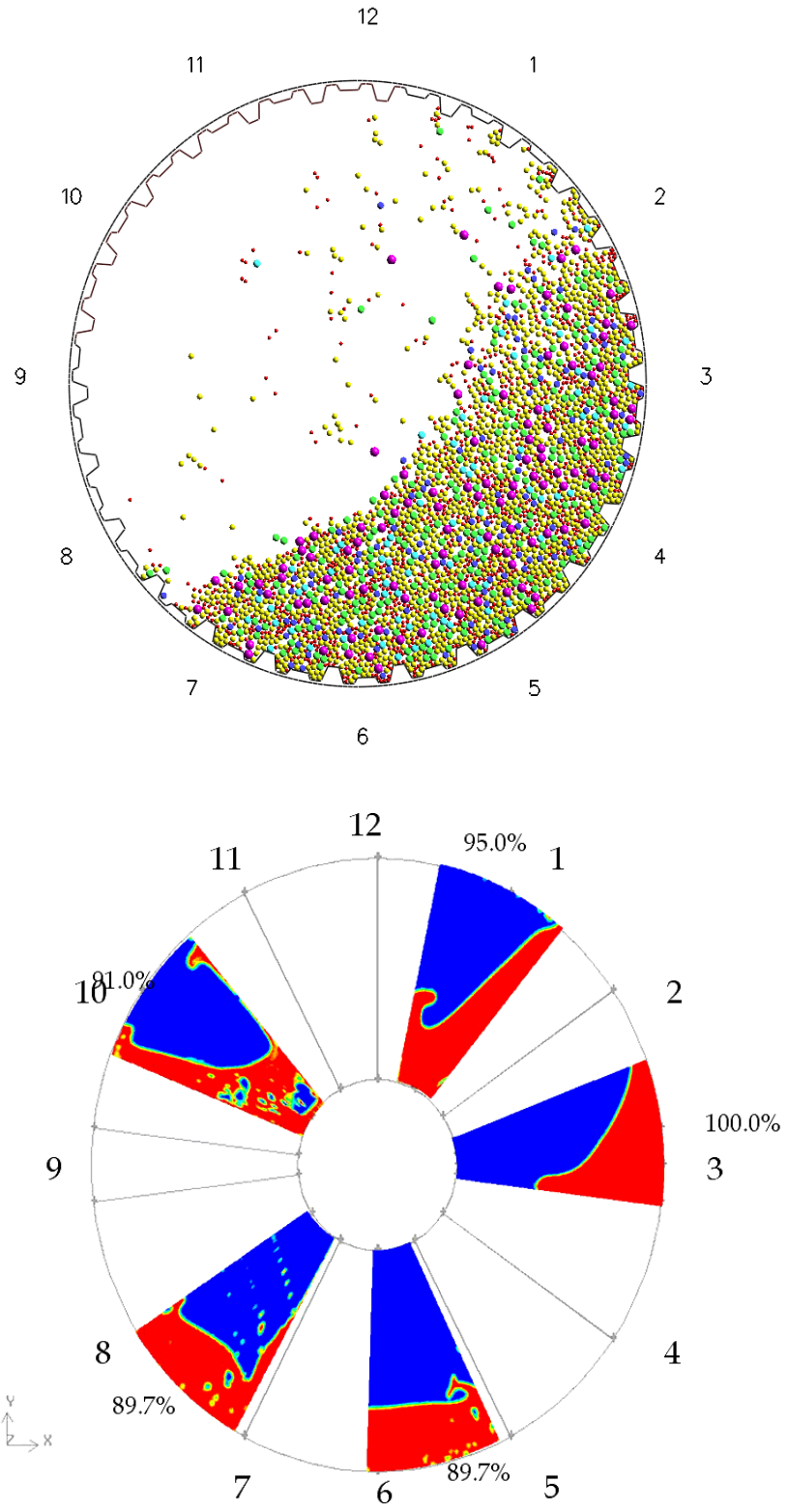

Figure 6.6 – DEM charge profile and CFD prediction of free surface profiles as the mill discharges, Morila OC SAG mill, 66% solids (Diameter 7.8 m and length 5.47 m)

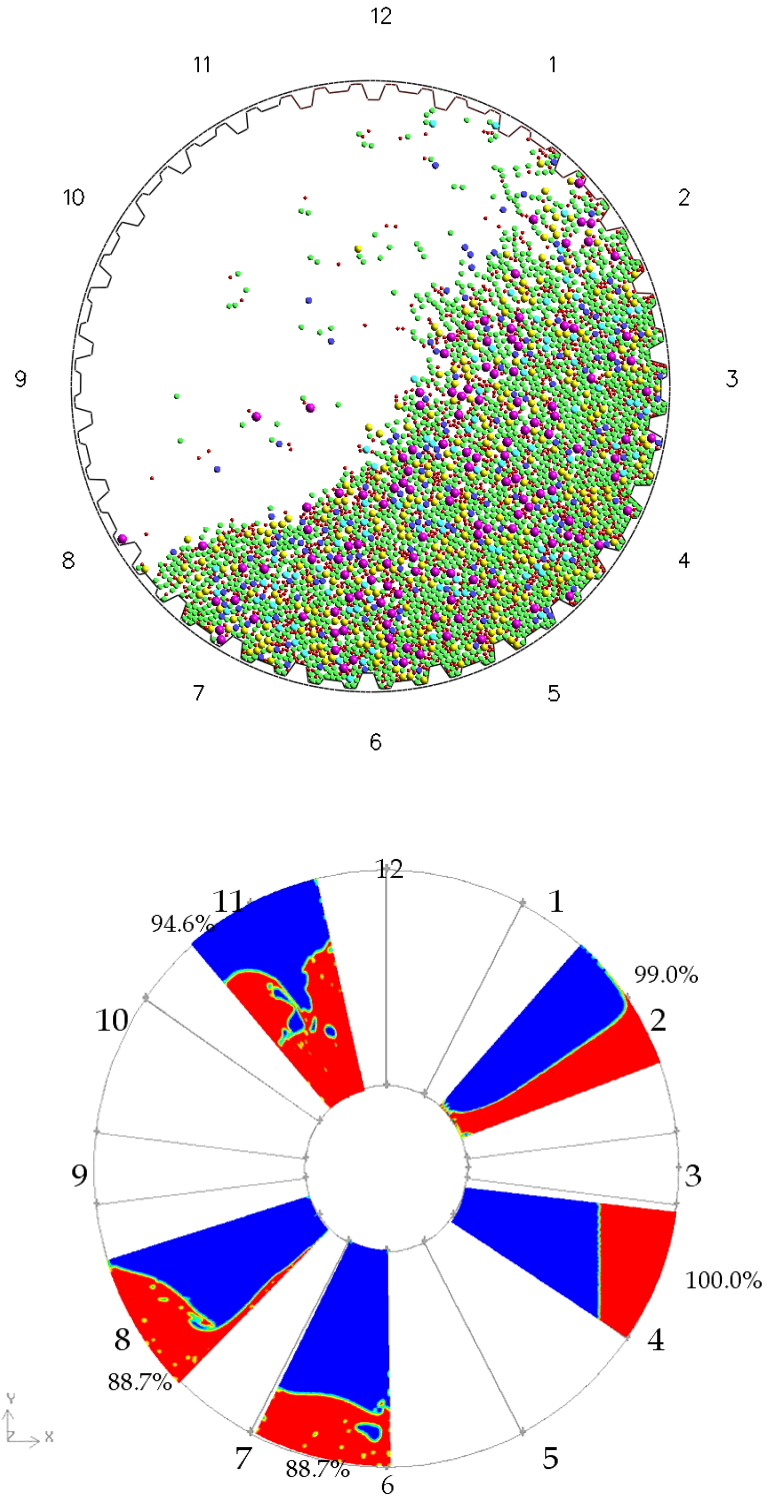

Figure 6.7 – DEM charge profile and CFD prediction of free surface profiles as the mill discharges, Morila OC SAG mill, 79% solids (Diameter 7.8 m and length 5.47 m)

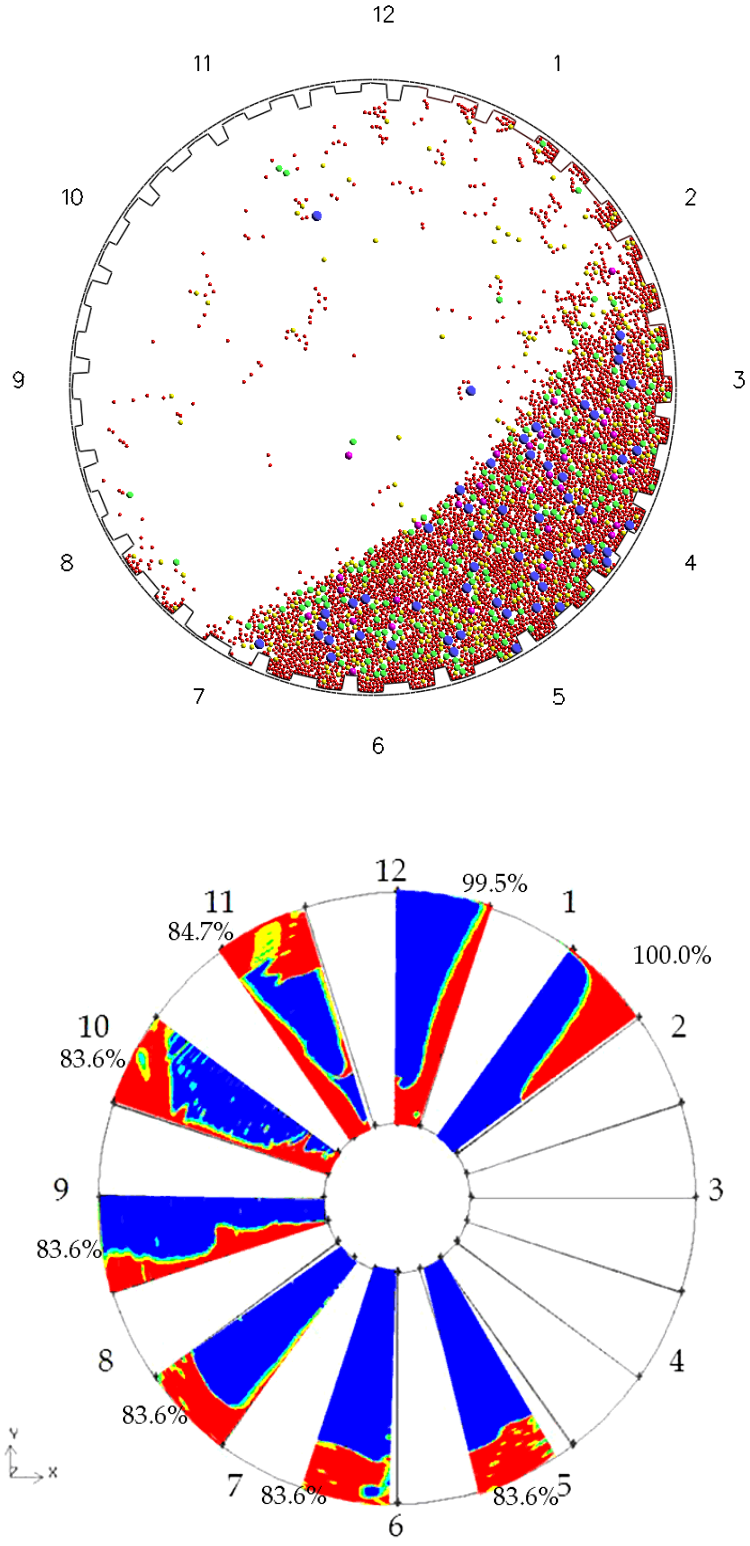

Figure 6.8 – DEM charge profile and CFD prediction of free surface profiles as the mill discharges, UG2 AG mill (Diameter 5.92 m and length 7.1 m)

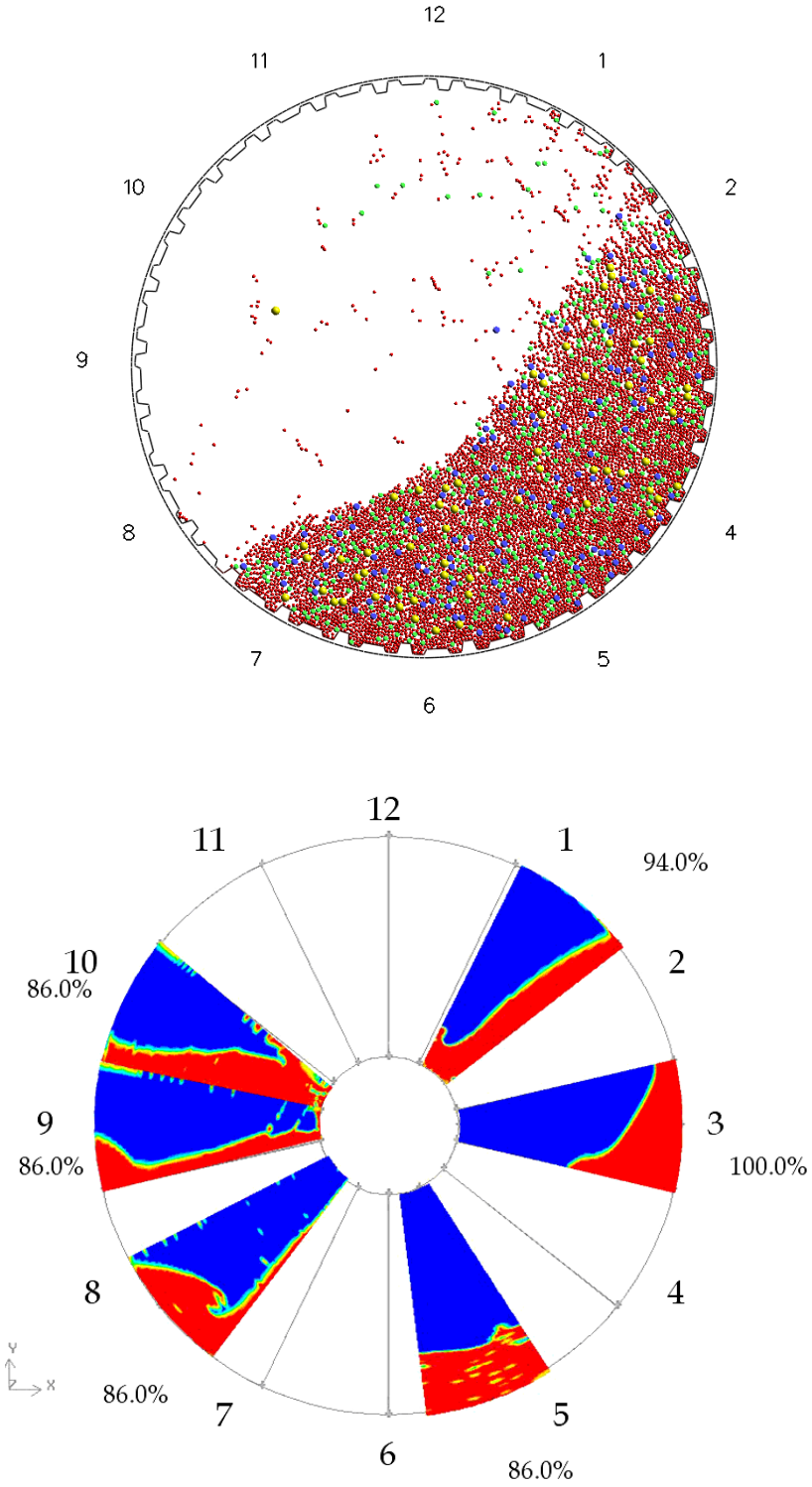

Figure 6.9 – DEM charge profile and CFD prediction of free surface profiles as the mill discharges, Lead/ Zinc/ Silver AG mill (Diameter 8.37 m and length 4.03 m)

As observed on the mill circles, the discharge towards the mill center starts at around the 1 o'clock – 12 o'clock regions in counterclockwise rotation; once the channel passes over the horizontal at the 9 o'clock region the discharge stops and the remaining slurry levels out in the pulp lifter channel. Approximately 15 to 20% of the fluid volume in the pulp lifter channel, on the average, is discharged in one full revolution. The comparisons of survey data and CFD predictions for volumetric flow rate, in terms of cubic meters per hour, and solid flow rate, in terms of tons per hour, are given in Table 6.1. In the first, left, two columns of the table, the survey data and CFD predictions are compared in terms of volumetric flow rate while the comparison based on the solids flow rate is given in the last, right, two columns. For instance, the volumetric flow rate for the Lead/Zinc/Silver AG mill is given by the survey data is 600 $m^3.h^{-1}$, and CFD predicted volumetric flow rate for the mill is 536 $m^3.h^{-1}$, which corresponds to 89% of flow rate in the survey data. It is seen that CFD predictions are, on the average, of 87% of flow rates in the survey data. Quantitatively analyzing the results, it is seen that the effects of the pulp lifter channel volume and the percent critical speed are significant. Also, the slurry properties are important in determining the volumetric flow rate. The percent critical speed and the volumetric flow rate imply an inverse relation, as would be expected. The volumetric flow rate increases as the pulp lifter channel volume increases. The slurry properties, slurry density and slurry viscosity, are identified as the secondary variables affecting the volumetric flow rate. The volumetric flow rate increases with increasing slurry density, however to a relatively much lesser extent.

Table 6.1 – Volumetric flow rate results: Published data (Powell & Valery 2006) vs. CFD predictions

	Volumetric flow rate ($m^3.h^{-1}$)		Solid flow rate (tph)	
	Survey data	CFD prediction	Survey data	CFD prediction
Los Bronces	841	754	919	823
Los Bronces	1322	1152	1505	1312
Gold ore	1318	1134	1781	1532
Morila OC	424	354	482	403
Morila OC	403	371	640	586
Navachab	306	224	425	311
UG2 AG mill	221	230	401	417
Lead/ Zinc/ Silver AG mill	600	536	1190	1063

The effect of slurry viscosity is intuitive. The resistance to flow increases as the viscosity increases, and also the turbulent momentum transfer is notably controlled by the shear stresses, hence the viscosity. To put it another way, the turbulence is characterized by high Reynolds numbers. The Reynolds number is a dimensionless number quantifying the ratio of inertial forces to viscous forces; the viscous forces are represented by the dynamic viscosity in the formulation. It is evident that the viscous forces do influence the pulp flow dynamics since the turbulence is represented by Reynolds stresses, which in turn are directly or indirectly formulated in terms of viscosity. The pulp lifter assembly for the ArcelorMittal Mont-Wright AG mill is shown by Figure 6.10. Here, the pulp lifter assembly is made up of thirty-six channels in the outer periphery.

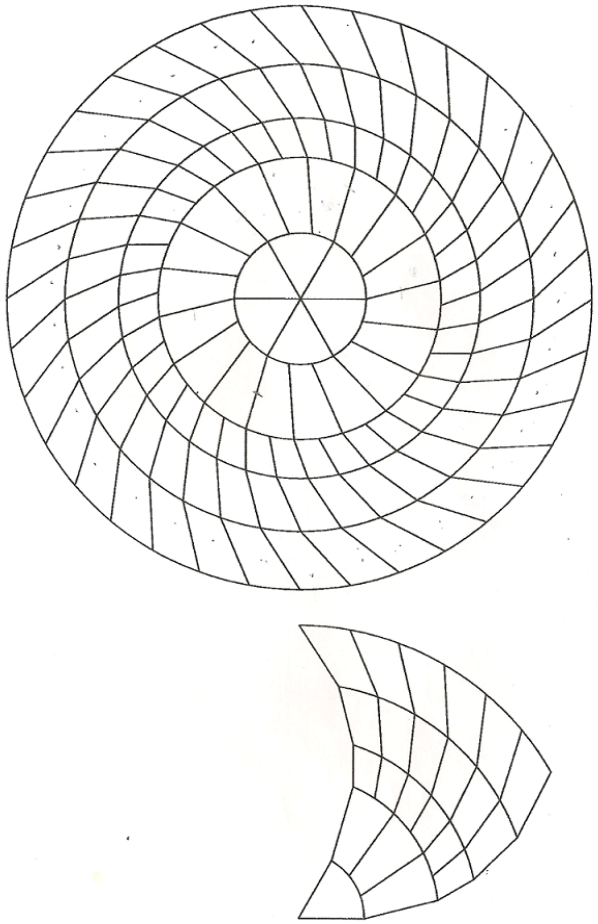

Figure 6.10 – Pulp lifter assembly for the ArcelorMittal Mont-Wright AG mill

As the assembly extends from the periphery to the interior, two adjacent pulp lifter channels are combined into one, resulting in the representation of the assembly by eighteen larger channels. Finally, the assembly is made into six larger pulp lifter channels in the most interior part of the structure. Figure 6.11 shows the DEM-CFD profiles for the ArcelorMittal Mont-Wright AG mill. Accordingly, two channels converging into one has been constructed with GAMBIT in the CFD computation. The CFD predictions on the ArcelorMittal Mont-Wright AG mill data yield a volumetric flow rate of 1631 $m^3.h^{-1}$ (1274 tph) in comparison to on-site survey data of 1630 $m^3.h^{-1}$(1273 tph).

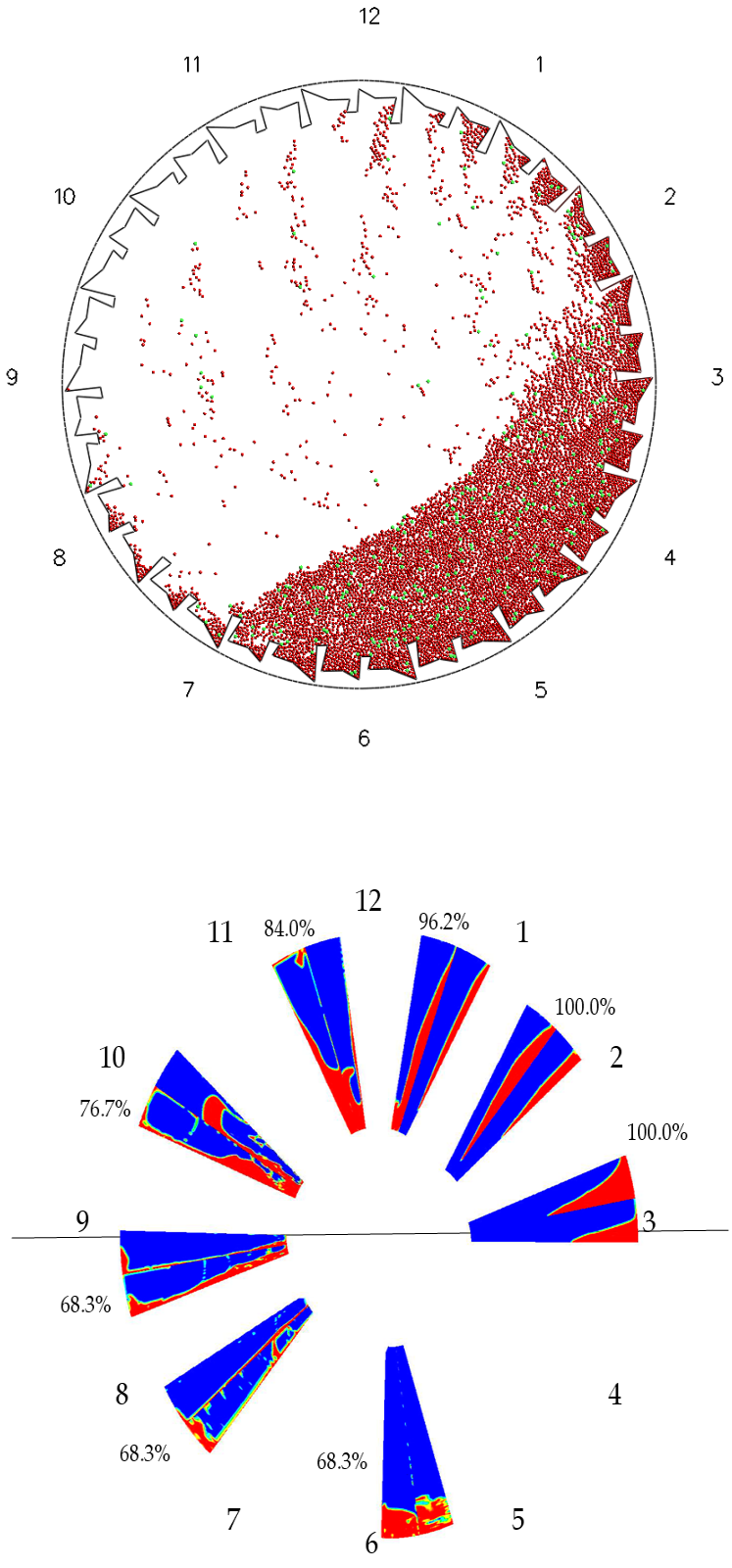

Figure 6.11 – DEM charge profile and CFD prediction of free surface profiles as the mill discharges, ArcelorMittal Mont-Wright AG mill (Diameter 9.76 m and length 3.5 m)

In general, CFD predictions for volumetric flow rates are lower than the survey volumetric flow rates, showing that the simplified approach does not fully describe the process. Other than that, absence of solids in modeling influences the quality of predictions since the turbulence induced by solids affects the flow behavior significantly. That proves, on the one hand, that the description of the physical process on a one-on-one basis to the best possible extent in computational modeling is crucial. On the other hand, it is also important that the pulp flow modeling includes both solids and fluid so that the process is described in much detail.

6.1. Summary

Applications of the CFD methodology on plant scale mills are presented in the current chapter. The simulation results are given in terms of DEM profiles for charge motion and CFD discharge profiles for the slurry. The pulp lifter channel volume, the percent critical speed, and the slurry properties are distinguished as the most significant variables in determining the volumetric flow rate. The volumetric flow rate increases as the pulp lifter channel volume and slurry density increase whereas an increase in percent critical speed causes a decrease in the volumetric flow rate. The CFD predictions are reassuring in the sense that not only the volumetric flow rate is closely captured, but also the simulation results provide free surface profiles inside the pulp lifter assembly. The nonlinear features of the flow behavior are once more verified by the results; although the variables affecting the process and relative significance can be identified, it is hard to relate to distinct patterns which would enable one to anticipate the outcome based on the input. It is only possible to make some qualitative predictions.

CHAPTER 7

SUMMARY AND CONCLUSIONS

Computational fluid dynamics methodology for assessing the free surface profiles and volumetric flow rate out of the mill has been presented. The transient multiphase turbulent pulp flow in the pulp lifter channel has been modeled by the use of the volume of fluid model for multiphase flow and standard $k - \varepsilon$ model for turbulence. The simulations were computed on a multiprocessor system in view of the computational power needed to simulate the entire pulp lifter assembly. The superposition principle was used to represent the whole system using the computed results from a single pulp lifter channel.

The experimental results have been provided for validation of the accuracy of the simulation results. The methodology was also employed for plant scale analyses. CFD predictions captured both the free surface profiles and volumetric flow rates of plant scale mills.

The results indicate the significance of the mill rotational speed on the discharge performance and hence on mill throughput.

The effective discharge flow diminishes as the mill rotational speed is increased; the mill should be operated at subcritical speed for optimum discharge (Mokken 1975). However, the breakage rate is diminished as the mill rotational speed is decreased.

Concisely, the mill rotational speed should be set such that the breakage rate and discharge rate are balanced. Both the ease and the rapidness add to the advantages of CFD simulations. The operational and the design parameters can be varied as required to gain insight into resulting volumetric flow rate as the mill rotational speed changes. Consequently, the results obtained by the modeling study of material transport provide a guide to enhance the milling performance.

The pulp lifter channel volume also proves to be important, affecting the volumetric flow rate out of the mill directly. Secondary factors such as the slurry properties do affect the discharge performance, although to a much lesser extent.

CFD analyses shed light on the design and the operations, particularly enabling a detailed understanding of the physics of flow through pulp lifter channels. Provided that the process is accurately described by a physical model with appropriate boundary conditions, it is possible to utilize the proposed model in the design and further modification of current day pulp lifter assemblies.

The flow problem is mainly based on the domain and the boundary. The domain is represented by the geometry of the channel in three dimensions. Also, the characteristic material properties of the flow problem such as density and viscosity are assigned to the domain. The boundary conditions assigned are complementary in defining the flow problem. Further, rotation of the domain and boundaries sets the correct centrifugal and gravitational forces.

Therefore, the correct representation of the channel geometry is important since it is the basis of the CFD computations. That being the case, the proposed model can further be expanded to study the pulp flow associated phenomena, such as flow back and

carry over, identified in Chapter 2. Alternative models for multiphase flow and turbulence modeling can improve the volumetric flow rate predictions.

The flow resistance caused by the presence of solids is one of the most important factors giving rise to momentum loss in the system. In the future, to account for the effect of solids accurately, the porous media model available in FLUENT can be incorporated into the computations instead of mimicking only the slurry effect. Having the viscous loss term and inertial loss term explicitly defined in the formulation, the porous media model can not only enhance the configuration of the domain but also improve the turbulent field calculations.

APPENDIX A

ADDITIONAL DYNAMIC FREE SURFACE PROFILES: EXPERIMENTAL RESULTS AND CFD PREDICTIONS

Additional results for dynamic free surface profile experiments are provided here. Figure A.1 through Figure A.3 present the experimental results accompanied by the CFD predictions for the dynamic free surface profiles of various glycerol solution concentrations with different volume fillings at 11.7 revolutions per minute. The experimental dynamic free surface profiles with corresponding CFD predictions for various glycerol solution concentrations with different volume fillings at 18.4 rpm mill rotational speed are demonstrated by Figure A.4 through Figure A.6 while Figure A.7 through Figure A.9 show the experimental results and the corresponding CFD predictions for various glycerol solution concentrations with different volume fillings at 26.2 rpm mill.

Finally, Figure A.10 through Figure A.12 present the experimental results and CFD predictions for various glycerol solution concentrations with different volume fillings at 34 rpm.

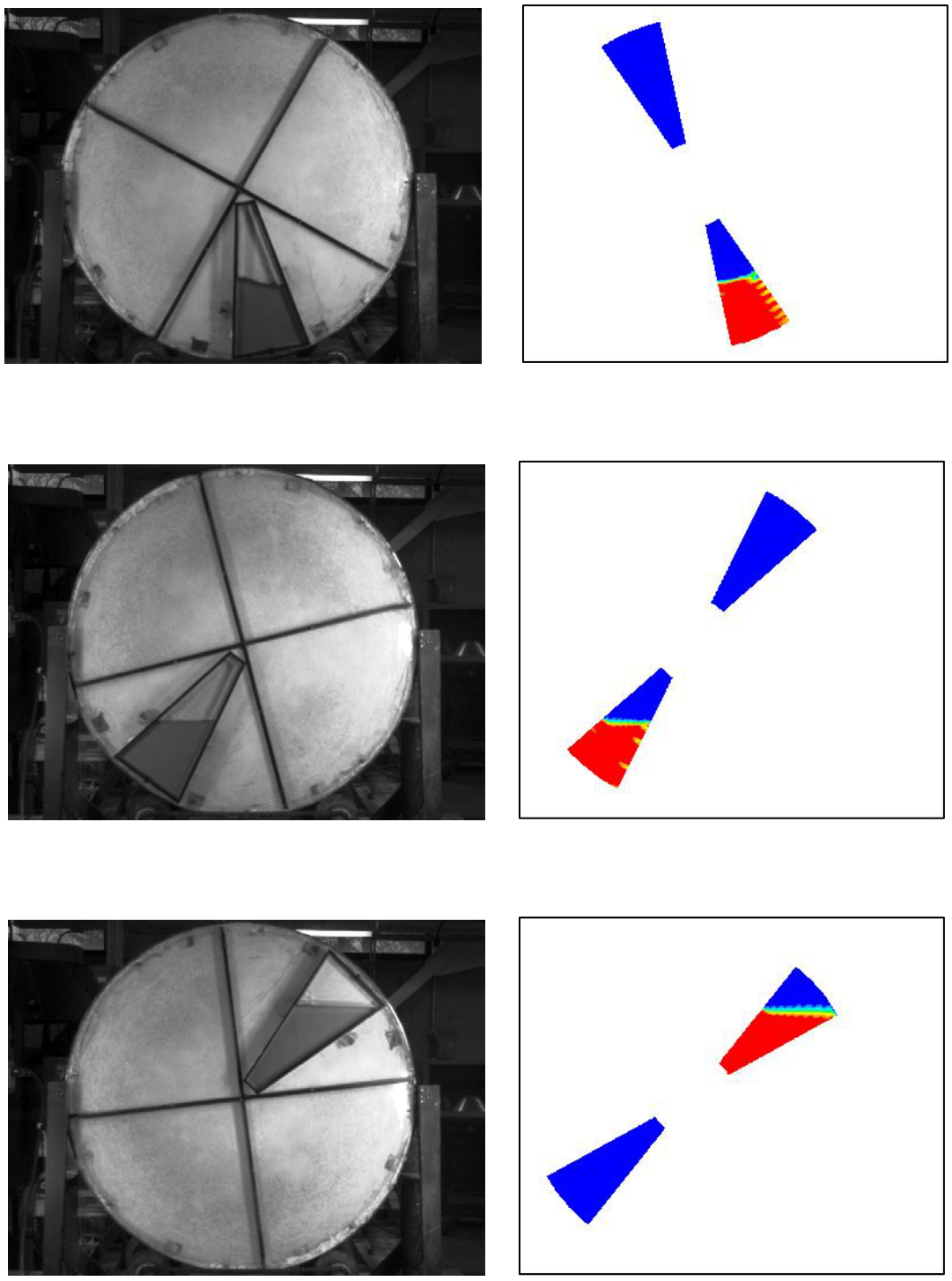

Figure A.1 – Experimental and CFD free surface profiles glycerol solution (75% by volume) with volume filling of 800 cm^3 (61.5% of channel volume) at 11.7 rpm

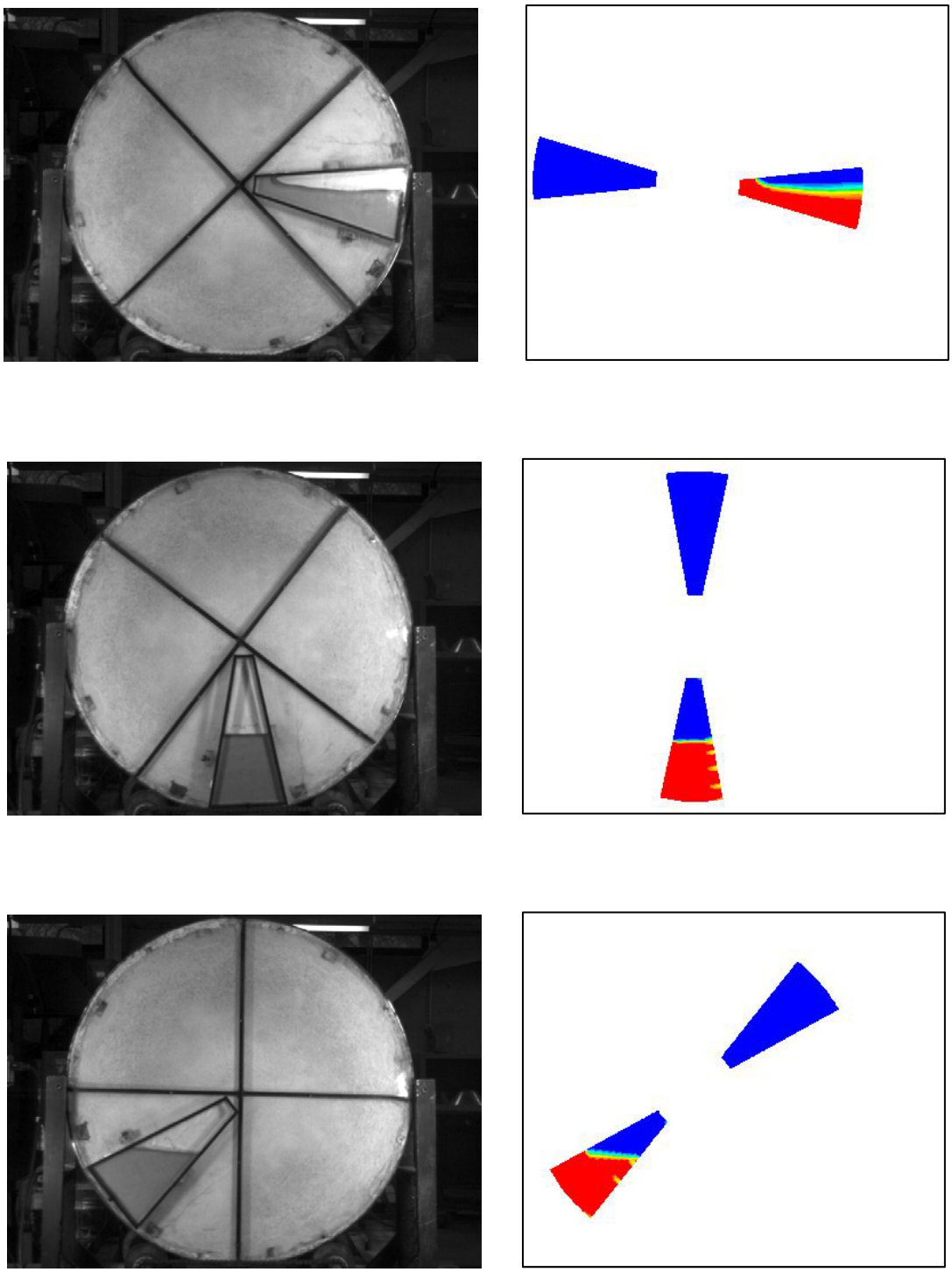

Figure A.2 – Experimental and CFD free surface profiles for glycerol solution (70% by volume) with volume filling of 800 cm^3 (61.5% of channel volume) at 11.7 rpm

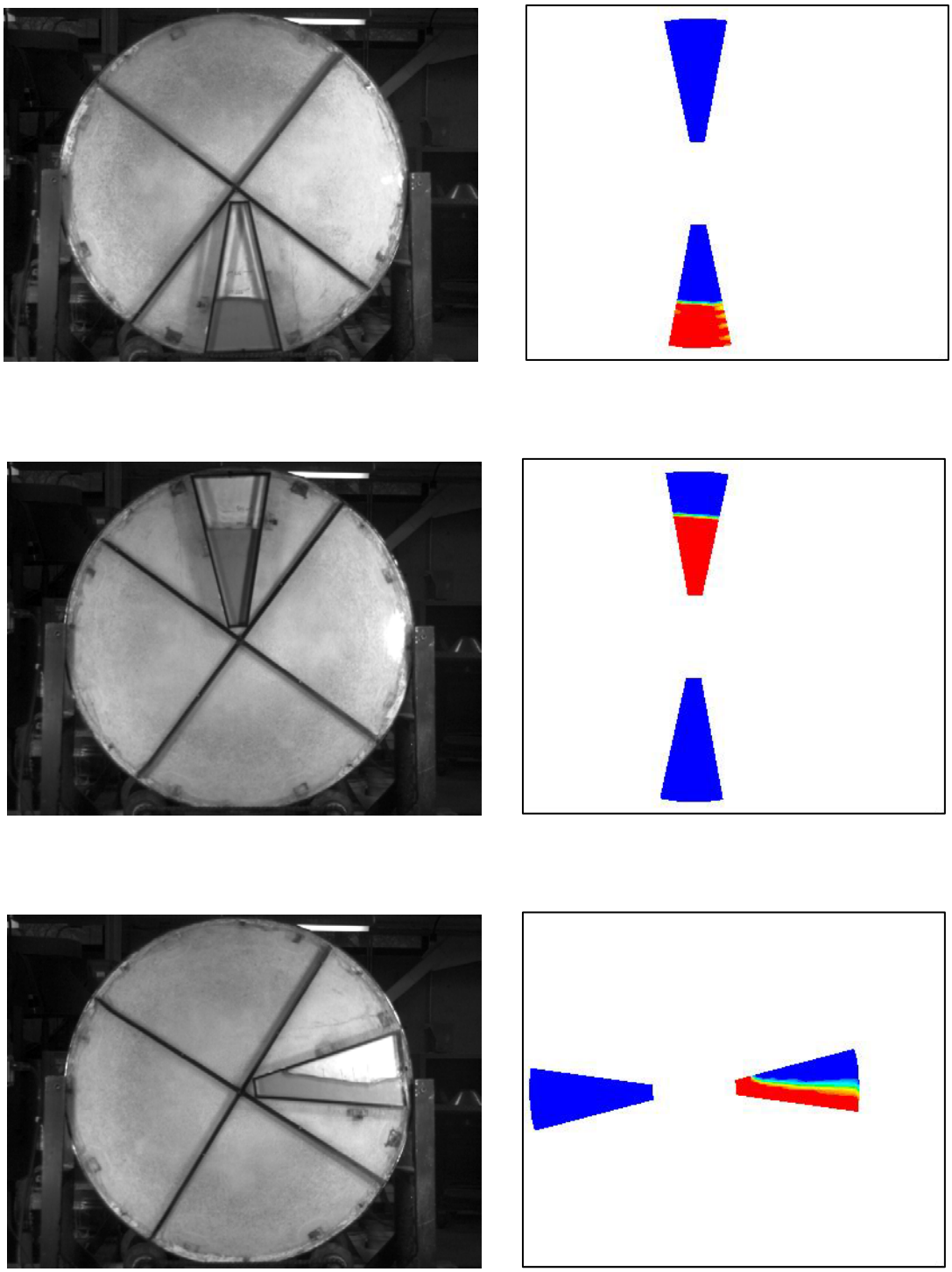

Figure A.3 – Experimental and CFD free surface profiles for glycerol solution (65% by volume) with volume filling of 650cm^3 (50% of channel volume) at 11.7 rpm

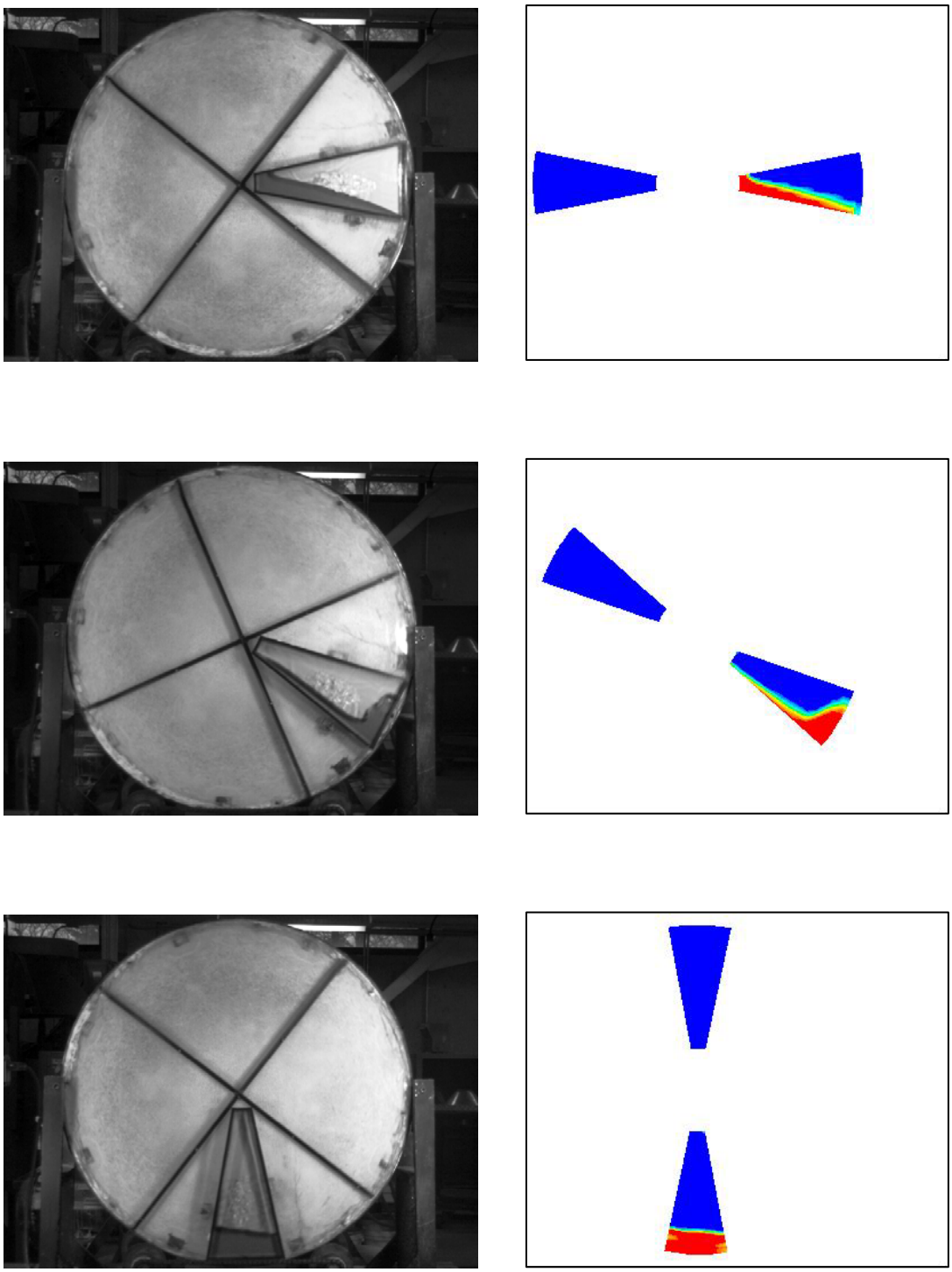

Figure A.4 – Experimental and CFD free surface profiles for glycerol solution (75% by volume) with volume filling of 350 cm^3 (27% of channel volume) at 18.4 rpm

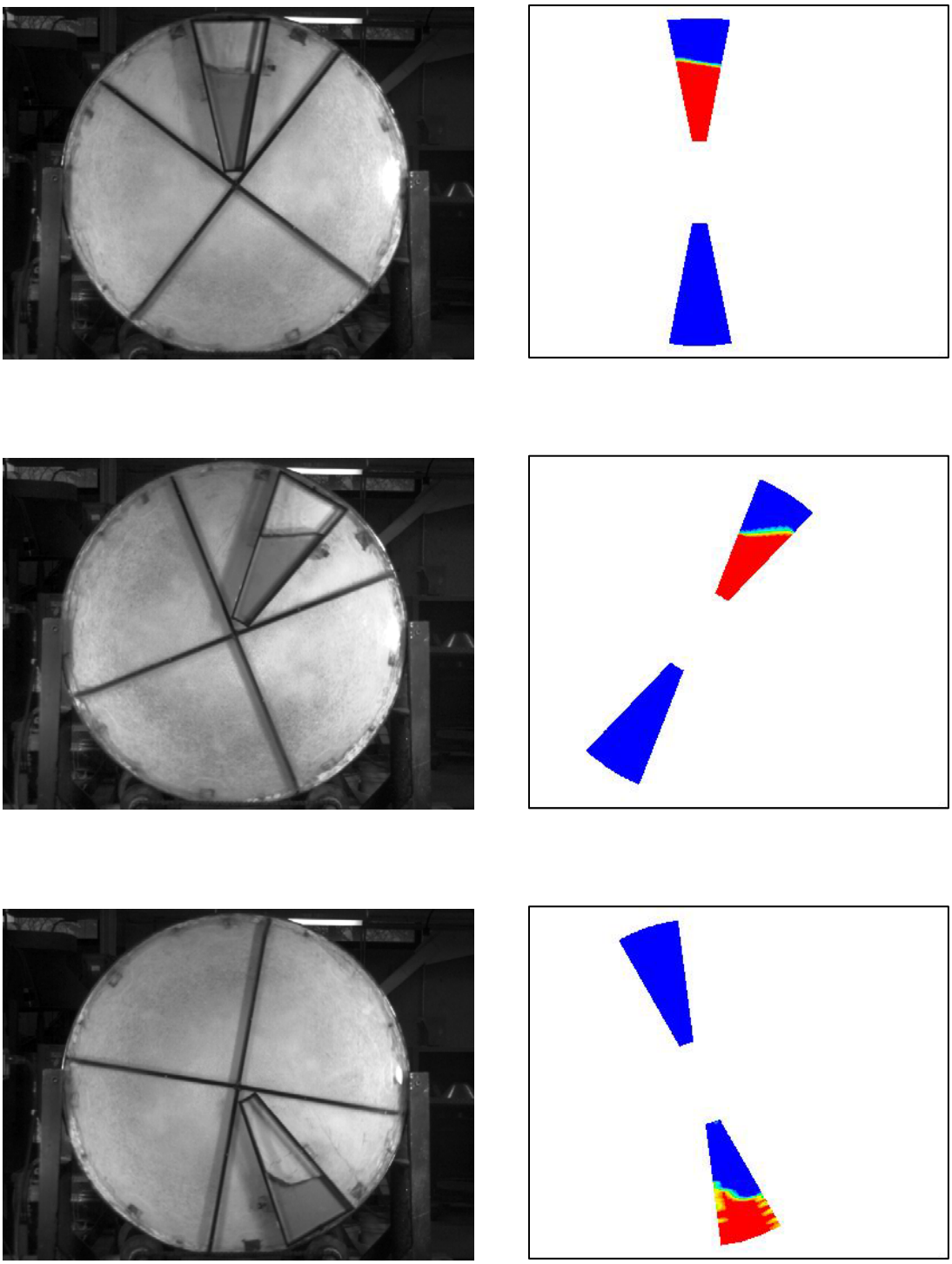

Figure A.5 – Experimental and CFD free surface profiles for glycerol solution (70% by volume) with volume filling of 650 cm^3 (50% of channel volume) at 18.4 rpm

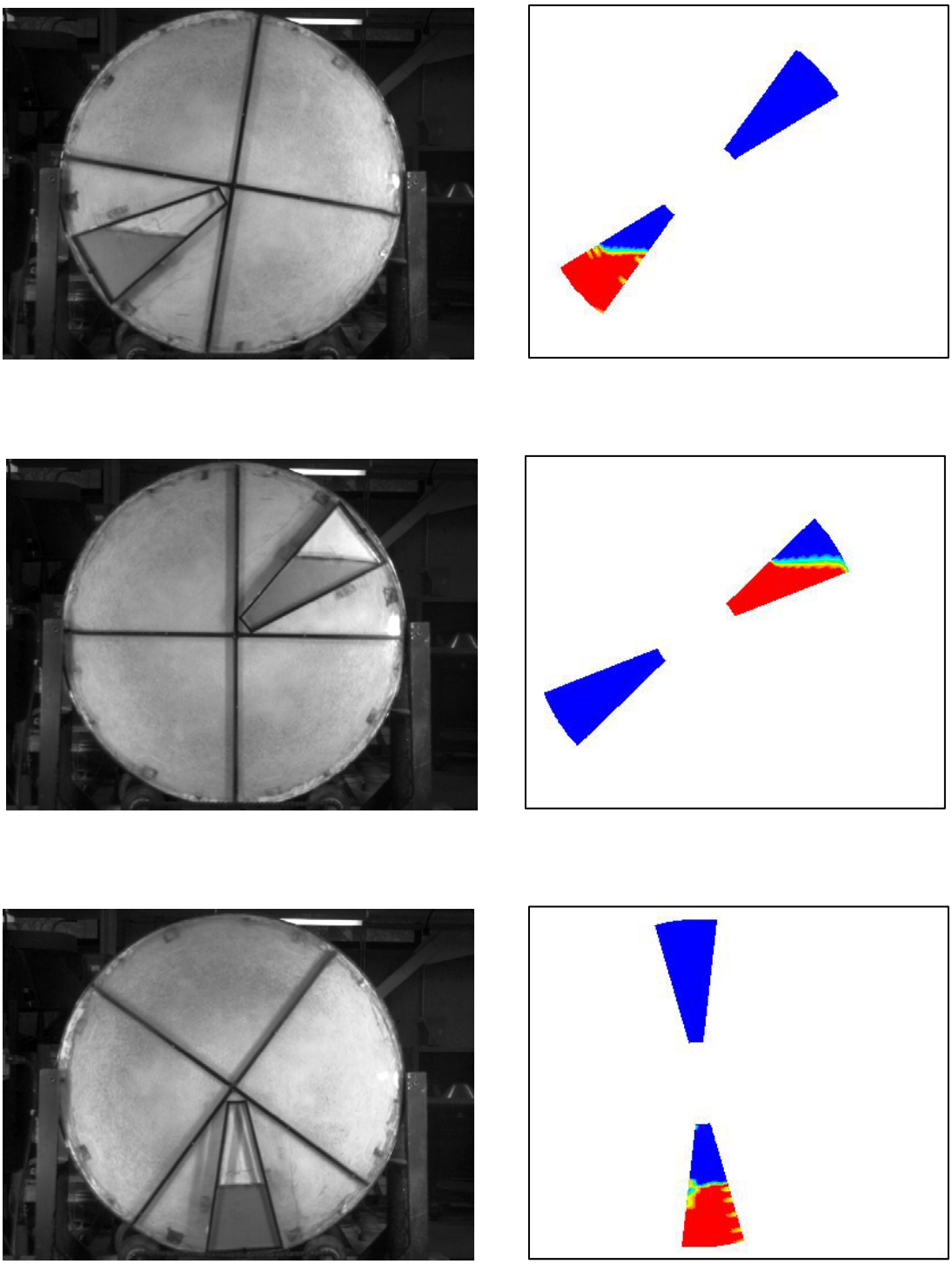

Figure A.6 – Experimental and CFD free surface profiles for glycerol solution (65% by volume) with volume filling of 800 cm^3 (61.5% of channel volume) at 18.4 rpm

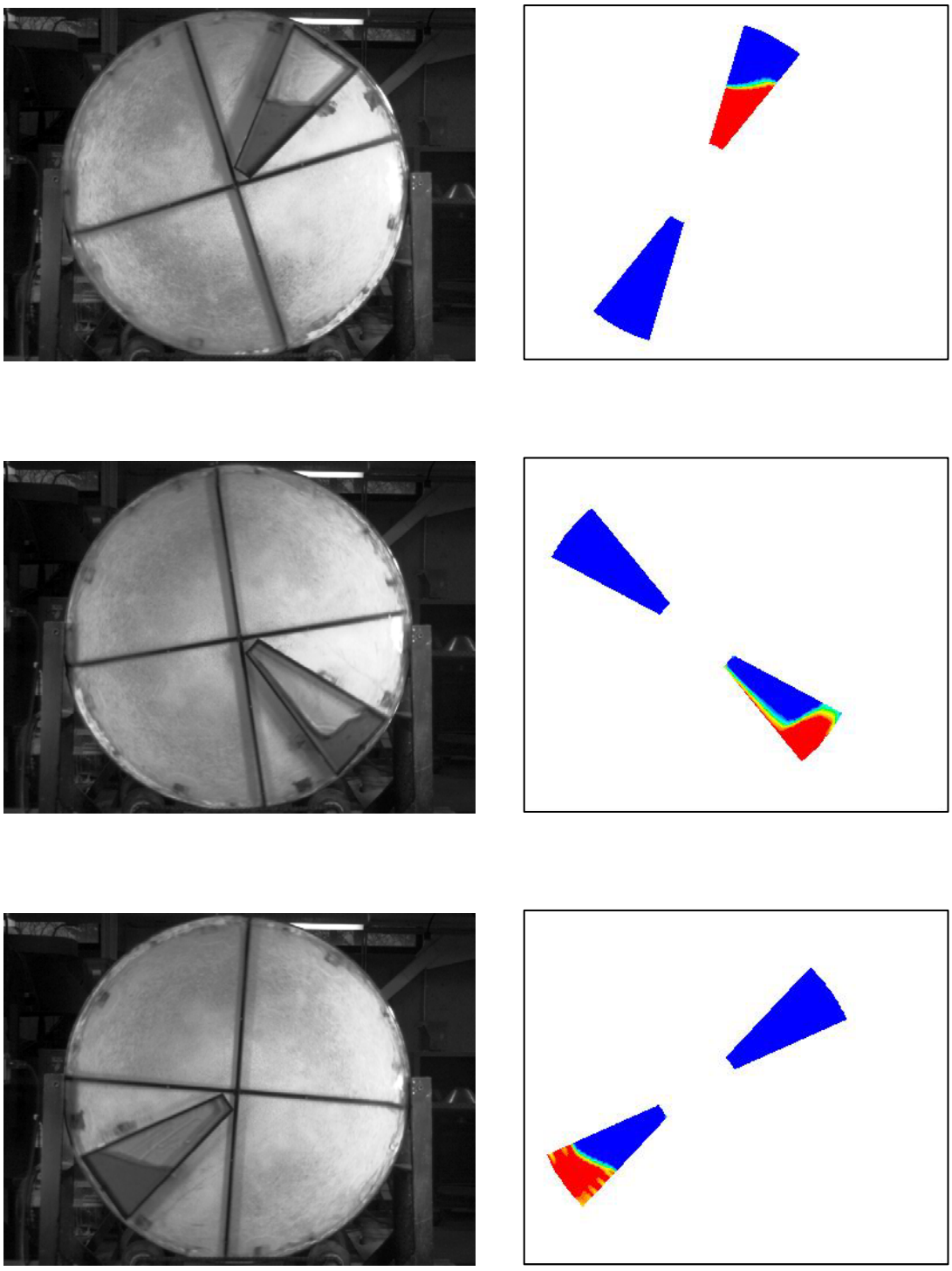

Figure A.7 – Experimental and CFD free surface profiles for glycerol solution (75% by volume) with volume filling of 500 cm^3 (38.5% of channel volume) at 26.2 rpm

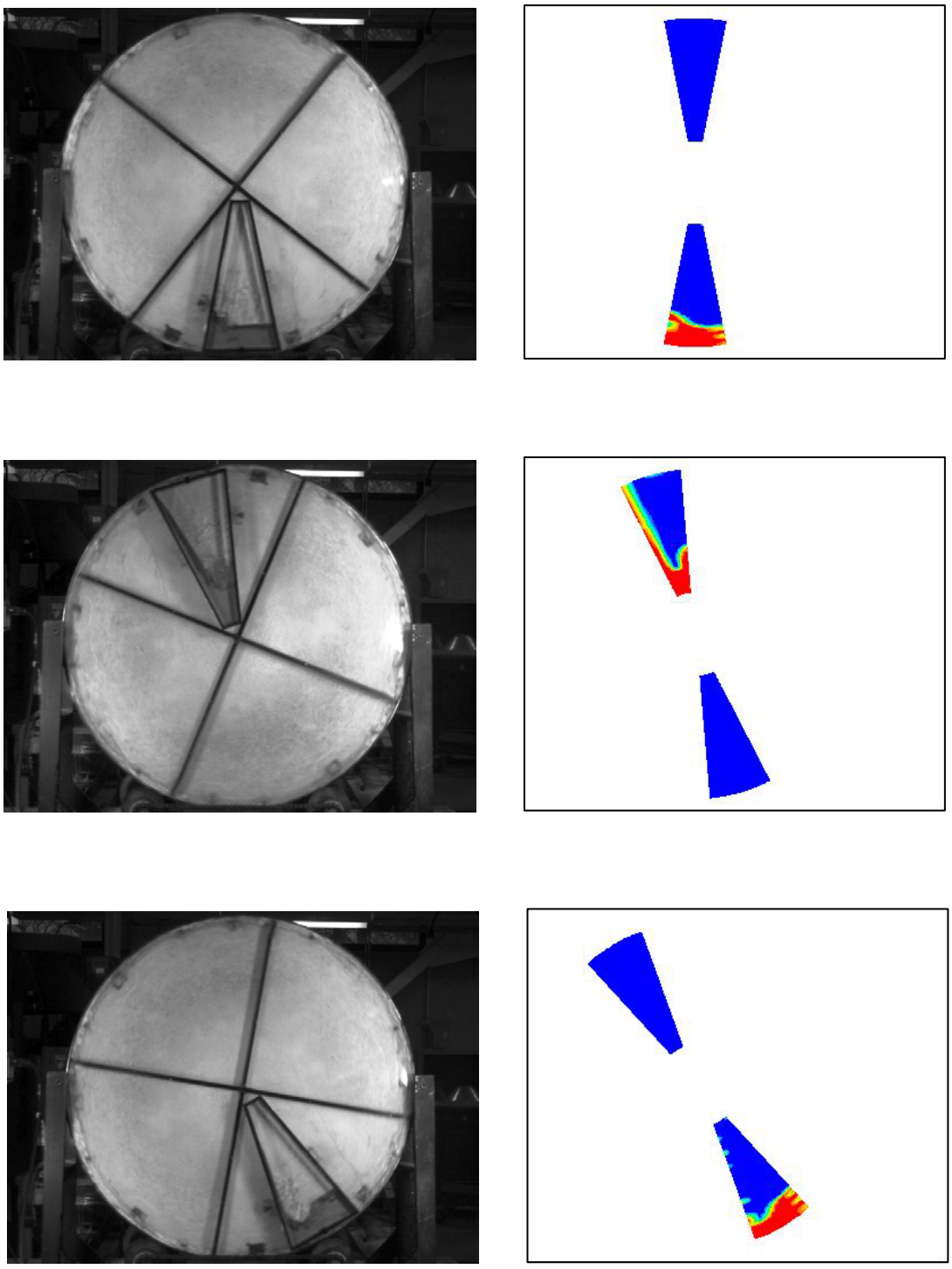

Figure A.8 – Experimental and CFD free surface profiles for glycerol solution (70% by volume) with volume filling of 350 cm^3 (27% of channel volume) at 26.2 rpm

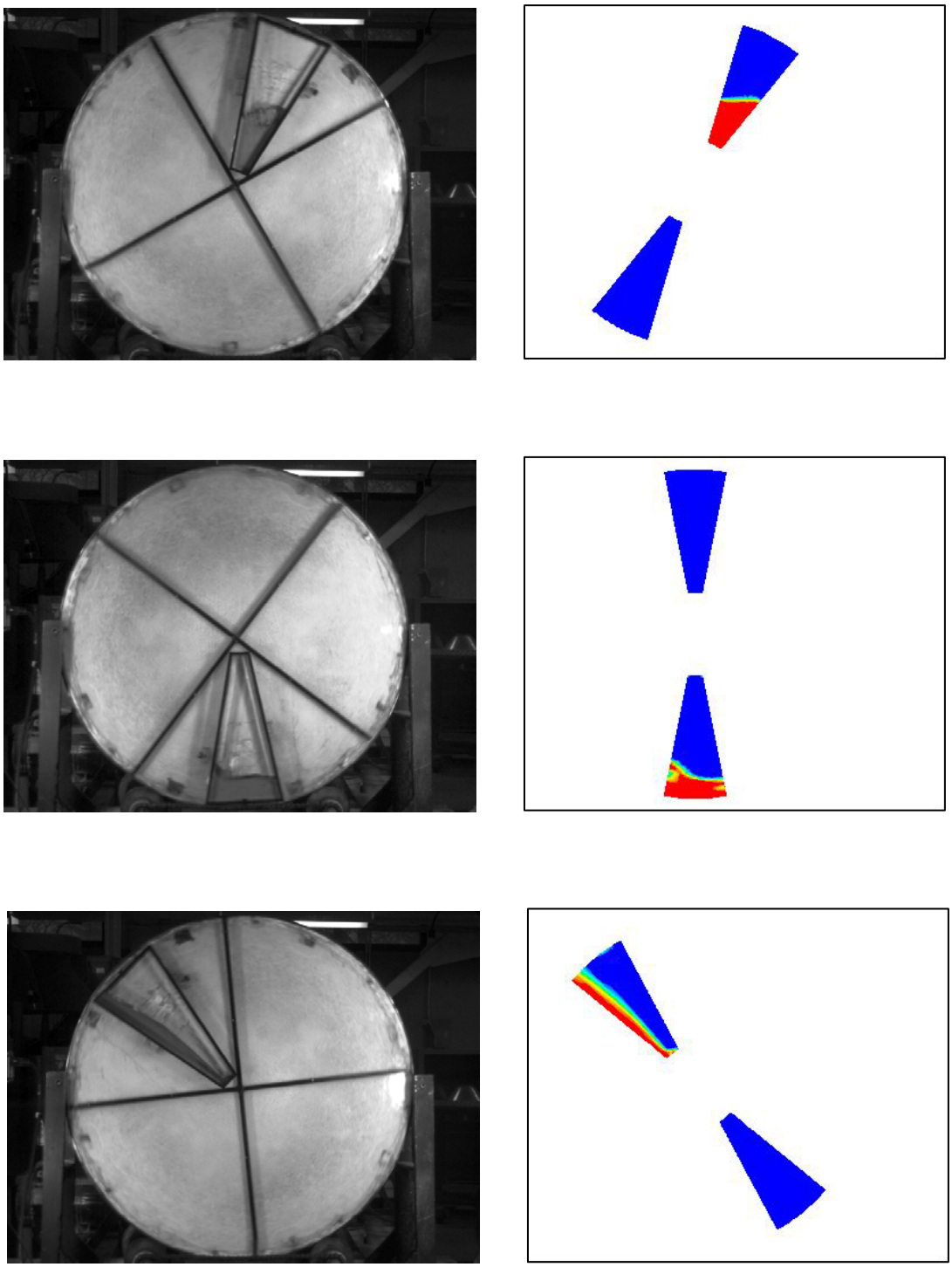

Figure A.9 – Experimental and CFD free surface profiles for glycerol solution (65% by volume) with volume filling of 350 cm^3 (27% of channel volume) at 26.2 rpm

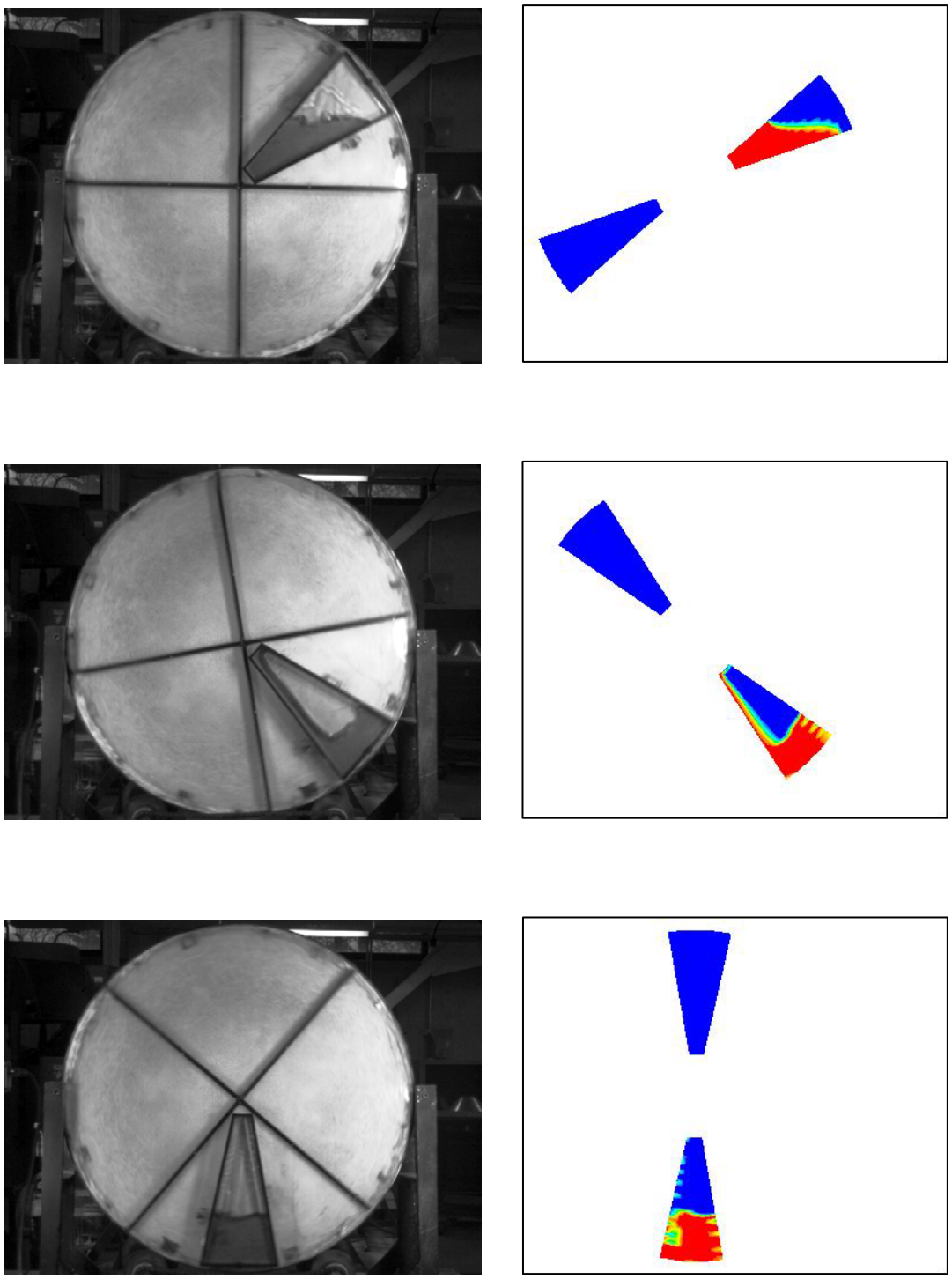

Figure A.10 – Experimental and CFD free surface profiles for glycerol solution (75% by volume) with volume filling of 650 cm^3 (50% of channel volume) at 34 rpm

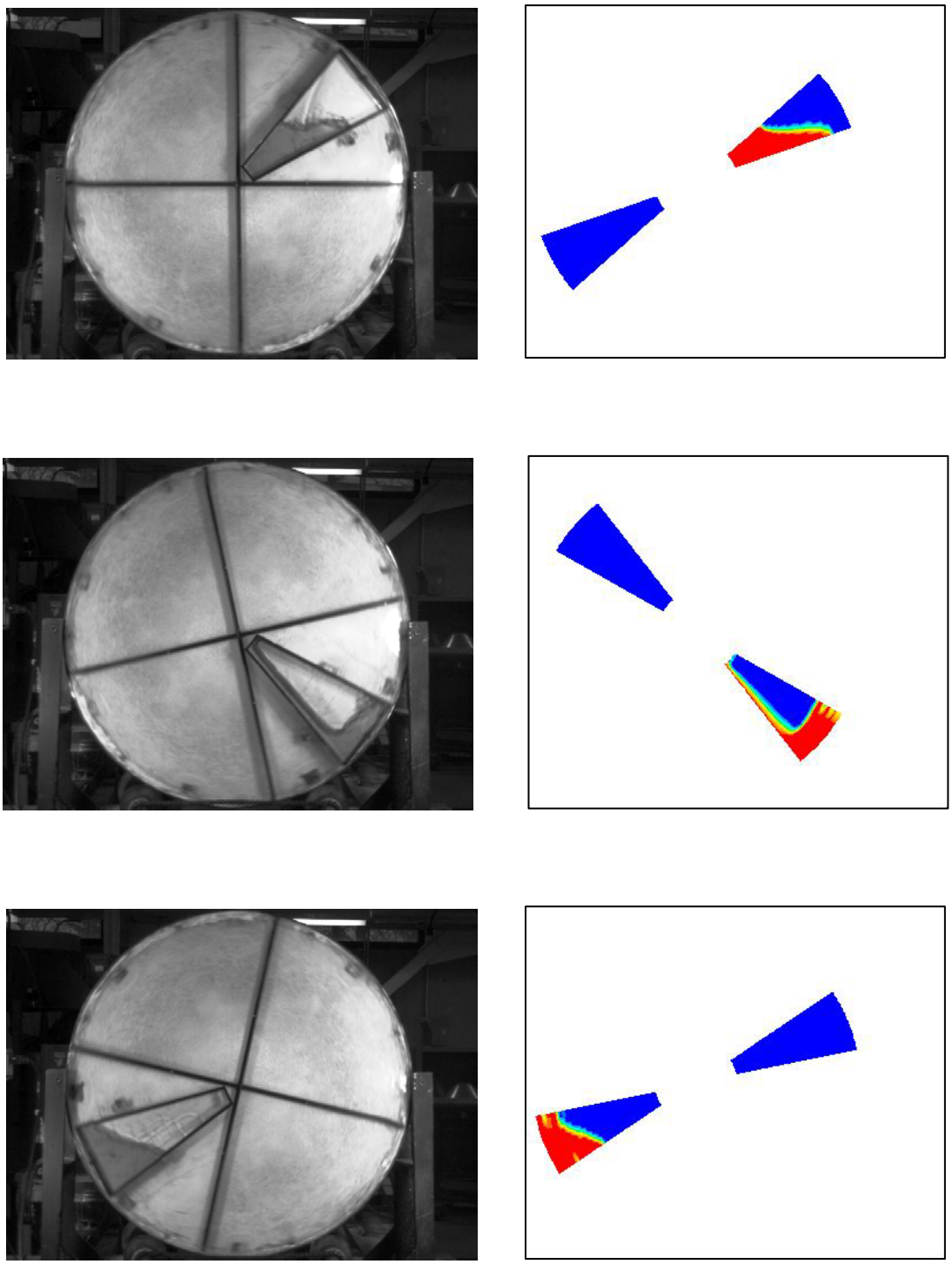

Figure A.11 – Experimental and CFD free surface profiles for glycerol solution (70% by volume) with volume filling of 500 cm^3 (38.5% of channel volume) at 34 rpm

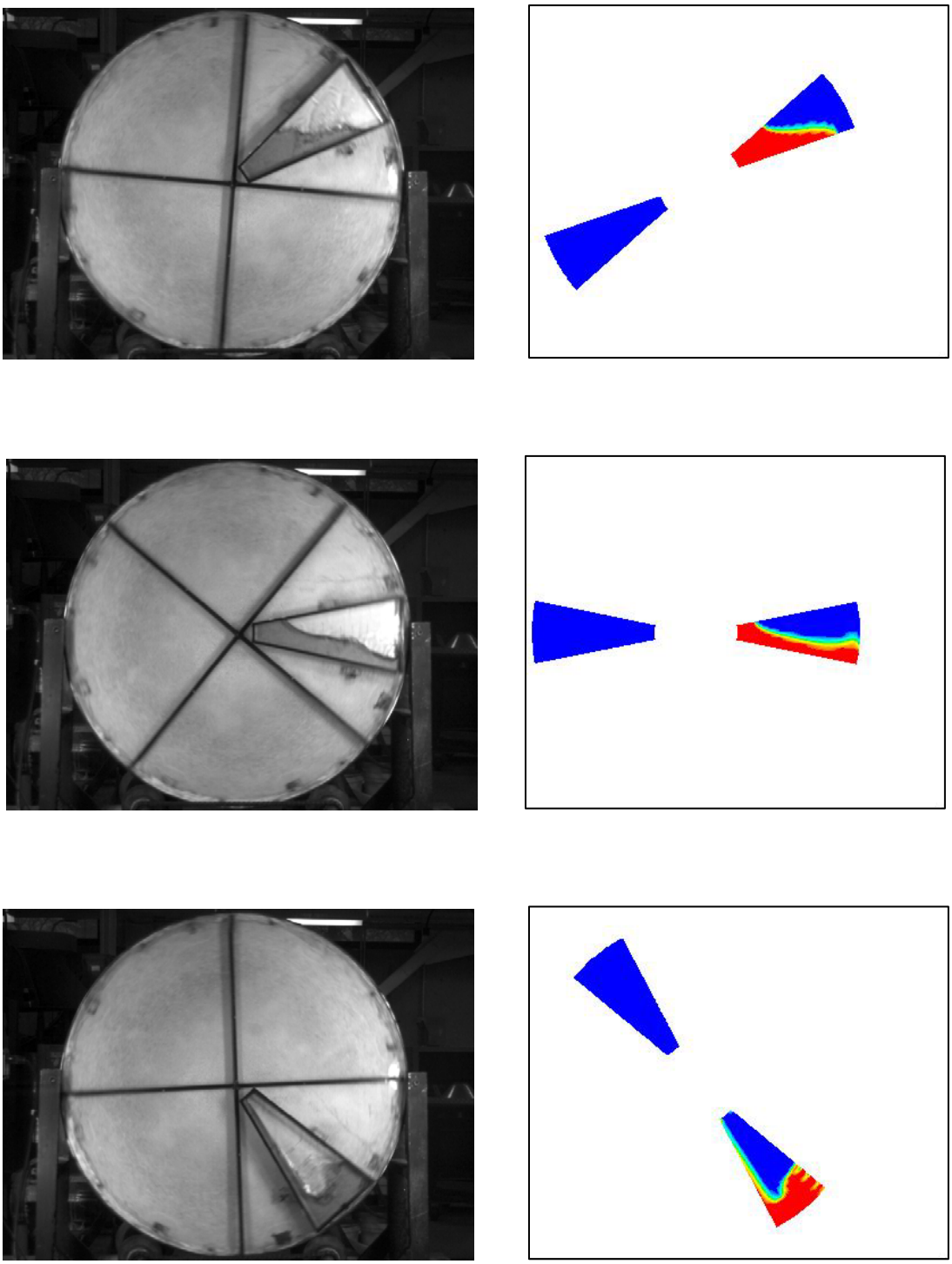

Figure A.12 – Experimental and CFD free surface profiles for glycerol solution (65% by volume) with volume filling of 500 cm^3 (38.5% of channel volume) at 34 rpm

APPENDIX B

EXPERIMENTAL DATA FOR THE DYNAMIC DISCHARGE PROFILE EXPERIMENTS

The experimental data for the dynamic discharge profile experiments are shown in Table B.1, Table B.2, and Table B.3.

Table B.1 specifies the data for the experiments run with two holes at 26.2 revolutions per minute and 34 rpm while Table B.2 demonstrates the data for the experiments run with two holes at 26 rpm, 29 rpm, 32 rpm, and 35 rpm mill rotational speeds. Table B.3 presents the data for the experimental runs with three holes at 26 rpm, 29 rpm, 32 rpm, and 35 rpm.

Table B.1 – Volume of discharge recorded for glycerol solution (85% by volume) (μ = 61 mPa.s) in experiments

Test	Speed (rpm)	Initial volume (cm^3)	Volume discharged in one revolution (cm^3)
1	26.2	650	107
2		650	106
3		650	110
4		650	107
5		650	110
6	26.2	350	65
7		350	64
8		350	66
9		350	65
10		350	65
11	34	650	64
12		650	64
13		650	66
14		650	64
15		650	64
16	34	350	35
17		350	36
18		350	37
19		350	36
20		350	37

Table B.2 – Volume of discharge recorded for glycerol solution (85% by volume) (μ = 83.5 mPa.s) in experiments with two holes

Test	Speed (rpm)	Initial volume (cm^3)	Volume discharged in one revolution (cm^3)
1	26	500	57
2		500	57
3		500	55
4		500	55
5		500	55
6	26	350	40
7		350	41
8		350	41
9		350	43
10		350	44
11	29	500	45
12		500	45
13		500	45
14		500	45
15		500	45
16	29	350	31
17		350	33
18		350	33
19		350	34
20		350	31

Table B.2 Continued

Test	Speed (rpm)	Initial volume (cm^3)	Volume discharged in one revolution (cm^3)
1	32	500	37
2		500	38
3		500	38
4		500	37
5		500	37
6	32	350	27
7		350	28
8		350	29
9		350	27
10		350	26
11	35	500	30
12		500	31
13		500	30
14		500	32
15		500	31
16	35	350	21
17		350	22
18		350	21
19		350	22
20		350	21

Table B.3 – Volume of discharge recorded for glycerol solution (85% by volume) (μ = 83.5 mPa.s) in experiments with three holes

Test	Speed (rpm)	Initial volume (cm^3)	Volume discharged in one revolution (cm^3)
1	26	500	81
2		500	80
3		500	82
4		500	81
5		500	83
6	26	350	51
7		350	51
8		350	52
9		350	52
10		350	52
11	29	500	65
12		500	66
13		500	65
14		500	66
15		500	66
16	29	350	46
17		350	45
18		350	45
19		350	45
20		350	45

Table B.3 Continued

Test	Speed (rpm)	Initial volume (cm^3)	Volume discharged in one revolution (cm^3)
1	32	500	53
2		500	54
3		500	53
4		500	53
5		500	53
6	32	350	38
7		350	38
8		350	37
9		350	37
10		350	38
11	35	500	42
12		500	43
13		500	44
14		500	43
15		500	43
16	35	350	30
17		350	29
18		350	27
19		350	30
20		350	31

APPENDIX C

COMPUTATIONAL FLUID DYNAMICS FREE SURFACE PROFILE PREDICTIONS FOR PILOT SCALE MILL

Appendix C reports the free surface profiles of the fluid, water, without any discharge in a mill having a diameter of 98 cm. The profiles are computed as the mill rotates in clockwise direction at 34.2 revolutions per minute corresponding to 80% of the mill critical speed. There are sixteen pulp lifter channels and the pulp lifter depth is 3 cm. The trunnion diameter is 25 cm.

The mill is filled with water up to 27% of the mill volume for the simulation, and the simulation results show the free surface profiles for one full revolution of the mill at the indicated mill rotational speed.

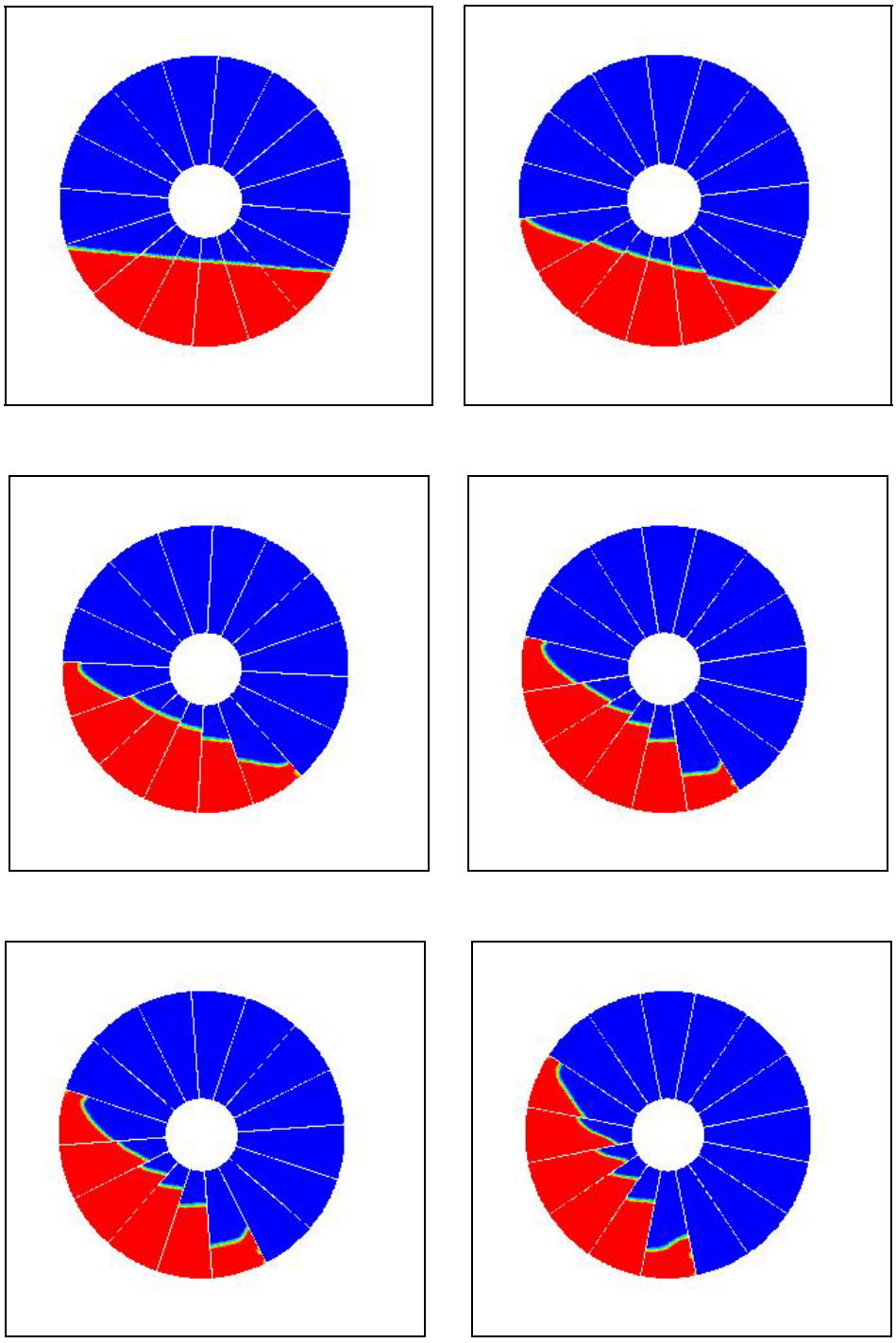

Figure C.1 – The successive free surface profiles of fluid volume in a mill of diameter 98 cm, as the mill rotates at 80% of the mill critical speed in clockwise direction

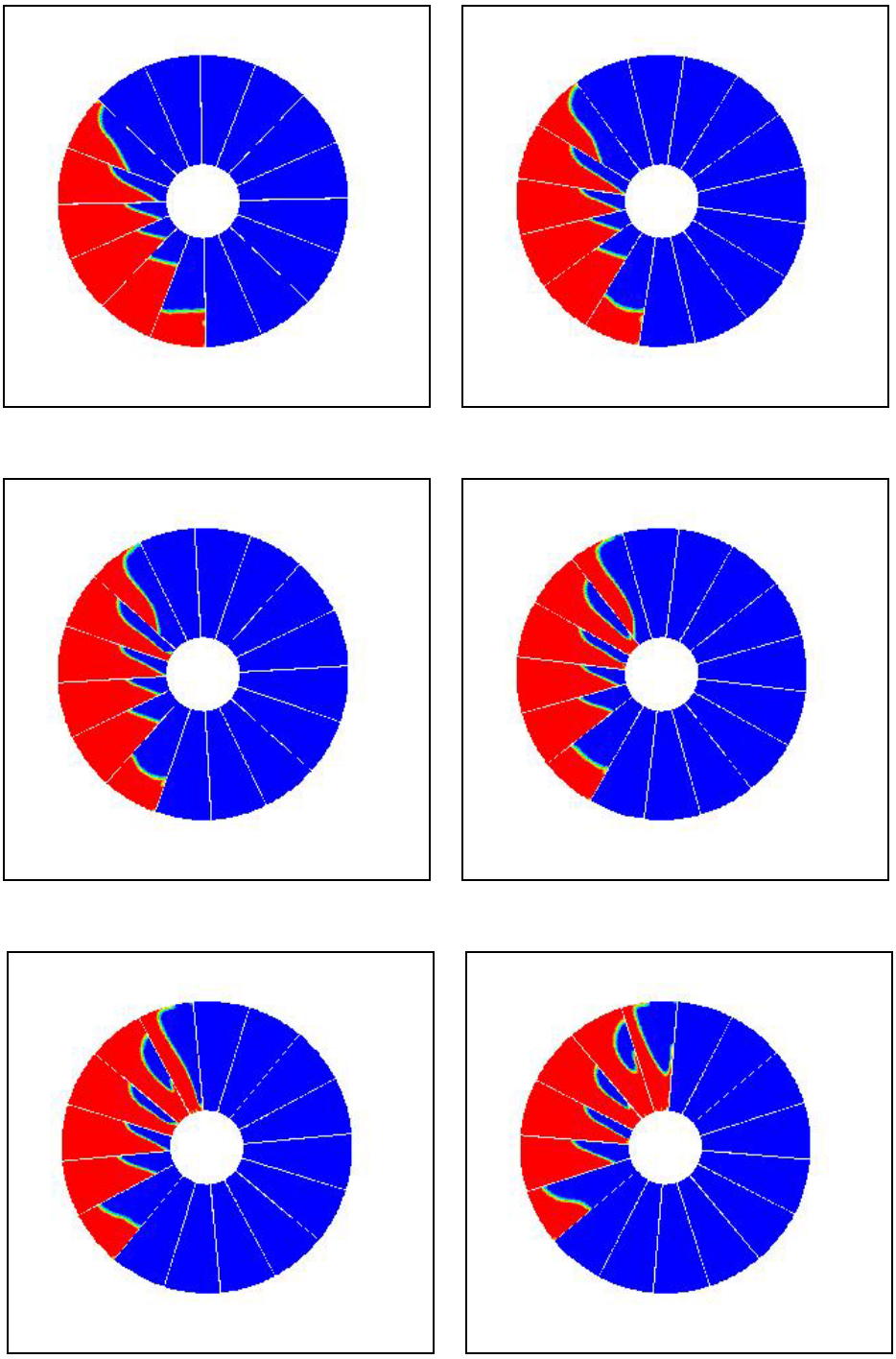

Figure C.1 Continued

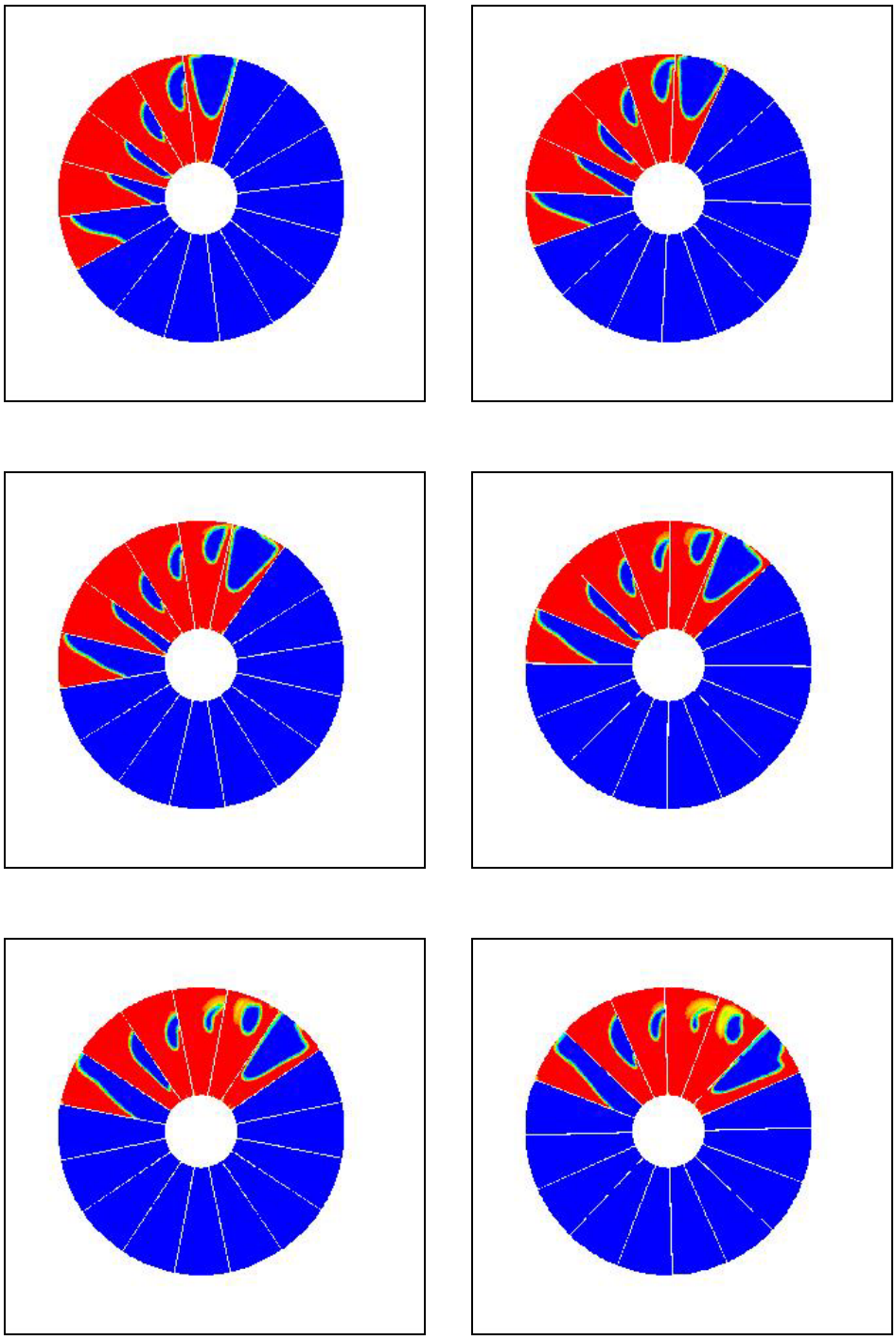

Figure C.1 Continued

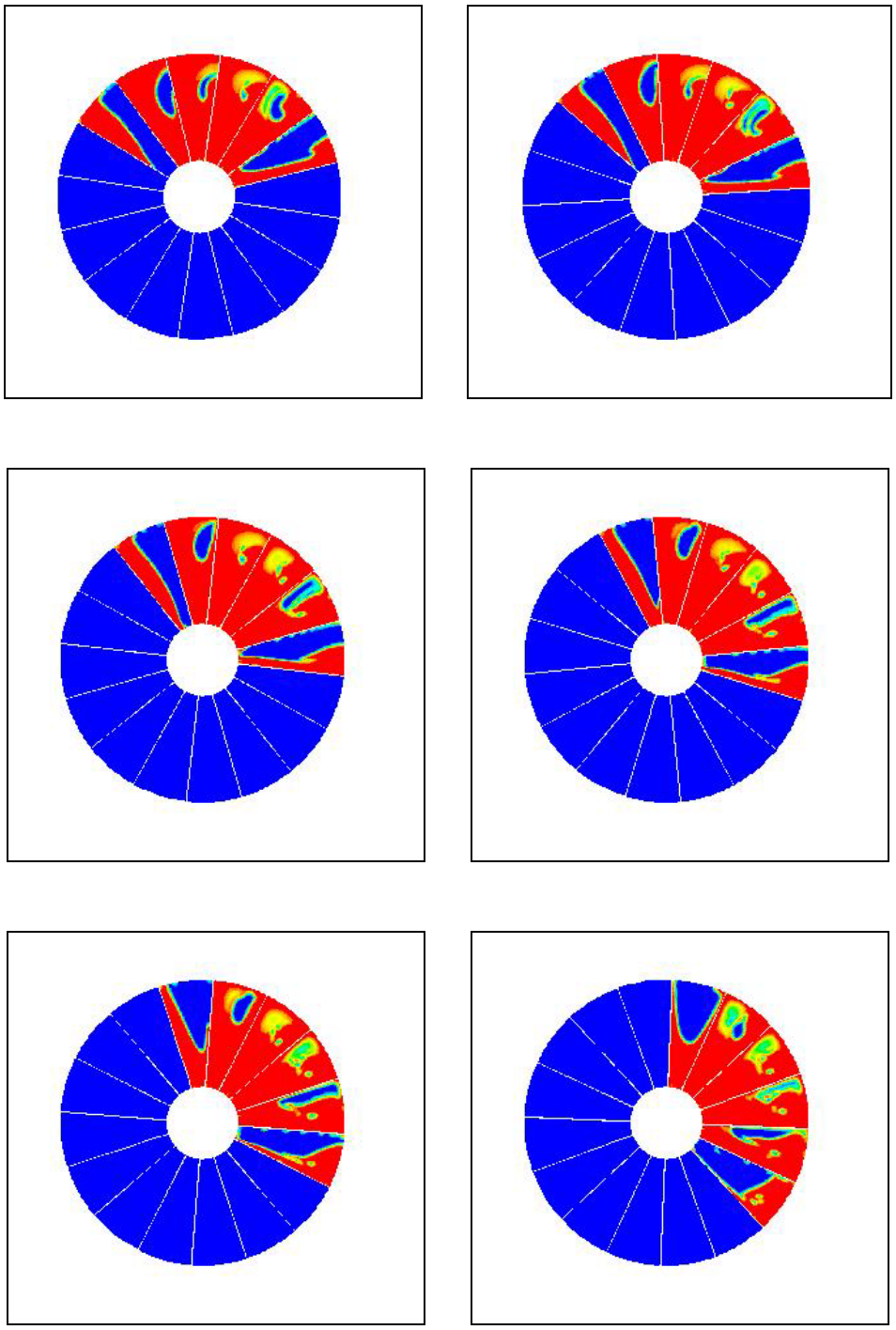

Figure C.1 Continued

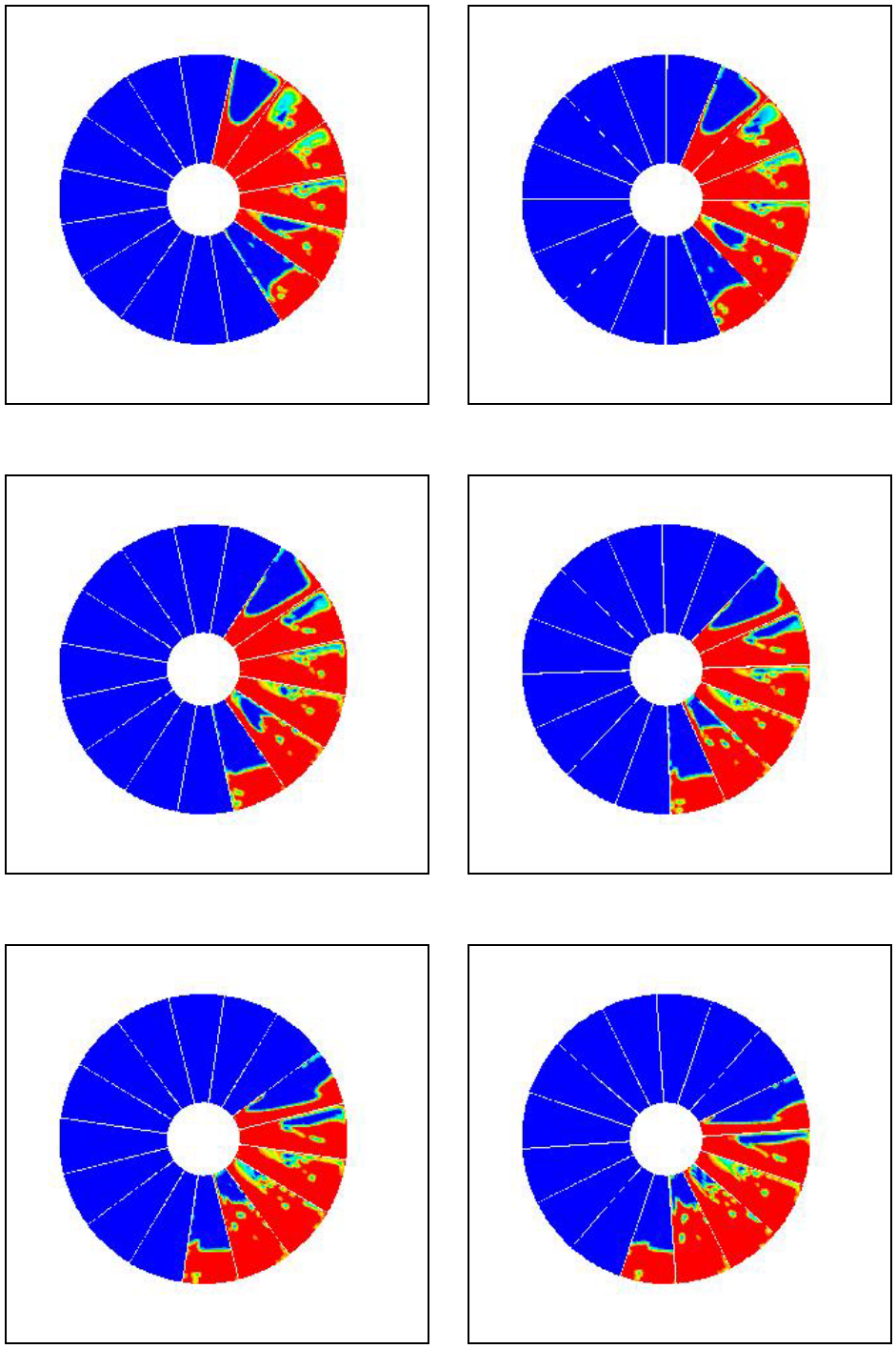

Figure C.1 Continued

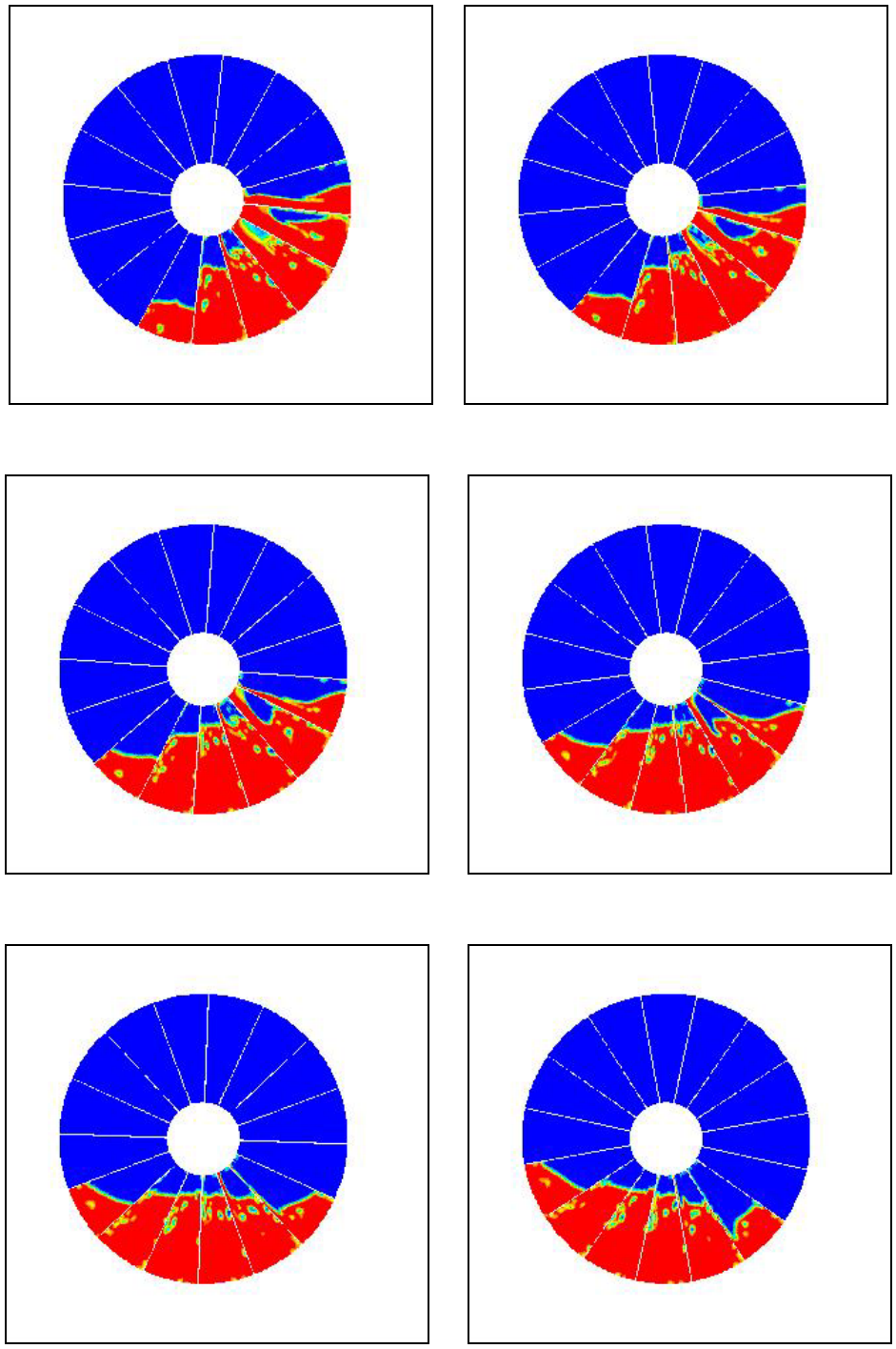

Figure C.1 Continued

REFERENCES

Austin LG, Menacho JM and Pearcy F 1987, 'A general model for semi-autogenous and autogenous milling', *Proceedings of the Twentieth International Symposium on Application of Computers and Mathematics in the Mineral Industries,* Johannesburg, SAIMM, pp. 107-126.

Bird RB, Stewart WE and Lightfoot EN 2007, *Transport Phenomena*, revised second edition, John Wiley and Sons, Inc., New York.

Cleary PW, Sinnott, M and Morrison, RD 2006, 'Prediction of slurry transport in SAG mills using SPH fluid flow in a dynamic DEM based porous media', *Minerals Engineering*, vol. 19, no. 15, pp. 1517-1527.

Cleary, PW, Prakash, M, Ha, J, Stokes, N and Scott, C 2007, 'Smooth particle hydrodynamics, status and future potential', *Progress in Computational Fluid Dynamics*, vol. 7, pp. 70-90.

Cleary, PW and Morrison, RD 2009, 'Particle methods for modelling in mineral processing', *International Journal of Computational Fluid Dynamics,* vol. 23, no. 2, pp. 137-146.

Dong H and Moys MH 2003, 'Load behavior and mill power', *International Journal of Mineral Processing,* vol. 69, pp. 11-28.

Ferziger JH and Peric M 2001, *Computational Methods for Fluid Dynamics*, third edition, Springer, Verlag, Berlin.

Fluent 6.3 user's guide 2006, Fluent Inc., Lebanon, USA.

Herbst, JA 2004, 'A microscale look at tumbling mill scale-up using high fidelity simulation', *International Journal of Mineral Processing*, vol. 74, pp. 299-306.

Hirt CW and Nichols BD 1981, 'Volume of fluid (VOF) method for the dynamics of free boundaries', *Journal of Computational Physics,* vol. 39, no. 1, pp. 201-225.

Latchireddi, S and Morrell S 1997, 'A laboratory study of the performance characteristics of mill pulp lifters', *Minerals Engineering*, vol. 10, no. 11, pp. 1233-1244.

Latchireddi, S and Morrell S 2003a, 'Slurry Flow in Mills: Grate-Only Discharge Mechanism (Part-1)', *Minerals Engineering*, vol. 16, pp. 625-633.

Latchireddi, S and Morrell S 2003b, 'Slurry Flow in Mills: Grate-Pulp Lifter Discharge Systems (Part 2)', *Minerals Engineering*, vol. 16, pp. 635-642.

Liu, MB and Liu GR 2010, 'Smoothed Particle Hydrodynamics (SPH): An overview and recent developments', *Archives of Computational Methods in Engineering,* vol. 17, pp. 25-76.

Marek M, Aniszewski W and Boguslawski A 2008, 'Simplified volume of fluid method for two-phase flows', *Task Quarterly*, vol. 12, no. 3, pp. 255-265.

Mishra, BK and Rajamani, RK 1992, 'The Discrete element method for the simulation of ball mills', *Applied Mathematical Modelling*, vol. 16, no.11, pp. 598-604.

Mishra BK 2003, 'A review of computer simulation of tumbling mills by the discrete element method: Part I – contact mechanics', International Journal of Mineral Processing, vol. 71, pp. 73-93.

Mishra BK 2003, 'A review of computer simulation of tumbling mills by the discrete element method: Part II – practical applications', International Journal of Mineral Processing, vol. 71, pp. 95-112.

Mokken AH, Blendulf GKI and Young GJC 1975, 'A study of the arrangements for pulp discharge on pebble mills, and their influence on mill performance', *Journal of the South African Institute of Mining and Metallurgy*, pp. 257-289.

Monaghan JJ 1992, 'Smoothed particle hydrodynamics', *Annual Reviews of Astronomy and Astrophysics*, vol. 30, pp. 543-574.

Morrell, S and Kojovic, T 1996, 'The Influence of Slurry Transport on the Power Draw of Autogenous and Semi-Autogenous Mills', *Proceedings of the International Conference on Autogenous and Semiautogenous Grinding Technology,* SAG1996, Vancouver, BC, Canada, pp. 48-57.

Morrell, S and Stephenson, I 1996, 'Slurry discharge capacity of autogenous and semi-autogenous mills and the effect of the grate design', *International Journal of Mineral Processing*, vol. 46, pp. 53-72.

Morrell S 2004, 'A new autogenous and semi-autogenous mill model for scale-up, design and optimisation', *Minerals Engineering*, vol. 17, pp. 437-445.

Morrell, S and Latchireddi, S 2000, 'The Operation and Interaction of Grates and Pulp Lifters in Autogenous and Semi-Autogenous Mills', *Proceedings of the Seventh Mill Operators' Conference*, AusIMM, Kalgoorlie, Australia, pp. 13-20.

Morrison, RD and Cleary, PW 2008, 'Towards a Virtual Comminution Machine', *Minerals Engineering*, vol. 21, pp. 770-781.

Moys, MH 1986, 'The effect of grate design on the behavior of grate discharge mills', *International Journal of Mineral Processing*, vol. 18, pp. 85-105.

Nordell LK, Potapov, AY and Herbst, JA 2001, 'Comminution simulation using discrete element method (DEM) approach - From single particle breakage to full-scale SAG mill operation', *Proceedings of the International Conference on Autogenous and Semiautogenous Grinding Technology,* SAG2001, Vancouver, BC, Canada, pp. 235-251.

Pope, SB 2000, *Turbulent Flows*, Cambridge University Press, Cambridge, UK.

Powell, MS and Valery, Walter 2006, 'Slurry pooling and transport issues in SAG mills', *Proceedings of the International Conference on Autogenous and Semiautogenous Grinding Technology,* SAG2006, Vancouver, BC, Canada, pp. 134-152.

Powell MS and Morrison RD 2007, 'The future of comminution modelling', *International Journal of Mineral Processing*, vol. 84, pp. 228-239.

Rajamani, RK and Mishra, BK 2001, 'Three dimensional simulation of charge motion in plant size SAG mills', *Proceedings of the International Conference on Autogenous and Semiautogenous Grinding Technology,* SAG2001, Vancouver, BC, Canada, pp. 48-57.

Rajamani, RK, Latchireddi, S, and Mishra, BK 2003, 'Discrete element simulation of ball and rock charge and slurry flow through grate and pulp lifters', *Proceedings of the SME Annual Meeting,* Society of Mining Engineers, Cincinnati, Ohio, preprint 03-108, pp. 1-5.

Royston, D and Denlay, D 1999, 'Design and performance of curved SAG mill pulp lifters', *Proceedings of the SME Annual Meeting,* Society of Mining Engineers, Denver, Colorado, preprint 99-52, pp. 1-3.

Royston, D 2000, 'Curved pulp lifters for AG and SAG mills - current experience', *Proceedings of the SME Annual Meeting,* Society of Mining Engineers, Salt Lake City, Utah, preprint 00-14, pp. 1-3.

Royston, D 2005, 'SAG mill pulp lifter design, discharge and backflow', *Proceedings of the SME Annual Meeting,* Society of Mining Engineers, Salt Lake City, Utah, preprint 05-49, pp. 1-6.

Royston, D 2007a, 'Practical experience in the design and operation of semi-autogenous grinding (SAG) mill liners', *Proceedings of the Ninth Mill Operators' Conference*, Ninth Mill Operators', Fremantle, WA, pp. 147-154.

Royston, D 2007b, 'Semi-autogenous grinding (SAG) mill liner design and development', *SME Publications, Minerals and Metallurgical Processing*, vol. 24, no. 3, pp. 121-132.

Shi, FN and Napier-Munn, TJ 2002, 'Effect of Slurry Rheology on Industrial Grinding Performance', *International Journal of Mineral Processing*, vol. 65, pp. 125-140.

Song M, Qiu X, Potapov A and Nordell L 2001, 'MILLSTAT-A software package for statistical analysis of mill databases', *Proceedings of the International Conference on Autogenous and Semiautogenous Grinding Technology,* SAG2001, Vancouver, BC, Canada, pp. 85-100.

Sussman M and Puckett EG 2000, 'A coupled level set and volume-of-fluid method for computing 3D and axisymmetric incompressible two-phase flow', Journal of Computational Physics, vol. 162, pp. 301-337.

Taggart AF 1945, *Handbook of Mineral Dressing*, second edition, John Wiley and Sons, Inc., New York.

Wilcox, DC 1993, Turbulence Modeling for CFD, First edition, DCW Industries, Inc., La Canada, California.

Zhang X, Sudharsan NM, Ajaykumar R and Kumar K 2005, 'Simulation of free surface flow in a tank using the Navier Stokes model and unstructured finite volume method', *Journal of Mechanical Engineering Science*, vol. 219, pp. 251-266.